การสังเคราะห์และพิสูจน์เอกลักษณ์ของตัวเร่งปฏิกิริยาซีโอไลต์บีตาที่ขยายรูพรุนเพื่อการแตกตัวของน้ำมันเตา

นางสาวณิชารีย์ วงศ์สวัสดิ์กุล

วิทยานิพนธ์นี้เป็นส่วนหนึ่งของการศึกษาตามหลักสูตรปริญญาวิทยาศาสตรมหาบัณฑิต

สาขาวิชาปิโตรเคมีและวิทยาศาสตร์พอลิเมอร์

คณะวิทยาศาสตร์ จุฬาลงกรณ์มหาวิทยาลัย

ปีการศึกษา 2552

SYNTHESIS AND CHARACTERIZATION OF ENLARGED-PORE ZEOLITE BETA CATALYST FOR HEAVY FUEL OIL CRACKING

Miss Nicharee Wongsawatgul

A Thesis Submitted in Partial Fulfillment of the Requirements
for the Degree of Master of Science Program in Petrochemistry and Polymer Science
Faculty of Science
Academic Year 2009

Thesis Title	SYNTHESIS AND CHARACTERIZATION OF ENLARGED-PORE ZEOLITE BETA CATALYST FOR HEAVY FUEL OIL CRACKING
By	Miss Nicharee Wongsawatgul
Field of Study	Petrochemistry and Polymer Science
Thesis Advisor	Assistant Professor Soamwadee Chaianansutcharit, Ph.D.

Accepted by the Faculty of Science, Chulalongkorn University in in Partial Fulfillment of the Requirements for the Master's Degree

……..……Dean of the Faculty of Science
(Professor Supot Hannongbua, Dr. rer. nat.)

THESIS COMMITEE

……..……Chairman
(Associate Professor Sirirat Kokpol, Ph.D.)

……..……Thesis Advisor
(Assistant Professor Soamwadee Chaianansutcharit, Ph.D.)

……..…… Examiner
(Associate Professor Wimonrat Trakarnpruk, Ph.D.)

……..……External Examiner
(Dr. Pornsawan Assawasaengrat, D.ENG)

ณิชารีย์ วงศ์สวัสดิ์กุล : การสังเคราะห์และพิสูจน์เอกลักษณ์ของตัวเร่งปฏิกิริยาซีโอไลต์บีตาที่มีรูพรุนขนาดกลางเพื่อการแตกตัวของน้ำมันเตา. (SYNTHESIS AND CHARACTERIZATION OF ENLARGED-PORE ZEOLITE BETA CATALYST FOR HEAVY FUEL OIL CRACKING) อ.ที่ปรึกษาวิทยานิพนธ์หลัก: ผศ. ดร. โสมวดี ไชยอนันต์สุจริต 104 หน้า

ซีโอไลต์บีตาที่ขยายรูพรุนสังเคราะห์ได้ภายใต้ภาวะไฮโดรเทอร์มัล โดยศึกษาเปรียบเทียบผลกระทบจากตัวแปรต่างๆ ได้แก่ แหล่งซิลิกา ชนิดและอัตราส่วนของสารต้นแบบ อุณหภูมิและระยะเวลาในการตกผลึก ได้พิสูจน์เอกลักษณ์ของสารตัวอย่างที่เตรียมได้ด้วยเทคนิคการเลี้ยวเบนของรังสีเอ็กซ์ การดูดซับไนโตรเจน กล้องจุลทรรศ น์แบบส่องกราด อินดักทีฟลีคัปเปิลพลาสมาอะตอม - มิคอีมิสชั่นสเปกโตรสโคปิก อะลูมิเนียมนิวเคลียร์แมจิกแองเกิลสปินนิวเคลียร์แมกเนติกเรโซแนนซ์ ข้อมูลการวิเคราะห์แสดงให้เห็นว่า ซีโอไลต์บีตาที่ขยายรูพรุนสามารถเตรียมได้จากซิลิกาเอชเอ็มเอสที่เผาไล่สารต้นแบบ และตกผลึก ที่อุณหภูมิ 135 องศาเซลเซียส เป็นเวลา 3 วัน ขนาดรูพรุนจะใหญ่กว่าซีโอไลต์บีตาอ้างอิง ขนาดรูพรุนจะเพิ่มขึ้นเมื่อ ใช้สารต้นแบบผสมระหว่างเททราเอทิลแอมโม-เนียมไฮดรอกไซด์และเฮกซาเดกซิลเอมีน แต่มีโครงสร้างของแซดเอชเอ็มสิบสองปน โครงสร้างแซดเอชเอ็มสิบสองเพิ่มขึ้นเมื่ออุณหภูมิและระยะเวลาการตกผลึกเพิ่มขึ้น ได้ศึกษาสมบัติเชิงเร่งปฏิกิริยาของซีโอไลต์บีตาที่ขยายรูพรุนที่สังเคราะห์ได้ในการแตกตัวของน้ำมันเตาเพื่อได้ไฮโดรคาร์-บอนขนาดเล็กภายใต้ภาวะต่างๆ พบว่าค่าการเปลี่ยนรูปของน้ำมันเตาเป็นผลิตภัณฑ์เมื่อใช้ซีโอไลต์บีตาที่ขยายรูพรุนเป็นตัวเร่งปฏิกิริยาสูงกว่าเมื่อเทียบกับซีโอไลต์บีตา และการแตกตัวโดยใช้ความร้อน ภาวะที่เหมาะสมในการแตกย่อยน้ำมันเตาในงานวิจัยนี้คือ 380 องศาเซลเซียส เป็นเวลา 40 นาที อัตราส่วนของตัวเร่งปฏิกิริยาต่อน้ำมันเตาเป็น 10 เปอร์เซ็นต์ อัตราการไหลของแก๊สไนโตรเจนที่ 20 ลูกบาศก์เซนติเมตรต่อนาที องค์ประกอบหลักของแก๊สที่ได้จากการแตกย่อยน้ำมันเตา คือ 1,3 บิวทา-ไดอีน แ ละสารที่มีจุดหลอมเหลวสูงกว่านอมัลเพนเทน(C_5^+) ของเหลวเบาประกอบด้วยสารไฮโดรคาร์บอนในช่วงแกโซลีน และของเหลวหนักในช่วงเคโรซีน ตัวเร่งปฏิกิริยาที่ใช้แล้วสามารถให้นำกลับมาใช้ใหม่ได้ง่ายด้วยการเผาและความว่องไวยังไม่เปลี่ยนแปลงมากนัก

สาขาวิชา ปิโตรเคมีและวิทยาศาสตร์พอลิเมอร์ ลายมือชื่อนิสิต .....

ปีการศึกษา 2552 ลายมือชื่อ อ.ที่ปรึกษาวิทยานิพนธ์หลัก .....

5072273223: MAJOR PETROCHEMISTRY AND POLYMER SCIENCE
KEYWORDS: ENLARGED-PORE ZEOLITE BETA / HMS / HEAVY FUEL OIL

NICHAREE WONGSAWATGUL: SYNTHESIS AND CHARACTERIZATION OF ENLARGED-PORE ZEOLITE BETA CATALYST FOR HEAVY FUEL OIL CRACKING. THESIS ADVISOR: ASST. PROF. SOAMWADEE CHAIANANSUTCHARIT, Ph.D., 104 pp.

The enlarged-pore zeolite beta (h-BEA) was synthesized under hydrothermal condition. The effects of different parameters were investigated *e.g.* silica source, type and ratio of template and crystallization temperature and time. The prepared samples were characterized by X-ray powder diffraction (XRD), nitrogen adsorption analysis, scanning electron microscopy (SEM), inductively couple plasma atomic emission spectroscopic (ICP-AES) and Al nuclear magic angle spin nuclear magnetic resonance (^{27}Al MAS NMR) techniques. The analysis data indicated that the enlarged-pore zeolite beta could be prepared from calcined Si-HMS and crystallized at 135°C for 3 days. Its pore diameter was larger than comparative zeolite beta. The pore size was more increased when mixed tamplate between tetraethylammonium hydroxide and hexadexylamine was used but ZSM-12 was a coexisting phase. The latter phase was predominated with increasing the crystallization temperature and time. The synthesized enlarged-pore zeolite betas were tested for catalytic cracking of heavy fuel oil to produce light hydrocarbon fuel on various conditions. It was found that conversion of heavy fuel oil into products over the enlarged-pore zeolite beta was higher than of zeolite beta and thermal cracking. The optimal condition for cracking of heavy fuel oil in this research was 380°C for 40 min, 10wt% of catalyst to heavy fuel oil and N_2 flow of 20 cm^3/min. The major components of gas fraction from heavy fuel oil cracking were 1,3-butadiene and the hydrocarbon having boiling point higher than n-pentane (C_5^+). The distillate oil was mainly composed of hydrocarbon in the gasoline range and heavy oil was mainly in the kerosene range. The used catalyst could be regenerated easily by simple calcination and its activity still does not change significantly.

Field of Study Petrochemistry and Polymer science Student's Signature .....
Academic year 2009 Advisor's Signature .....

ACKNOWLEDGEMENTS

The success of this thesis can be attributed to the extensive support and assistance from Assistant Professor Dr. Somwadee Chaianansutcharit, author's advisor. The author deeply thanks for her valuable advice and guidance in this research and her kindness throughout this study.

The author would like to gratitude to Associate Professor Dr. Sirirat Kokpol, Associate Professor Dr. Wimonrat Trakranpruk and Dr. Pornsawan Assawasaengrat as the chairman and members of this thesis committee, respectively, for all kindness and useful advice in this research.

The author would like to thank Department of Petrochemistry and Polymer Science, Chulalongkorn University for valuable knowledge and experience and gratefully appreciate the Graduate School, Chulalongkorn University and Center of Excellence for Petroleum, Petrochemicals and Advanced Materials, Chulalongkorn University for partially financial support, Department of Chemistry, Chulalongkorn University for analysis instruments and Shell Co., Ltd. for supplying heavy fuel oil.

The author also thanks members of Materials Chemistry and Catalyst Research Unit for generosity, especially their very good corporation in work, sharing of colorful emotion and friendly working atmosphere. The author truly realizes their support and standing by her throughout work.

For all of her friends, she greatly appreciates their encouragement and discussion throughout the course of her the research and study. Finally, she would like to express her deepest gratitude to her beloved family for their entirely care and support, endless love and eternal understanding throughout her life. The usefulness of this thesis, she dedicates to her family, all teachers who have taught since her childhood.

CONTENT

Page

Page

LIST OF TABLES

LIST OF FIGURES

Figure **Page**

Figure **Page**

Figure **Page**

LIST OF SCHEMES

LIST OF ABBREVIATIONS

BET	Brunauer-Emmett -Teller
BJH	Barret, Joyner, and Halenda
°C	Degree Celsius
cps	Counts Per Second
g	gram (s)
GC	Gas Chromatography
h	hour (s)
HFO	Heavy Fuel Oil
ICP-AES	Inductively Coupled Plasma-Atomic Emission Spectroscopy
M	molar
MAS-NMR	Magic-anglespinning-nuclear magnetic resonance
mg	milligram (s)
min	minute (s)
ppm	part per million or mg/l
SEM	Scanning Electron Microscopy
TEAOH	Tetraethylammoniumhydroxide
TPD	Temperature-Programmed Desorption
XRD	X-ray diffraction
%	percent

CHAPTER I

INTRODUCTION

1.1 Motivation

As the world demand in energy is increased, and the oil recovery is decreased, as shown in Figure 1.1, the conventional crude oils have become more expensive. Therefore objective of this work is to convert and upgrade heavy petroleum fraction into valuable liquid products by using catalytic cracking process.

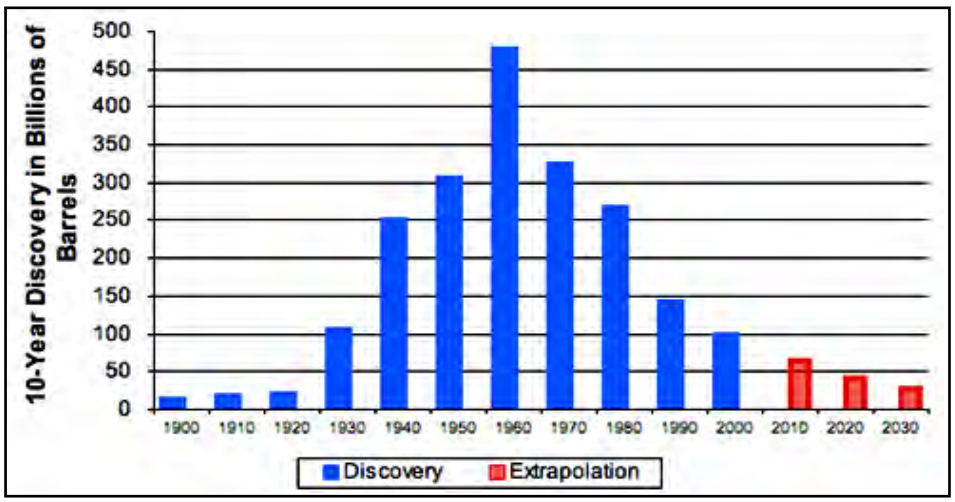

Figure 1.1 World oil recoveries over 10 year periods [1].

In recent years, development of new porous materials combining the advantageous properties of microporous zeolites and ordered mesoporous alumino-silicates [2] has been explored. The porous materials are called the composite materials. Although these composites promote the cracking activity and produce more hydrocarbons with higher market value, these materials not present the actual combination of both structures. At the same time, there has been increasing an interest in developing the pore size of microporous zeolite materials to meet the demands in both industrial and fundamental studies for the treatment of large molecules, such as processing the heavy ingredients of crude oils or separating and synthesizing large organic molecules [3]. Therefore, the objective of this work is to synthesize and

characterize enlarged-pore zeolite beta under the hypothesis that the enlarged-pore zeolite beta allows the large molecules in heavy petroleum fraction to diffuse through the pore and degrade to lighter hydrocarbon. This enlarged-pore zeolite beta also keeps acidity and crystallinity of the structure.

1.2 Background

Crude oil, petroleum, is the term for unprocessed oil, which coming out of the under-ground. Crude oil is a fossil fuel made naturally from decayed animals and plants for millions of years ago. Heat and pressure from mud layers turn the dead organisms into petroleum or crude oil. After crude oil is removed from the ground, it is refined into many hydrocarbon fractions as shown in Figure 1.2. The oldest and common refining process is called fractional distillation which differentiates hydrocarbons based on boiling temperature. There are three main fractions from this process, as follows

(1) Light fraction, this portion consists of hydrocarbons with the lowest boiling temperature. There are categorized into three fractions.

- Liquefied petroleum gas (LPG)

  LPG is small alkanes which consists of 1 to 4 carbon atoms (C_1-C_4), commonly known by methane, ethane, propane, and butane. The boiling temperature is less than 40°C. It is liquefied under pressure at the oil source and is used for heating and making plastics.

- Naphtha or Ligroin

  Naphtha is mixing of C_5-C_9 alkanes. The boiling temperature ranges about 60-100°C. It is used as intermediate for making gasoline.

- Petrol or Gasoline

  Gasoline is a liquid which is mixed of C_5-C_{12} alkanes and cycloalkanes. The boiling point ranges about 104-200°C. It is used as motor fuel.

(2) Medium fraction contains of hydrocarbons with medium boiling temperature. There are two fractions in this part.

- Kerosene

  Kerosene is mixed liquid between alkanes (C_9-C_{16}) and aromatics. The boiling point ranges about 175-250°C. It is used as fuel for jet engines, tractors and starting material for making other products

- Gas oil or Diesel distillate

  Diesel distillate is a liquid which are C_{12}-C_{25} alkanes. The boiling temperature ranges about 250- 350°C. It is used for diesel fuel, heating oil, and starting materials for making other products.

(3) Heavy fraction contains hydrocarbons with high boiling temperature. There are three fractions in this part

- Lubricating oil

  Lubricating oil is a liquid which is long chain C_{20}-C_{50} alkanes, cycloalkanes and aromatics. The boiling temperature ranges about 300-370°C. It is used for motor oil, grease and other lubricants.

- Heavy fuel oil or Fuel oil

  Heavy fuel oil is a liquid which is long chain C_{20}-C_{70} alkanes, cycloalkanes and aromatics. The boiling point ranges about 370-600°C. It is used for industrial fuel, ocean liner fuel and starting material for making other products.

- Residual

  Residual is solid which is multiple ring compounds with higher C_{70} atoms. The boiling temperature is greater than 600°C. It is used as coke, asphalt, tar, waxes, and starting material for making other products.

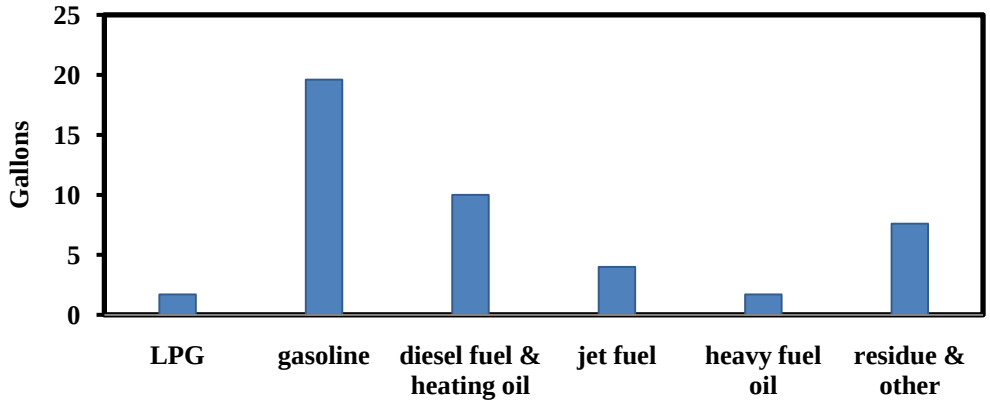

Figure 1.2 Products made from a barrel of crude Oil [4].

1.3 Heavy Fuel oil

Fuel oil or Heavy fuel oil or bunker fuel or bunker C or black oil is one of heavy fraction obtained from petroleum distillation as above-mentioned. They are viscous liquids with characteristic scent and dark color. There are mixtures of high molecular weight compounds having a typical boiling range from 370 to 600°C [5-7]. It has high density; some heavy fuel oil can be above 1,000 kg/m^3, which has environmental implications in the event of a spillage into fresh water. It consists of aromatic, aliphatic and naphthenic hydrocarbons, typically having carbon numbers from C_{20} to C_{70}, together with asphaltenes and smaller amounts of heterocyclic compounds containing sulphur, nitrogen and oxygen. It has suspension of asphaltenes which are highly polar aromatic compounds of very high molecular weight (2000-5000). It also contains organo-metallic compounds from their presence in the original crude oils. The most important metal is vanadium. Some crude sources, for example, from the Caribbean area and Mexico are particularly high in vanadium and this is reflected in high vanadium contents in heavy fuel oils produced from these crudes. Vanadium is a major significance for fuels burned in both diesel engines and boilers because when combined with sodium (perhaps from seawater contamination) and other metallic compounds in critical proportions it can form high melting point ashes which are corrosive to engine exhaust valves. Other elements that are in heavy fuel oil include nickel, iron, potassium, sodium and hydrogen sulphide. The high concentration of hydrogen sulphide (H_2S) has been collected in the headspaces of storage tanks of heavy fuel oils [8-9]. Heavy fuel oils are used in medium to large industrial plants,

marine applications and power stations in combustion equipment such as boilers, furnaces and diesel engines.

Since consumption and price of heavy fuel oil are less than gasoline and diesel fuel, as shown in Figure 1.3 and Figure 1.4, heavy fuel oil was used as upgrading feedstock to produce more valuable fractions. The process for upgrading via breakdown larger hydrocarbon into smaller hydrocarbons to give more useful molecules is called cracking.

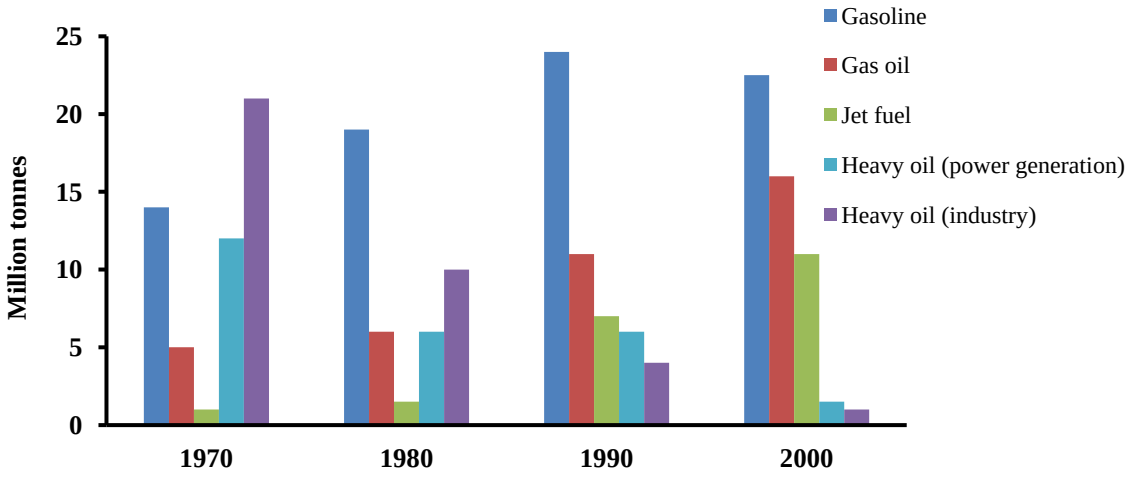

Figure 1.3 Energy uses by fuel type in 1970 to 2000 [10].

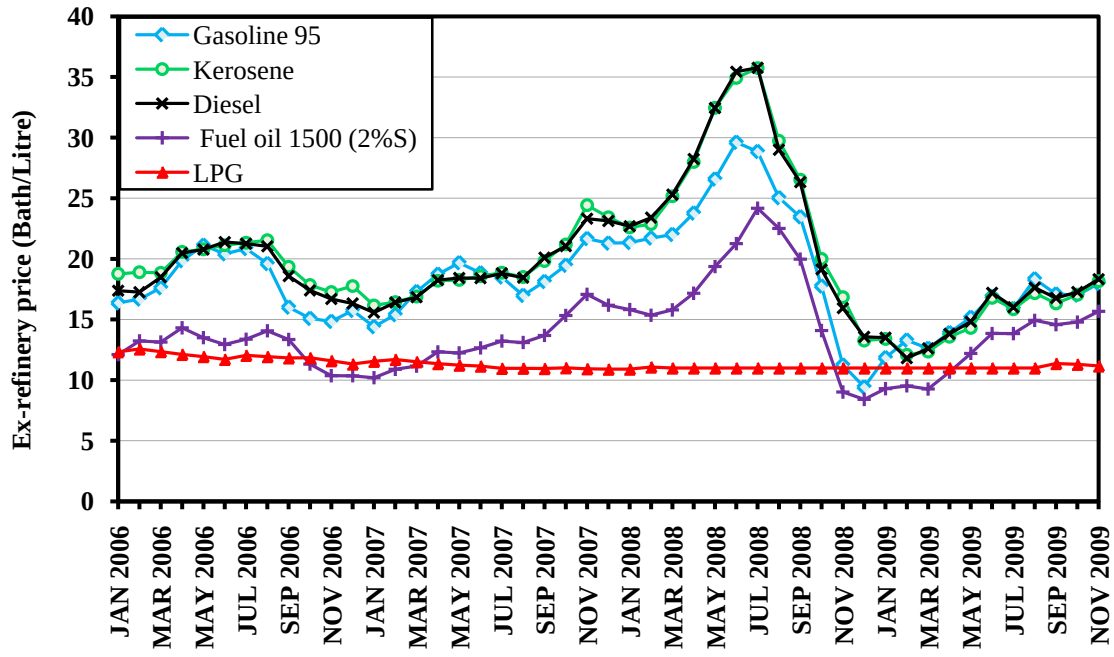

Figure 1.4 Comparison of ex-refinery oil price [11].

1.4 Cracking Process

The cracking process is essentially cleavage of large hydrocarbons into smaller hydrocarbons called petrochemicals. Petrochemical products can be used as raw materials in the production of new petrochemicals and plastics, without any decrease in their qualities and limitation of their applications. This process consists of three types of reaction: thermal cracking, catalytic cracking, and hydrocracking.

1.4.4 Thermal Cracking Process

Thermal cracking or thermolysis process requires high temperature to break down the bonds in the backbone of residues from the bottom of distillation process [12]. Three main forms of feedstock recycling of polymers by thermolysis are shown in Figure 1.5. When decomposition process is carried out in the absence of air, this is termed pyrolysis. When it is performed in hydrogen atmosphere, it is referred to hydrogenation. If it is carried out in the presence of a controlled amount of oxygen, it is known as gasification. Depending on the conversion route employed, the end products vary in composition and quality.

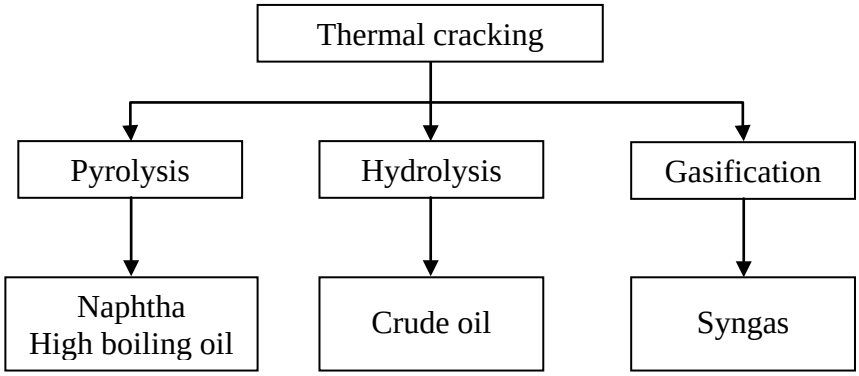

Figure 1.5 Overview of feedstock recycling for hydrocarbon feedstock by thermal cracking [12].

Thermal cracking process is usually occurred at temperature between 500-800°C. In the process, large hydrocarbon molecules can be converted into thermolytic oil, solid coke and volatile fraction that may be separated into condensable hydrocarbon oil and a non-condensable high calorific value gas. The proportion of

each fraction and their precise composition depend primarily on the nature of feedstock and the process condition.

Thermal cracking processes generally proceed via radical pathways through a random scission mechanism that generates a mixture of linear olefins and paraffins over a wide range of molecular weights [13].

A proportion of species which directly generated from the initial degradation reaction are transformed into secondary products due to the occurrence of inter- and intra-molecular reactions. The extent and the nature of these reactions depend both on the reaction temperature and the position of the products in the reaction zone. The design of reactor also affects.

Thermal cracking mechanism

Thermal cracking processes generally proceed via radical pathways [13]. The principal reaction of thermolysis involves hydrogenation or dehydrogenation concurrently with fragmentation of the carbon skeleton. The process is initiated by hemolytic cleavage of carbon-carbon bond into two free radicals as Equation 1. The initial radicals may then abstract hydrogen atom in hydrocarbon chain (in-chain hydrogens) as shown in equations 2 and 3 since in-chain hydrogens have lower bond strength than do the hydrogen atom at chain-end or considerate from stabilities of obtained radical. Stabilities of radical is ordered by 3°-radical > 2° -radical > 1° -radical > CH_3-radical. Thus, radicals preferentially attack the in-chain hydrogens to obtain more stable radical. All in-chain hydrogens are equivalent in their ease of homolysis in comparison with homolysis of primary hydrogen from methyl group. The intermediate radical may undergo C-C bond homolysis (β-scission) to form olefins as ethylene and propylene and a new alkyl group as shown in equations 4 and 5. Disproportionation leads to a new olefin and an alkane with the same number of carbon atoms in equation 6.

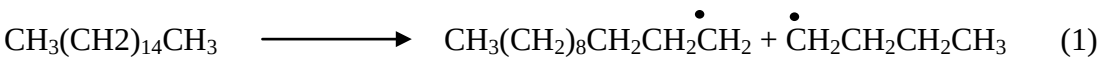

$$CH_3(CH2)_{14}CH_3 \longrightarrow CH_3(CH_2)_8CH_2CH_2\dot{C}H_2 + \dot{C}H_2CH_2CH_2CH_3 \quad (1)$$

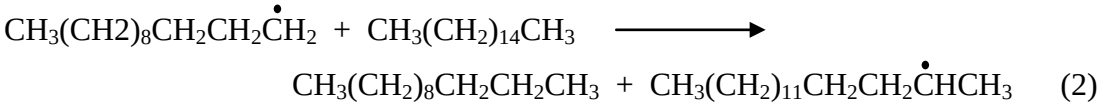

$$CH_3(CH2)_8CH_2CH_2\dot{C}H_2 + CH_3(CH_2)_{14}CH_3 \longrightarrow CH_3(CH_2)_8CH_2CH_2CH_3 + CH_3(CH_2)_{11}CH_2CH_2\dot{C}HCH_3 \quad (2)$$

$$\dot{C}H_2CH_2CH_2CH_3 + CH_3(CH_2)_{14}CH_3 \longrightarrow CH_3CH_2CH_2CH_3 + CH_3(CH_2)_{11}CH_2\dot{C}HCH_2CH_3 \quad (3)$$

$$CH_3(CH_2)_8CH_2CH_2\dot{C}H_2 \longrightarrow CH_3(CH_2)_8\dot{C}H_2 + CH_2{=}CH_2 \quad (4)$$

$$CH_3(CH_2)_{11}CH_2CH_2\dot{C}HCH_3 \longrightarrow CH_3(CH_2)_{11}\dot{C}H_2 + CH_2{=}CHCH_3 \quad (5)$$

$$2\,\dot{C}H_2CH_2CH_2CH_3 \longrightarrow CH_2{=}CHCH_2CH_3 + CH_3CH_2CH_2CH_3 \quad (6)$$

Methyl and ethyl radicals are the only stable radicals formed in the temperature range of 500-800°C. Obviously, all higher radicals decompose into alkanes and either methyl and ethyl radicals or atomic hydrogen. The obtained alkanes then react via hydrogen abstraction to give methane, ethane and alkenes as in Figure 1.6. The overall result of thermal cracking is changed in hydrogen content and carbon skeleton.

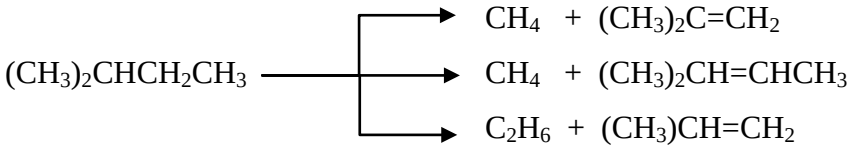

Figure 1.6 Reaction scheme of hydrogen abstraction [13]

In cracking of alicyclic alkanes, the reaction proceeds by abstraction of a hydrogen atom followed by β-scission. The cyclopentyl radical may undergo successive hydrogen abstraction to form cyclopentadiene.

Under certain conditions dehydrogenation is becoming an important reaction during pyrolysis, lower molecular weight (hydrogen rich) alkanes undergo dehydrogenation with hydrogen participated in the hydrogen transfer reactions. For example, ethane is transformed to ethylene, propane and propylene. In contrast, C-C bond breaking is the characteristic transformation of all other higher-molecular weight (more hydrogen-deficient) hydrocarbons. The higher molecular weight hydrocarbons are more reactive than hydrocarbons with lower molecular weight. Thus, paraffins most easily undergo thermal cracking, whereas olefins, cycloalkanes, and aromatics exhibit the decreasing order of cracking.

Under pyrolytic condition, higher molecular weight hydrocarbons and cycloalkanes undergo cracking temperature above 300°C, generally between 500-800°C. The pyrolysis reaction forms alkenes by carbon-hydrogen scissions as shown in Equations 7 to 9.

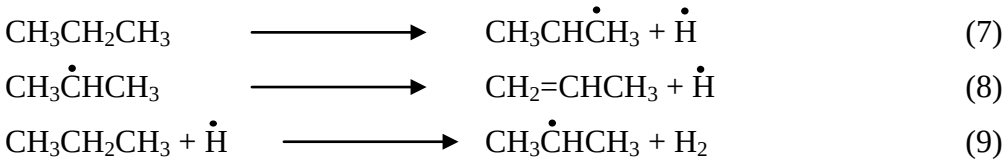

During pyrolysis, rearrangement of hydrogen atom or alkyl group migration occurs because of the failure of free radicals in isomerization. As a result, small branched alkanes are produced.

1.4.5 Catalytic Cracking Process

Catalytic cracking process is important and widely used in refinery for converting heavy oils into more valuable gasoline and lighter products [14], which are important feedstock for petrochemical industry. Originally, cracking was accomplished thermally but the catalytic process has almost completely replaced thermal cracking because the reaction occurs at low temperature. Gasoline product has high octane number and heavy oils and unsaturated gases are less produced.

Products from catalytic cracking units are more stable than those from thermal cracking units due to lesser olefins content in the liquid products. This reflects a higher hydrogen transfer activity, which leads to more saturated hydrocarbons.

The feeds for catalytic cracking units vary from gas oils to crude residues. Heavier feeds containing higher concentration of basic and polar molecules as well as asphaltenes reduce the catalyst activity and lower the quality of gasoline. For example, basic nitrogen compounds are readily adsorbed on the catalyst acid sites and temporary deactivation. Polycyclic aromatics and asphaltenes contribute strongly to coke formation. Thus, these feed stocks are often pretreated to decrease the metallic and asphaltene contents. Hydrotreatment, solvent extraction, and propane deasphalting are important treatment processes.

Catalytic cracking mechanism

A major difference between thermal and catalytic cracking is that catalytic cracking occur through carbonium ion intermediate, compared to the free radical intermediate in thermal cracking. Carbonium ions are longer lives and more selective than free radicals. The mechanism of catalytic cracking illustrates different ways by which carbonium ions may be generated in the reactor.

The reaction from carbomium ion can be classified to:

1. Isomerization to a more stable carbonium ion through a methyl shift:

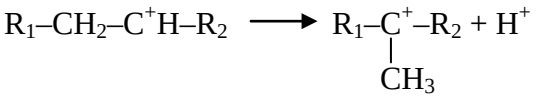

(1)

2. Oligomerization with olefin in a bimolecular reaction to form a larger adsorbed carbonium ion:

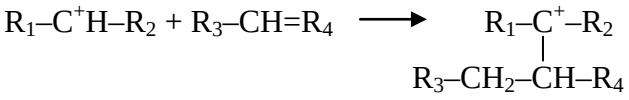

(2)

3. Desorption with deprotonation to form an olefin (the opposite of adsorption):

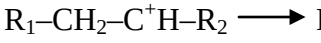

(3)

4. Desorption with hydride abstraction from a paraffin to form new paraffin (H-transfer reaction):

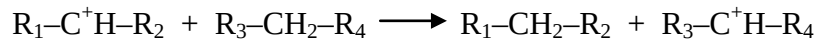

(4)

5. Desorption with hydride abstraction from (cyclic) olefins or coke (precursors) to form paraffin and a more aromatic compound (H-transfer reaction):

(5)

The reactions (2), (4) and (5) can occur if the pore size of the catalyst is large enough for the reactive intermediates or they should occur on the external surface of catalyst.

The most important cracking reaction is the carbon-carbon beta bond scission (β-scission). A bond at a position beta to the positive-charged carbon breaks heterolytically, yielding olefin and another carbonium ion.

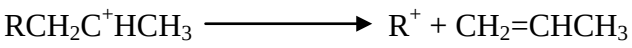

Another β-scission can occur with the new carbonium ion, rearrange to a more stable carbonium ion, react with a hydrocarbon molecule in the mixture, and produce paraffin. It may also occur on either side of the carbonium ion. For example, cracking of secondary carbonium ion from long chain paraffin could be represented as follows:

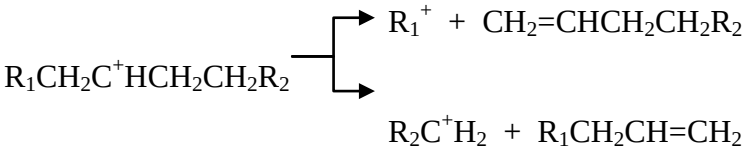

Aromatization of paraffins can occur through a dehydrocyclization reaction. Olefinic compounds formed by the beta scission can form a carbonium ion intermediate with the configuration conductive to cyclization. During the cracking process, fragmentation of polynuclear cyclic compounds may occur, leading to formation of simple cycloparaffins. These compounds can be a source of C_6, C_7 and C_8 aromatics through isomerization and hydrogen transfer reactions.

Coke formed on the catalyst surface is thought to be due to polycondensation of aromatic nuclei. The reaction can occur through a carbonium ion intermediate of benzene ring. The polynuclear aromatic structure has a high C/H ratio.

1.4.6 Hydrocracking

Hydrocracking is a thermal process (>350°C) in which hydrogenation accompanies cracking. Relatively high pressure (100-200 psi) is employed and the overall result is a change in character or quality of the products [15]. The products are combined between the catalytic cracking products and the hydrogenation products. The hydrocracking reaction is catalyzed by dual-function catalysts: the cracking function provided by acid catalyst and metal catalyst gives hydrogenation function.

The mechanism proceeds through initial reactions of catalytic cracking occur, but some of the secondary reactions are inhibited by the presence of hydrogen. The methyl groups attached to secondary carbons are more easily removed than those

attached to tertiary carbon atoms, whereas methyl groups attached to quaternary carbons are the most resistant to hydrocracking.

The effect of hydrogen on naphthenic hydrocarbon is ring scission followed by immediate saturation of each end of the fragment produced. The ring is preferentially broken at favored positions, although all the C-C bond positions are attached to some extent. Aromatic hydrocarbons are resistant to hydrogenation under mild conditions, but under more severe conditions the main reactions are conversion of aromatics to naphthenic rings and scissions within the alkyl side chains. Naphthenes may also be converted to paraffins. Polynuclear aromatics are more readily attacked than the single-ring compounds. The reaction proceeds by a stepwise process in which one ring at a time is saturated and opened.

1.5 Catalyst

The products from pure thermal degradation show a wide range of carbon numbers. That requires further process for improving its quality [16]. The catalytic cracking and hydrocracking allow the reaction to be performed at lower temperature. The selectivity and distribution of product can be controlled by a right selection of catalyst type as well as the rate of reaction is modified by the catalyst. The most well known catalyst is zeolite, one type of catalytic porous materials. Porous materials are defined for a set of pores embedded in a matrix of mostly solid material. The pores are voids in the material itself, which can be isolated or interconnected. Porous materials can be classified according to the IUPAC definitions into three main types depending on their pore size [17] as summarized in Table 1.1.

Table 1.1 IUPAC Classification of porous materials

Type of material	Pore size (Å)	Examples
Micropores	< 20	zeolites, activated carbon
Mesopores	20 – 500	M41s, SBA-15, pillared clays
Macropores	> 500	glasses

1.5.1 Zeolite

Zeolites are porous materials [18-19], which can apply for catalytic applications such as oil refining (as cracking catalysts and as adsorbents), petrochemical industry, and synthesis of chemicals. Because zeolites provide high activities and selectivities, they become the important material on catalytic cracking as a catalyst to support the breaking down of large hydrocarbon molecules into smaller ones at temperature around 400-500°C.

Zeolites [20], a type of molecular sieves, are crystalline aluminosilicate of alkali and alkaline earth metals. Zeolites occur in nature and are obtained by synthesis. Their structures are “framework” which is an extensive three-dimensional network that built up from connection of tetrahedral $[SiO_4]^{4-}$ linkage. The replacement of aluminium for silicon gives the tetrahedral $[AlO_4]^{5-}$, introducing excess negative charge in the framework structure which is strongly acidic [21]. This charge is balanced by inorganic or organic cations located in channels or cages of the framework, extra-framework positions. The charge-balancing cations are usally mobile and undergo ion-exchange. Chemically, zeolites are represented by the empirical formular:

$$M_{x/n}\,[(AlO_2)_x\,(SiO_2)_y].\ w\ H_2O$$

Where M is the exchangeable cations of valence n, usually from the group I or II ions, although other metals, nonmetals, and organic cations are also possible and n represents the cation oxide state. The value of x is equal to or greater than 1 because Al^{3+} does not occupy adjacent tetrahedral sites, otherwise it results in the negative charged units next to each other, and w is the number of water molecules. Water molecules inhabit in the channels and cavities, as the cations that neutralize the negative charge created by the presence of the AlO_2^- tetrahedral unit in the structure. The sum (x+y) is the total number of tetrahedral in the unit cell. The position, [ ], represents the framework composition. The structure of zeolite is shown in Figure 1.7.

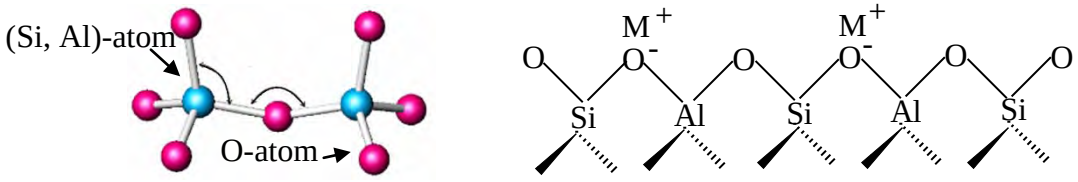

Figure 1.7 The structure of zeolites.

Zeolites are classified according to the structural parameter which is the size of pore opening where molecules diffuse into. The pore size is related to the ring size defined as the numbers of $(Al,Si)O_4$ tetrahedral linked together to form secondary building units (SBUs) [22]. There are three pore openings in the zeolite system: the small (8-member ring), medium (10-member ring), and large (12-member ring) pores. The porosity and shape selectivity are very important for zeolite catalyst because it is related to the diffusion ability. Shape selectivity in zeolites has been divided into three categories: reactant shape selectivity, product shape selectivity, and transition state shape selectivity. These are depicted in Figure 1.8. One type of molecules will react preferential and selectively in a shape-selective catalyst if they can diffuse through the pore, while large molecules will be absolutely unable to diffuse through the pores and only react on the external non-selective surface of zeolite [23]. The product molecules from high diffusively reactants are deformable and pass through opening, which are smaller than their critical diameters, are higher than the bulky. Hence, not only size but also the dynamics and structure of the molecules must be taken into account.

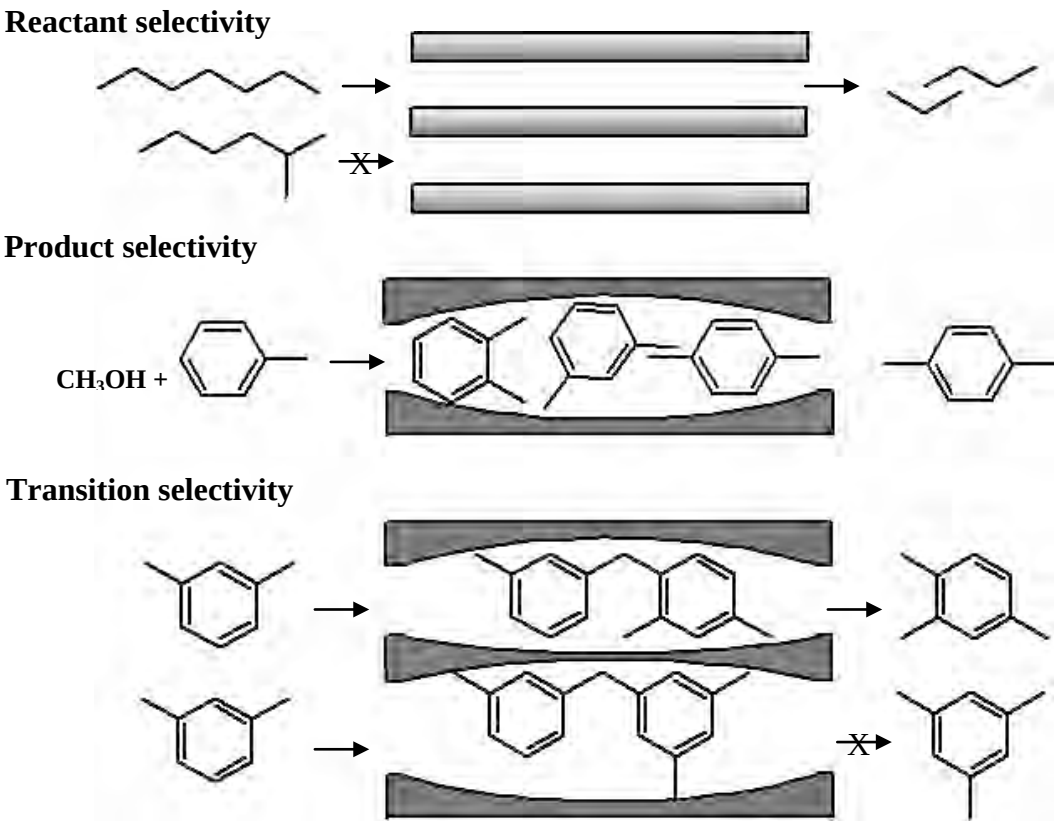

Figure 1.8 Diagram depicting three types of selectivity [20].

The catalytic abilities of zeolites can be attributed to their superior properties, in comparison with other types of materials, which are the combination of high internal surface area, high acidity, selective sorption, molecular sieve properties, and ion exchange. High internal surface area and acidity give rise to high activity, while high selective sorption capacity and molecular sieve properties result in high reaction selectivity. If the cationic charge-balances are exchanged to H^+, they can have a very high number of strong acid sites which related to high activity [24].

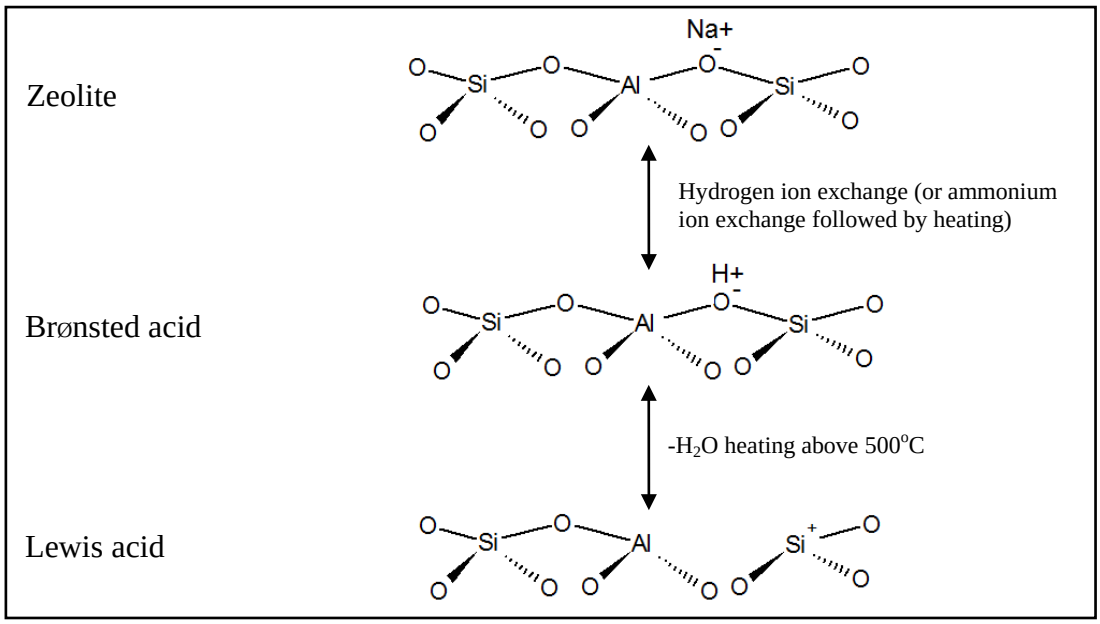

Figure 1.9 The generation of Brønsted and Lewis acid sites of zeolites.

Most industrial applications of zeolites, such as the cracking reaction, are based on acidity of catalysts. This means that the activity of catalyst is depended on the number of acid sites arising from the hydroxyls within the zeolites pore structure. These hydroxyls are generated by ammonium exchange followed by a calcination step. Normally, synthesized zeolites usually have Na^+ balancing the framework charges, but these Na^+ ions can be readily exchanged for proton by direct reaction with an acid, giving hydroxyl groups, the Brønsted acid sites. If the zeolite is not stable in acid solution, it is common to use ammonium compounds such as NH_4OH, NH_4Cl or NH_4NO_3 and then heat it for eliminating ammonia, and leaving a proton. Thus Brønsted acidity is at the proton donor site. When Brønsted sites are dehydrated by heating, tricoordinated Al ion is obtained and identified as a Lewis acid site. That

means Brønsted sites are converted into Lewis sites which is electron-pair acceptor property at the temperature is over 500°C, and water is driven off. The formation of these sites is shown in Figure 1.9. Hence the surfaces of zeolites can display both types of acid.

In the cracking process, both Lewis and Brønsted acid sites can promote carbonium ion formation. The following reactions illustrate different ways by which carbonium ions may be generated in the reactor:

1. Abstraction of a hydride ion by Lewis acid site from a hydrocarbon

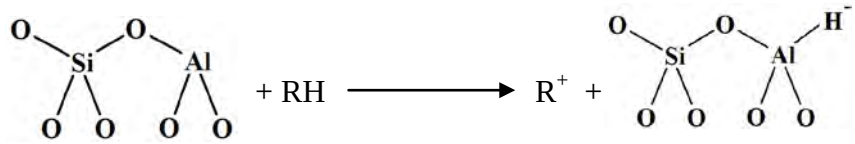

Lewis acid site

2. Reaction between a Brønsted acid site (H^+) and an olefin

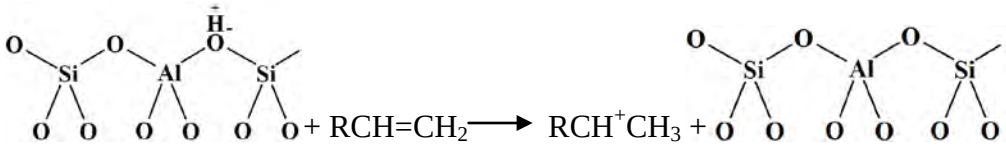

Brønsted acid site

3. Reaction of a carbonium ion formed from step 1 or 2 with another hydrocarbon by abstraction of a hydride ion

$$R^+ + RCH_2CH_3 \longrightarrow RH + RCH^+CH_3$$

Abstraction of a hydride ion from a tertiary carbon is easier than from a secondary carbon, which is easier than from a primary position. The formed carbonium ion can rearrange through a methyl-hydride shift similar to what has been explained in catalytic reforming. This isomerization reaction is responsible for a high ratio of branched isomers in the products.

1.5.2 Zeolite Synthesis

In general, zeolites are synthesized by a hydrothermal method in a closed cylindrical vessel, called an autoclave [25]. The zeolites are generated from a silica

source (*e.g.* a silica sol, fumed silica, or sodium water glass) and an alumina source (*e.g.* sodium aluminate or aluminium sulfate) and an alkali such as NaOH, and/or a quaternary ammonium compound which acts as a directing agent or template. These species are well suited for the preparation of homogeneous mixture in water that results in aluminosilicate gel. The gel is gradually crystallized in an autoclave at the optimal temperature under autogeneous pressure, which approximately equivalent to the saturated vapor pressure of water at the crystallized temperature. The crystallization time varies from a few hours to several days. The aluminosilicate gel is formed by copolymerization of silicate and aluminate species *via* a condensation mechanism. The gel composition and zeolite structure are controlled by size and structure of polymerizing species. In some cases, more than one type of zeolite is formed in succession. The type of zeolite and its property depended on three important variables: gross composition, reactant mixture components, temperature and time of crystallization. There are also some other factors such as stirring, nature (either physical or chemical) of reaction, and the order of mixing. These factors are called history-dependent factors. The synthesis method is shown in Scheme 1.1.

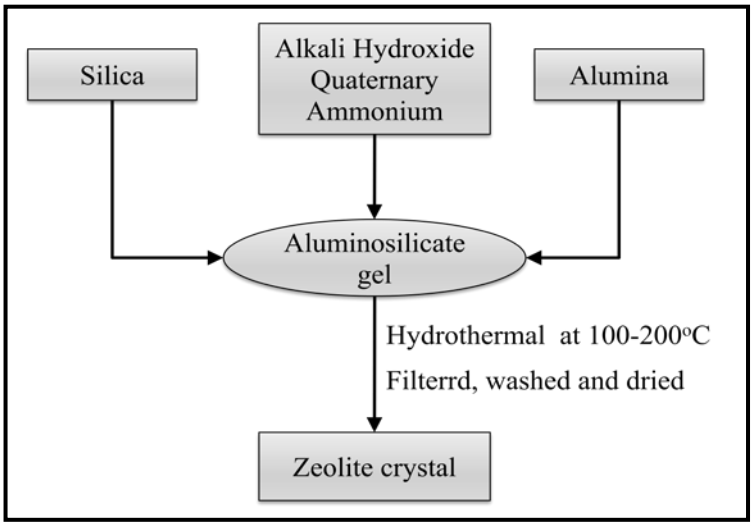

Scheme 1.1 The formation of zeolite by hydrothermal method.

Each component in reaction mixture, the SiO_2/Al_2O_3 mole ratio, the hydroxide content of gel, and the presence of inorganic cation, also contribute to specific characteristic of gel and to the structure of final material obtained besides the

organic additives as crystal-directing agent or template [26]. Temperature of crystallization influences zeolite phase and crystallization time. The crystallization period decreases with increasing temperature and the condition may favor the formation of other phases. For some mixtures when the temperature increases, the rate of crystallization increases. The high porous zeolites prefer crystallization at lower temperature while lower porosity zeolites do at higher temperature [27]. The crystallization parameters must be adjusted to produce only one zeolite phase, whereas maximum crystallization under minimal crystallization time.

After synthesis, zeolite are washed to remove water, dried, and calcined in air, *e.g.*, at 550°C to eliminate organic species. For most catalytic properties, the zeolite is converted into acidic form.

The synthetic zeolites fall into two families on the basis of extra-framework species. One family is similar to natural zeolite in the chemical compositions. These zeolites have low Si/Al ratio (less than 5). The other family of zeolites is made with organic structure-directing agent and have a Si/Al ratio larger than 5. There are several types of zeolite which were used as catalyst in catalytic cracking, such as ZSM-5, zeolite Y and zeolite beta.

1.5.3 Zeolite Beta

Zeolite beta is a large pore zeolite. It is known that the crystal size of zeolite catalyst can influence the reaction activity and selectivity [28]. Zeolite beta has been used as a cracking catalyst for higher production of olefins, as well as in the catalyst stability by increasing the crystallite size.

Structure and properties of zeolite beta

In 1967, zeolite beta with high silica (Si/Al>5) [29] was first synthesized by Wadlinger *et al.* [30] and using tetraethylammonium hydroxide as the organic template. The use of organic bases has a significant impact on development of high silica zeolite but the structure is very complex. The unit cell composition of zeolite beta is:

$$(TEA, Na)_n[(AlO_2)_n(SiO_2)_{64-n}]$$

Zeolite beta exhibits characteristic properties of the 12-membered ring, shown in Figure 1.10, connecting together in three dimensional channel system. There are two different types of channels: straight channel (100) and sinusoidal channel (001) [31-32]. These are shown in Figure 1.11.

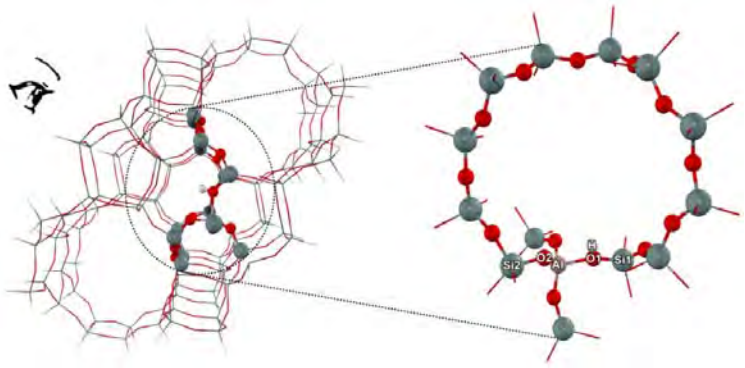

Figure 1.10 The ball-and-stick graphics represent the active region 14T including the main gateway to the intersection of zeolite beta (12-membered-ring) [33]

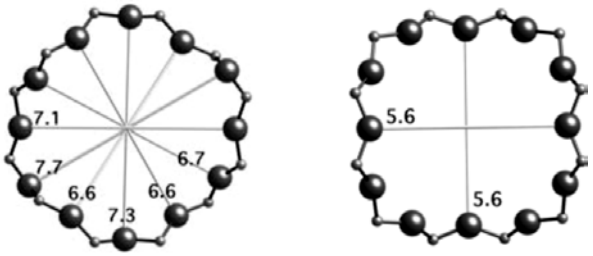

(a) (b)

Figure 1.11 The 12-ring viewed along (a) (100) plane and (b) (001) plane [34]

Their structures consist of intergrowth hybrid of two distinct structures termed Polymorphs A and B. These polymorphs grow in two dimensional sheets which randomly alternate in their structures. The smaller building units are double six-ring units connected by two four-ring and four, five-ring units. These are connected to form chains along the [001] direction, shown in Figure 1.12 [31]. The two polymorphs of zeolite beta, demonstrated in Figure 1.13, show only the T-atom positions (for simplicity) [35]. The oxygen atoms have been omitted for clarity.

1. Polymorph A: tetragonal crystal system, two different pore opening dimensions: 0.60x0.56 nm and 0.68x0.73 nm, there is arranged in an ABABAB. . . type configuration.

2. Polymorph B: monoclinic crystal system, two different pore opening dimensions:0.68x0.55 nm and 0.68x0.73 nm, there is arranged in an ABCABC. . . type configuration

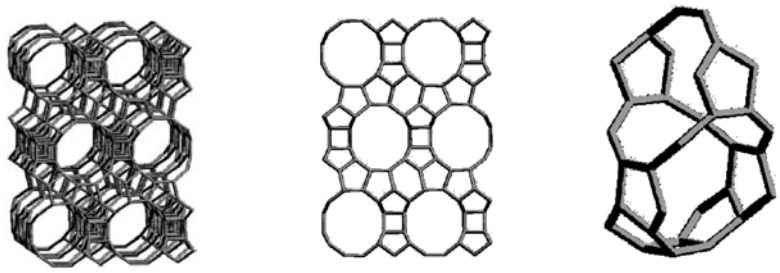

(a) (b) (c)

Figure 1.12 The framework of zeolite beta (a) view along [100] direction (b) projection viewed along [100] direction and (c) channel intersection viewed normal to [001] direction.

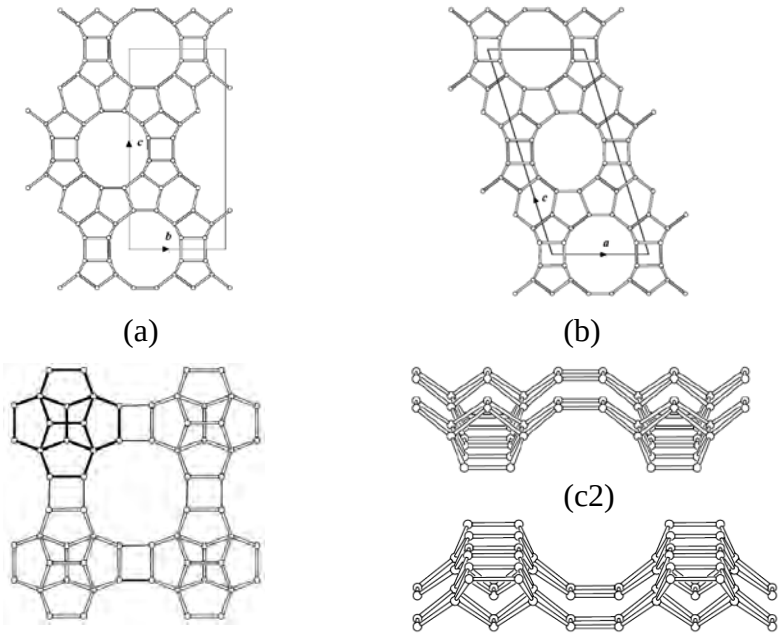

(a) (b)

(c2)

(c1) (c3)

Figure 1.13 Frameworks of (a) polymorph A, (b) polymorph B of zeolite beta and (c1) a layer or periodic building unit (PBU) of the beta family of structure types, the tetragonal beta layer, is composed of T16 units (in bold). The layers depicted in parallel projection (c2) and in perspective view (c3).

Zeolite beta was suggested as an active catalyst and a useful sorbent [30] because of its strong acidic property and pore system. The great potentials have taken for the catalytic cracking of aromatic, isobutane alkylation with n-butene, disproportionation of hydrocarbons, and isomerization [36]. Since zeolite beta combines three important characteristics: large pore (12 oxygen member rings), high silica to alumina ratio and three dimension network or pores, it can give a certain level of shape selectivity, high thermal and chemical stability.

1.6 Mesoporous Material

Even though zeolite beta is well-defined large microporosity, high hydrothermal stability and intrinsic acidity, it cannot be applied for treating the relatively large molecules presented in heavy fuel oils [37]. Thus, in 1992 scientists at Mobil Oil Research and Development announced the synthesis of the first broad family of mesoporous molecular sieves (denoted M41S) [38-39]. In contrast to zeolites which are synthesized with single, solvated organic molecules or metal ions as the template, supramolecular arrangements of molecules are used for the synthesis of M41S. One of them is MCM-41. The materials exhibit large specific surface areas, large pore volumes and pore size. These mesopore materials are of great interest for application in size- and shape- selective processes, *e.g.*, catalyst supports, adsorbents, or host structures for nanometer-sized guest compounds [40]. Unfortunately, the pore walls are not crystalline, but amorphous. Recently, there are many families of mesoporous materials, such as HMS (Hexagonal Mesoporous Silica) and SBA-15, with straight hexagonal structure by using different types of templates and verifying pH of gel. Comparison in inorganic materials the type of interaction between template and inorganic species and synthesis conditions of mesoporous structured is summarized in Table 1.2.

MCM-41 can be synthesized using quaternary ammonium salt as a template. SBA-15 can be synthesized by using amphiphilic tribock copolymer as a template in acid condition of hydrochloric acid. In case of HMS, it can be prepared in neutral and environmentally benign condition using primary amine as a template. Although these materials have the same hexagonal structure, some properties are different as shown in Table 1.3.

Table 1.2 Comparison in inorganic materials the type of interaction between template and inorganic species and synthesis conditions of mesoporous structured

Material	Template	Assembly	Media (pH)
MCM-41	Quaternary ammonium salt	Electrostatic	Basic or Acid
SBA-15	Amphiphilic triblock copolymer	Hydrogen bonding	Acid (pH = 1-2)
HMS	Primary amine	Hydrogen bonding	Neutral

Table 1.3 Properties of some hexagonal mesoporous materials [41]

Material	Pore size (Å)	Wall thickness (nm)	BET specific surface area (m^2/g)	Framework structure
MCM-41	15-100	1	>1000	Honey comb
SBA-15	46-300	3-6	630-1000	Rope-like
HMS	29-41	1-2	640-1000	Wormhole

Since mesoporous catalysts are higher accessibility of reactants as compared to zeolites, they are suitable catalyst for large size molecules cracking. Nevertheless, these materials have lower acidity and hydrothermal stability because of their amorphous nature of frameworks, which limit their use as catalysts in a wide range of industrial processes and reactions. Thus metal ions can be substituted for silica in pure silica mesoporous material to yield acidic materials. Many trivalent ions like Al^{3+}, B^{3+}, Ga^{3+}, Fe^{3+}, *etc.*, can be substituted into the structures. It is well-known that when metal ion is substituted into silicate structure, the negative charges of material can be balanced with proton and generates Brønsted acidity [42]. However the increased acidity of mesoporous material is still slightly lower than zeolite.

HMS is similar to MCM-41 with respect to high surface area and uniform mesoporous channels, but it possesses only short-range hexagonal symmetry. HMS

usually has thicker framework walls (1-2 nm) compared with MCM-41 (ca. 1 nm) that lead HMS to better thermal, hydrothermal, and mechanical stability [43] and greater attention for catalytic applications. Furthermore, the structure of HMS may provide better transport channels for reactants to access the active centers than MCM-41. The neutral templating route of HMS also has several advantages over the cationic templating route [44]. The synthesis is performed at room temperature, and Al is incorporated into the resulting material in proportions depending on Si/Al ratio of the reactant gel. Furthermore, Brønsted acid sites are directly generated by calcining the as-synthesized Al-HMS without the need of ammonium exchange. Mokaya and Jones [44] found that directly calcined Al-HMS with Si/Al ratio of 5 possessed acid sites very similar in strength to HY zeolite.

1.7 Hexagonal Mesoporous Silica (HMS)

HMS was firstly reported by Pinnavaia *et al.* [45] in 1994. It is a kind of mesoporous molecular sieves with wormholelike framework structure generated by a neutral templating route through hydrogen bonding pathway. This pathway is an interaction between neutral primary alkylamine and natural inoganic precursor at room temperature. The primary amine was used as structure directing agent or template, water and alcohol such as ethanol or propanol was used as solvent and co-solvent to improve template solubility, respectively, and silica was an inorganic precursor.

A hydrophobic alkyl chain length between C_8-C_{18} in primary amine templates can control pore size of HMS [46] and also modified auxiliary structure such as mesitylene is used to expand the pore of HMS. After template-directed synthesis procedure, the after-treatment process is needed to remove the surfactant template. Two methods normally used to remove surfactant templates are calcination and solvent extraction. Mesoporous materials generated through the charge-matching pathway, which were strong electrostatic interactions between organic and inorganic phase, mainly depend on calcination method to remove the templates, while materials generated through the hydrogen bonding pathways can rely on both methods. Calcination is widely adopted for its simplicity and efficiency, whereas noncorrosive solvent extraction possesses the outstanding advantages of surfactant recovery and

environmental friendliness [45]. Owing to the weak hydrogen bonding interactions, more than 90% of the neutral template can be recovered by a simple extraction procedure using ethanol [45] or acidified water [47] as extracting solvent, which is not possible in the case of the other pathways. The solvent extraction can be prevented the partial degradation of the mesoporous structure that could occur during calcinations in air at a relatively high temperature. Besides the mild synthesis condition of HMS and the non-polluted extracted template, there are many advantages of HMS motivated researchers to study its applications, for example [48] large surface area up to 900–1000 m^2g^{-1}, narrow pore size distribution of 3–4 nm and slightly less ordered structure. Furthermore, Brønsted acid sites are generated directly by calcining the as-synthesized Al-HMS without the need for ammonium exchange.

In recent years, there was investigation of synthesizing zeolite beta prepared from MCM-41[49]. The zeolite beta showed large pore diameter and pore volume and also kept acidity advantage of microporous. Thus, this work is interested on the synthesis of enlarged-pore zeolite beta prepared from Si-HMS. Because Si-HMS can be prepared in mild condition and spent less time to synthesize than MCM-41.

1.8 Literatures Review

In 2000, Aguado *et al.* [50] studied the catalytic of polyolefins cracking over zeolite beta at temperature of 400°C for 0.5 h. Zeolite beta was synthesized by fluoride method, hydrothermal method and amorfhous xerogel method. They found that zeolite beta which synthesized by amorphous xerogels method has small crystallites (<200 nm) and allows polyolefins to be degradated to fuel oil around 40-60% of conversion and 60-70% of selectivity towards C_5-C_{12} hydrocarbons. In contrast, zeolite beta which synthesized by the fluoride method has low activity for the cracking of polyolefins because of its large crystal size (12 mm) and poor aluminium incorporation.

In 2008, Groen *et al.* [51] synthesized composite zeolite beta by using fluoride method and alkaline post treatment in NaOH solution to extract silicon from the framework (desilication). The obtained desilicated zeolite beta has mesoporous surface area up to 370 m^2g^{-1} which larger than desilicated ZSM-5 and mordenite

(MOR) zeolite. However, the stability, crystallinity and micropore volume of desilicated zeolite beta was decreased. The activity of benzene alkylation with ethylene over desilicated zeolite beta decreased when compared to the untreated zeolite beta because the alkali treatment reduced the acidic properties associated with tetrahedrally coordinated aluminum in the zeolite beta.

In 2001, Guo *et al.* [52] synthesized zeolite beta/MCM-41 composite material through a two-step crystallization process. The first step was a synthesis of low crystallinity zeolite beta gel by controlling the crystallization time. Then the gel was added to surfactant cetyltrimethylammonium bromide (CTAB) in the second step. The gel condenses around the CTAB leading to the mesoporous wall of the composite. The zeolite beta/MCM-41 composite was compared with a mechanical mixture of zeolite beta and MCM-41. They found that the crystallinity and pore volume of the synthesized composite is larger than that of the mechanical mixture. The composite had more medium and strong Brønsted acid sites and showed better catalytic activity for *n*-heptane.

In 2006, Chen *et al.* [49] synthesized zeolite beta which made from mesoporous material by using mesoporous material, MCM-41, ammonium hydroxide and tetraethylammonium hydroxide (TEAOH) as silicon source, alumina source and directing agent, respectively. The zeolite beta was crystallized at the temperature of 140°C for 3 days by the hydrothermal method in an autoclave. The obtained zeolite beta was tested for catalytic properties on hydrothermal process of heavy oil comparing with zeolite beta prepared by using tetraethyl orthosilicate (TEOS) as silica source. The zeolite beta made from MCM-41 showed larger pore diameter and pore volume than the zeolite beta made from TEOS, and kept acidity advantage of microporous. Thus, it allowed large molecule in heavy feed oil to be degradated and more selective toward middle distillate oil, C_{10}-C_{16} hydrocarbons. Smaller unsaturated hydrocarbons products (C_2-C_5 olefin) were decreased.

In 1992, Beck *et al.* [38] explained the formation of silicate and aluminosilicate mesoporous molecular sieves, MCM-41. They found that low surfactant

concentrations gave a disordered structure; for all that, the ordered structure rapidly increased with increasing surfactant concentrations. With increasing the surfactant concentration, the hexagonal structure became progressively more disordered and wormhole-like structures were obtained. At the maximum surfactant concentration, the order of the mesoporous silica structure decreased.

In 2009, Van *et al*. [53] investigated the influence of cooling rate on the formation of the composite materials using zeolite beta nanoparticle seeds to form the mesopores. They found that the effect of the cooling rate on the nanoparticle seeds, after aging at high temperature, led to differences in porosity and crysrallinity of zeolite. A rapid quenching showed larger pore diameters and volumes in comparison with the composite material from slow cooling rate. Nevertheless, the mesoporous structure via slow cooling rate was more uniform, high aluminium content and better zeolitic characteristics.

In 2001, Cassiers *et al*. [54] studied a wide range of ordered mesoporous materials, in particular, MCM-41, MCM-48, HMS, FSM- 16, and SBA-15. They found that thermal stability was strongly related to the wall thickness and the silica precursor used during synthesis. The trend of stability was observed: MCM-41 (fumed silica), MCM-48 (fumed silica) > SBA-15 (TEOS) > FSM-16 (layered silicate) > HMS (TEOS), MCM-41 (TEOS), MCM-48 (TEOS). For the hydrothermal stability, it was influenced by wall thickness. By comparing hexagonal mesostructures with similar wall thicknesses, the following stability trend was observed: MCM-41 (fumed silica) > FSM16 (layered silicate) > HMS (TEOS), MCM-41 (TEOS). The mechanical stability was little influenced by the nature of the mesoporous molecular sieves.

In 2006, Li *et al.* [55] synthesized mesoporous ZSM-12 by desilication in alkaline treatment. The mesopore size and volume can be controlled to a certain extent by varying alkali concentration, treatment time and temperature. The concentration of NaOH solution was found to be the most dominant factor affecting the desilication process. They found that the content of tetrahedrally coordinated aluminum in the

zeolite frame work also controls the formation of mesopores by facilitating desilication process in alkaline medium. The ZSM-12 with relatively low Si/Al ratios, relatively high NaOH concentration was favorable for the generation of mesopores while preserving the microporous structure and acidic property of ZSM-12 while the samples with higher Si/Al ratios, lower NaOH concentrations favored the creation of mesopores. They also found that an as-synthesized ZSM-12 sample is much more difficult to be desilicated than calcined ZSM-12 samples of comparable Si/Al ratios due to hindering the interaction of hydroxide species (base) with Si–O–Si linkages.

In 2009, Loiha *et al.* [56] synthesized zeolite beta preparing from rice husk by acid leaching and used as a silica source under hydrothermal method at 135 °C and completed by crystallization for 3 days with various gel Si/Al ratios. They found that samples with gel Si/Al ratios of 8 to 20 contained only the pure phase of beta while the samples with gel Si/Al ratios ranging from 50 to 200 showed mixed phases of Beta and ZSM-12. The phase of ZSM-12 became more significant with a higher Si/Al ratio and was almost pure at the ratio of 200.

1.9 Objectives

1. To synthesize the enlarged-pore zeolite beta.
2. To study properties of the enlarged-pore zeolite beta.
3. To investigate the efficiency of enlarged-pore zeolite beta catalysts for cracking of heavy fuel oil upgrading.
4. To study the activity of regenerated enlarged-pore zeolite beta catalysts.

CHAPTER II

EXPERIMENTAL

2.1 Instruments, Apparatus and Analytical Techniques

Oven and furnace

Memmert UM-500 oven was used for hydrothermal process of zeolite beta and enlarged-pore zeolite beta at various crystallization temperature and time. It was also used for drying the catalysts at 110°C. Carbolite RHF 1600 muffle furnace was used for calcination to remove moisture and organic templates from the catalyst. As-synthesized zeolite beta was heated to 100°C with a heating rate of 1°C/min and dwelled at 100°C for an hour. After that the temperature was raised up 550°C with the same heating rate and dwelled at that temperature for 5 h. As-synthesized enlarged-pore zeolite beta was calcined at 100°C for 1 h and 550°C for 10 h with the heating rate of 1°C/min which similar to as-synthesized Si-HMS. After calcination, as-synthesized of zeolite beta, enlarged-pore zeolite beta and Si-HMS were named as calcined zeolite beta, calcined enlarged-pore zeolite beta and calcined Si-HMS. The heating programs of zeolite beta, enlarged-pore zeolite beta and Si-HMS are shown in Schemes 2.1 and 2.2, respectively.

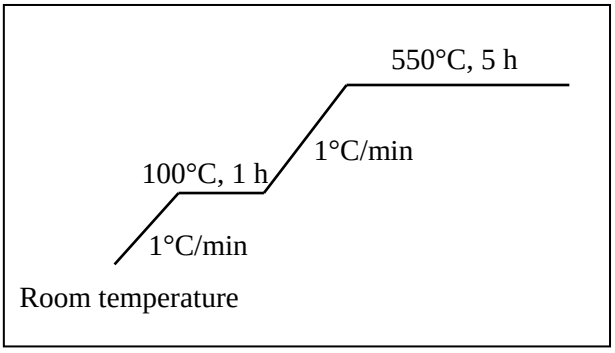

Scheme 2.1 The heating program of zeolite beta.

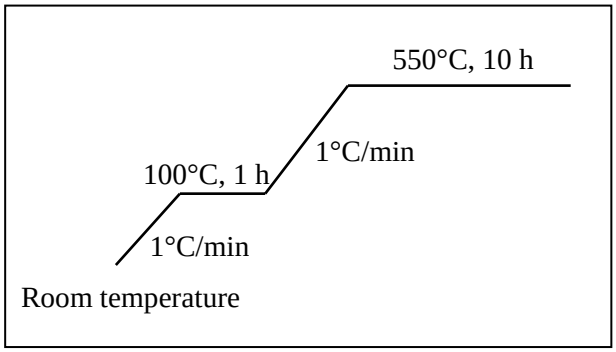

Scheme 2.2 The heating program of enlarged-pore zeolite beta and Si-HMS.

Powder X-ray Diffraction (XRD)

The X-ray diffraction patterns of as-synthesized and calcined of Si-HMS, zeolite beta and enlarged-pore zeolite beta were measured. The powder samples were placed on a holder and X-ray diffraction measurements were carried out by a Rigaku, Dmax 2200/Ultima^{+} diffractometer using a monochromator and Cu Kα radiation. The tube voltage and current were set at 40 kV and 30 mA, respectively. XRD patterns were collected in the 2-theta ranging from 5 to 50 degree with scan speed of 5 degree min^{-1} for zeolite beta and from 1.2 to 10 degree with scan speed of 2 degree min^{-1} for Si-HMS. For zeolite beta, enlarged zeolite beta and Si-HMS, the scattering slit, divergent slit, and receiving slit, were fixed at 0.5 degree, 0.5 degree, and 0.15 mm, respectively.

Scanning Electron Microscopy (SEM)

The morphology and particles size of calcined prepared Si-HMS, zeolite beta and enlarged-pore zeolite beta samples were determined by scanning electron microscope. The sample must be mounted on the stub (metal holder) by a mounting medium (carbon tape) and coated with gold for conductivity. The SEM micrographs of samples were obtained on JSM-5410 LV scanning electron microscope with 15 kV of acceleration voltage.

Nitrogen Adsorption-Desorption Technique

Nitrogen adsorption-desorption isotherm measurements were carried out using a BEL Japan BELSORP-mini 28SP adsorptometer for characterization of catalyst

porosity in terms of nitrogen adsorption-desorption isotherms, BET specific area, external surface area and pore size distribution of catalysts. Before analysis each calcined sample was weighed to approximately 40 mg and degassed at 400°C for 3 h under vacuum. Adsorption isotherms were measured at 77 K (liquid nitrogen) using nitrogen of 99.999% purity as an adsorbate. The analyses were performed at the Department of Chemistry, Faculty of Science, Chulalongkorn University.

Inductively Coupled Plasma Atomic Emission Spectrometry

Aluminum contents in the catalysts were analyzed using the Perkin Elmer Plasma-1000 inductively coupled plasma-atomic emission spectrometer (ICP-AES) at Scientific and Technology Research Equipment Centre, Chulalongkorn University.

^{27}Al MAS Nuclear Magnetic Resonance Spectroscopy

The signal of aluminum tetrahedral in catalysts was measured by ^{27}Al-magnetic angle spinning nuclear magnetic resonance (^{27}Al MAS NMR, Bruker DPX-300 spectroscopy operating at 78 MHz) at National Metal and Materials Technology Center, Pathumthani.

Gas Chromatography

Hydrocarbon gases from cracking processes were analyzed by a Varian CP 3800 gas chromatograph equipped with a 0.53 mm inner diameter and 50 m length of Alumina-PLOT column and a flame ionization detector (FID) detector. The column temperature was started at 35°C and maintained for 5 min. Then the temperature was increased to 140°C at a rate of 3°C/min and maintained for 10 min. The total time was 50 min. Liquid products were analyzed using the similar instrument as the gases products but equipped with a 0.25 mm inner diameter and 30 m length of CP-sil 5 column (equivalent to DB-1 column). The column temperature was started at 35°C and maintained for 20 min. Then the temperature was increased to 200°C at a rate of 5°C/min and maintained for 10 min. The total time was 63 min. The volumes of each sample injections are 3.0 μl and 1.0 μl for gas and liquid, respectively. The column heating programs of gas and liquid analysis are shown in Schemes 2.3 and 2.4, respectively.

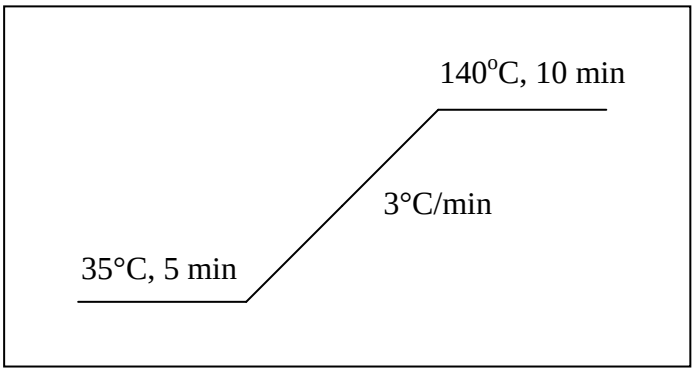

Scheme 2.3 The column heating program for gas analysis.

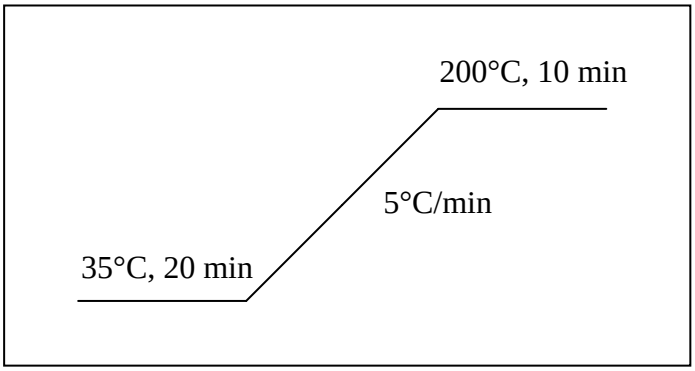

Scheme 2.4 The column heating program for liquid analysis.

2.2 Chemicals and Gases

1. Tetraethyl orthosillicate 98%, TEOS, $C_8H_{20}O_4Si$ (Fluka, reagent grade)
2. Aluminum isopropoxide, AIP, $C_9H_{21}AlO_3$ (Merck, reagent grade)
3. Tetraethylammonium hydroxide, TEAOH, $C_8H_{21}NO_4$ (Fluka, 40 wt%)
4. Hexadecylamine, HDA, $C_{16}H_{35}N$ (Fluka, reagent grade)
5. Hydrochloric acid, HCl, (Merck, 37 wt%)
6. Ethanol, C_2H_5OH (Fluka, reagent grade)
7. Heavy oil grade A was obtain from Shell Co., Ltd.
8. Standard gas mixture for GC analysis was kindly obtained from PTT Chemical Public Company Limited.
9. Standard liquid quantitative calibration mixture for GC analysis (Supelco)
10. Standard gasoline for GC analysis (Supelco)

2.3 Synthesis of Catalysts

2.3.1 Synthesis of Hexagonal Mesoporous Silica (Si-HMS)

Si-HMS synthesis was performed by modifying the procedures reported by Tuel *et al.* [57] and Pauly *et al*. [58]. The gel mole composition of $1SiO_2$: 0.25HDA: 8.3EtOH: $100H_2O$ was prepared by dissolving hexadecylamine (HDA, 0.05 mole), which acted as a directing agent, with the mixed solvent between ethanol (EtOH, 1.66 mole) and water (H_2O, 11.0 mole). The mixture was stirred for 30 min or until it became a homogeneous solution, called HDA-solution. Then tetraethyl orthosilicate (TEOS, 0.2 mole) and water (H_2O, 9.0 mole) were added to the HDA solution in sequence under vigorous stirring for 2 h, the gel was obtained. After ageing for 20 h at room temperature, the white solid product was filtered and washed several times with distilled water to neutral pH value. After the solid was air dried for a day at room temperature, as-synthesized Si-HMS was obtained. The template was removed by calcination of the as-synthesized sample at the temperature of 550°C for 10 h, the calcined Si-HMS was obtained. The synthesis procedure of Si-HMS was shown in Scheme 2.5. The prepared Si-HMS was used as silica source to further synthesize enlarged-pore zeolite beta.

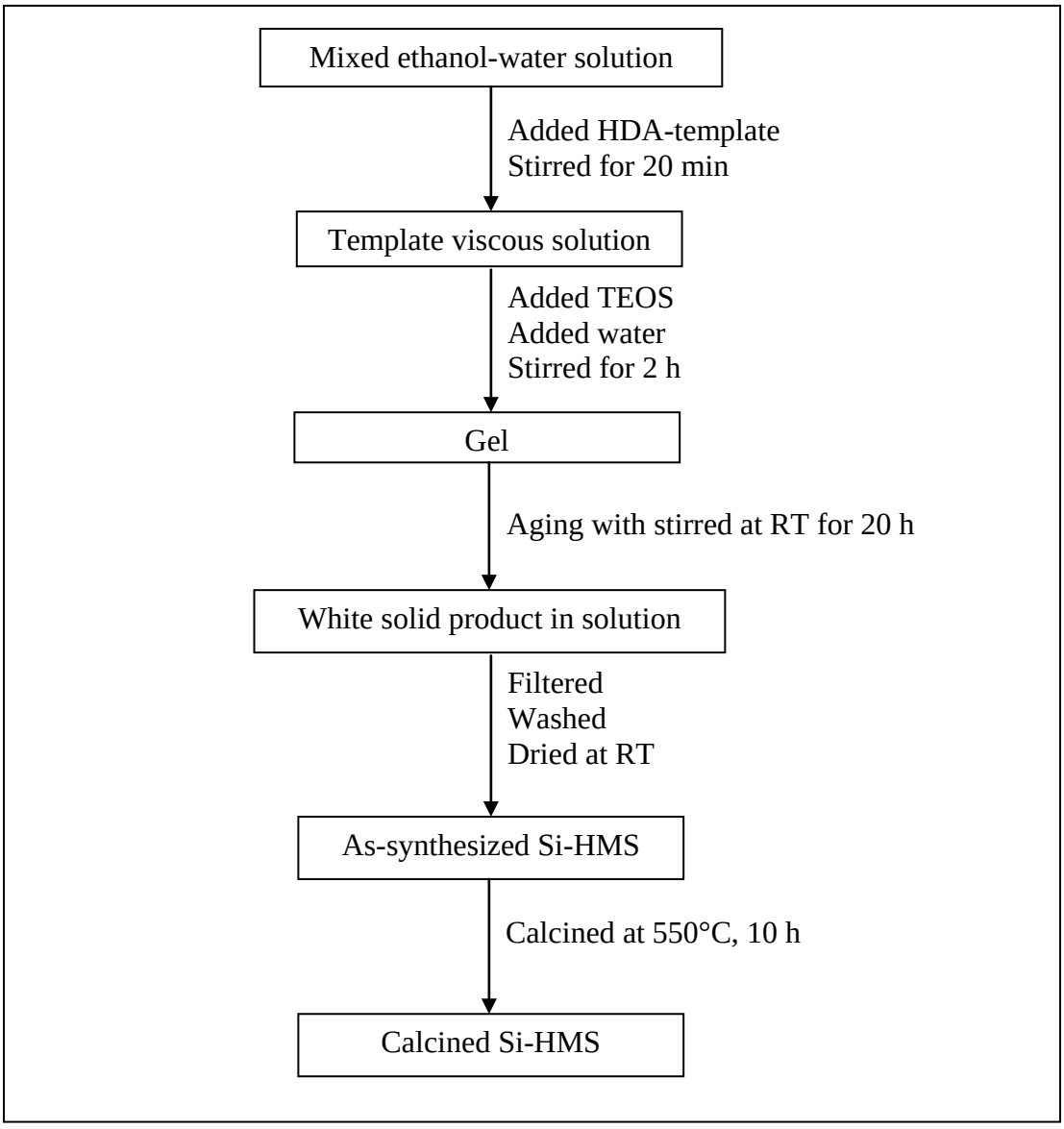

Scheme 2.5 Diagram of Si-HMS synthesis.

2.3.2 Synthesis of Enlarged-Pore Zeolite Beta

The zeolite beta with the Si/Al molar ratio in gel of 60 was prepared by Aguado *et al*. [50] using the gel mole composition of $1SiO_2$: $0.0083Al_2O_3$: 0.37TEAOH: $6.78H_2O$ and the procedure was summarized as follows.

The silica source, TEOS, was hydrolyzed with 0.05 N aqueous HCl ($6.0x10^{-4}$ mole) for 45 min in an ice bath (0°C) until a clear solution was obtained. Then 20%wt TEAOH template solution ($1.17x10^{-2}$ mole) was slowly added into the solution until the gel point was reached. The cogel was dried overnight at 110°C and crushed into powdered materials known as xerogel. Then a clear Al-TEAOH solution, prepared from dissolving isopropoxide (AIP, $1.91x10^{-2}$ mole) in 30%wt TEAOH solution (3.50 mole) at 0°C under a nitrogen atmosphere, was added to xerogel under the same condition and stirred for 18 h to obtain SiO_2-Al_2O_3 gel. The gel was then transferred into Teflon-lined autoclave for crystallization under autogeneous pressure at 135°C for 3 days. The obtained crystals were separated from the solution by centrifugation, washed several times with distilled water to neutral pH value and dried overnight at 110°C, and named as-synthesized zeolite beta (denoted as-synthesized BEA). Then, it was calcined at 550°C for 5 h to obtain calcined zeolite beta (denoted calcined BEA). The procedure was summarized in Scheme 2.6.

The enlarged-pore zeolite beta with Si/Al molar ratio in gel of 60 prepared by modified Aguado method [50] regarding to synthesis parameters. The synthesis parameters *e.g.* silica source, template type and ratio, crystallization temperature and time were investigated as follows.

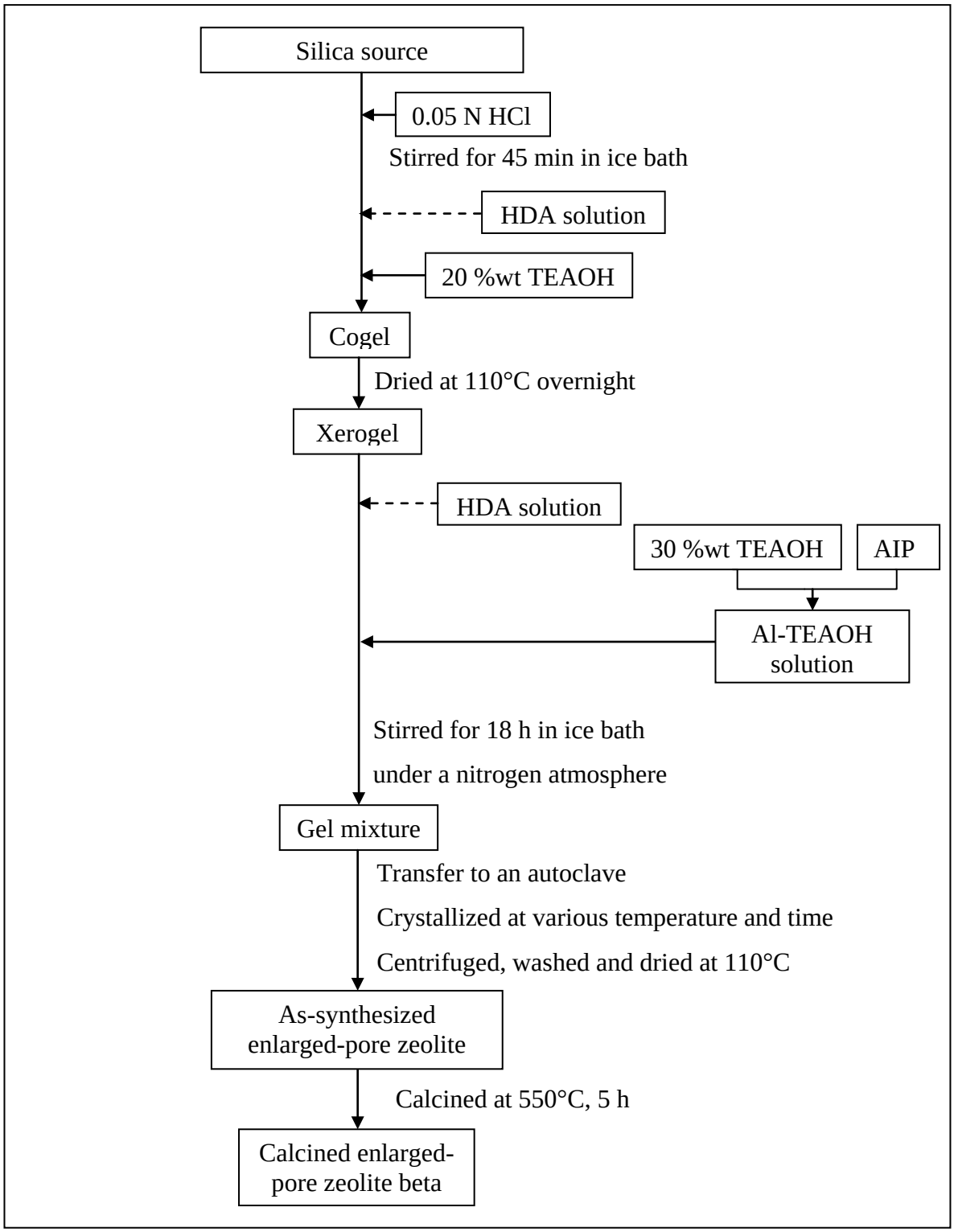

Scheme 2.6 Diagram of zeolite beta and enlarged-pore zeolite beta synthesis.

2.3.2.1.Effect of Silica Source

To investigate the effect of silica source on the synthesis of enlarged-pore zeolite beta, the gel composition of $1SiO_2$: $0.0083Al_2O_3$: 0.375TEAOH: $6.78H_2O$, was prepared from as-synthesized Si-HMS, calcined Si-HMS and TEOS. The synthesis procedure was described in Section 2.3.2. The material gel was crystallized in autoclave at 135°C for 3 days and calcined at 550°C for 5 h in the case of TEOS and 10 h in the case of as-synthesized Si-HMS and calcined Si-HMS. The starting materials of these samples were displayed in Table 2.1.

Table 2.1 Synthesis condition for zeolite beta and enlarged-pore zeolite beta with various silica sources

Sample codes	Si, Al -source	Template	Calcination
BEA	TEOS, AIP	TEAOH	550°C, 5 h
h'-BEA	As-synthesized Si-HMS, AIP	TEAOH	550°C, 10 h
h-BEA	Calcined Si-HMS, AIP	TEAOH	550°C, 10 h

2.3.2.2.Effect of Templates

To investigate the effect of template on the synthesis of enlarged-pore zeolite beta, TEAOH and HDA were used as summarized in Table 2.2. The materials were denoted h-BEA-Mn-T_{crys}-t_{crys}, (where Mn = mixed template, T_{crys} = crystallization temperature and t_{crys}=crystallization time). The synthesized Si-HMS in Section 2.3.2.1 was used as silica source. All gel materials were crystallized in autoclaves at 135°C for 3 days and calcined at 550°C for 10 h. The synthesis method was followed by description in Section 2.3.2.

During synthesis, the HDA solution, which consisted of HDA ($1.17x10^{-2}$ mole), ethanol (0.39 mole) and H_2O (2.57 mole), was added in the first time before addition of 20%wt TEAOH solution. The second time, the HDA solution, which consisted of HDA ($5.83x10^{-2}$ mole), EtOH (1.94 mole) and H_2O (12.83 mole) was

added into xerogel before adding with AIP-TEAOH solution. The procedure was summarized in Scheme 2.6

2.3.2.3.Effect of Crystallization Temperature and Time

To investigate the effect of crystallization temperature and time on the synthesis of enlarged-pore zeolite beta, the gel mole composition of $1SiO_2$: $0.0083Al_2O_3$: 0.315TEAOH: 0.061HDA: 1.69EtOH: $17.95H_2O$ (h-BEA-M4-T_{crys}-t_{crys}) was prepared and placed into autoclaves at different crystallization temperatures: 135, 140 and 145°C for 6, 9, 12 and 15 days. The synthesis method followed description in Section 2.3.2.

Table 2.2 Synthesis condition of enlarged-pore zeolite beta at various types of template and gel mole composition

Sample codes	Si, Al-source	Template	Gel mole Composition
h-BEA-M0-135-3	cal. HMS, AIP	HDA	$1SiO_2$: $0.0083Al_2O_3$: 0.376HDA: 12.48EtOH: $89.45H_2O$
h-BEA-M1-135-3	cal. HMS, AIP	HDA-TEAOH	$1SiO_2$: $0.0083Al_2O_3$: 0.247TEAOH: 0.128HDA: 3.93EtOH: $32.84H_2O$
h-BEA-M2-135-3	cal. HMS, AIP	HDA-TEAOH	$1SiO_2$: $0.0083Al_2O_3$: 0.295TEAOH: 0.081HDA: 2.36EtOH: $22.42H_2O$
h-BEA-M3-135-3	cal. HMS, AIP	HDA-TEAOH	$1SiO_2$: $0.0083Al_2O_3$: 0.315TEAOH: 0.061HDA: 1.69EtOH: $17.95H_2O$
h-BEA-M4-135-3	cal. HMS, AIP	HDA-TEAOH	$1SiO_2$: $0.0083Al_2O_3$: 0.326TEAOH: 0.050HDA:1.32EtOH: $15.46H_2O$
h-BEA	cal. HMS, AIP	TEAOH	$1SiO_2$: $0.0083Al_2O_3$: 0.376TEAOH: $6.78H_2O$

2.4 Elemental Analysis

In the fluoride treatment, 4.00 mg of calcined catalyst samples were digested with 10 ml of conc. HCl in a Teflon beaker then 10 ml of 48% HF was added into the Teflon beaker to get rid off silica in the form of volatile SiF_4. The samples were heated but not boiled until the solution was almost dried on a hot plate. The fluoride treatment was repeated twice. A 10 ml of 6 M HCl and 6 M HNO_3 mixture in the ratio of 1:3 was added slowly into the samples. The samples were warmed until they almost dried again. Then 10 ml of deionized water was added into the almost dry samples and warmed about 5 min to complete digestion. The solution was rinsed to a 50-cm^3 polypropylene volumetric flask and then adjusted the volume by deionized water. The flask was capped and shaken thoroughly. Finally, the solution was transferred into a plastic bottle with a treaded cap lined under a polyethylene seal.

2.5 Cracking of Heavy Fuel Oil

The cracking of heavy fuel oil (denoted HFO) was carried out using enlarged-pore zeolite beta as catalyst compared with zeolite beta. This cracking was performed in a closed reactor, which is a glass tube with 4.4 cm. in diameter and 37 cm. in length, under atmospheric pressure. The cracking apparatus was shown in Figure 2.1. The process diagram is shown in Scheme 2.7. A total of 10 g of heavy fuel oil and 1.0 g of catalyst were loaded into the reactor. For thermal cracking, only heavy fuel oil was loaded into the reactor. Before a cracking process, the reactor was set up, and purged with N_2 gas at flow rate of 20 ml/min to remove air. The cracking process was started with heating the tube reactor to the reaction temperature with heating rate of 20°C/min by a split-tube furnace equipped with a programmable temperature controller and a K-type thermocouple. The temperature was maintained at the reaction temperature for various times. The product fraction was flowed from the reactor by the nitrogen gas through a condenser. While the gas fraction was passed through the condenser and collected into a Tedlar bag, the liquid product was condensed in a condenser at a temperature of cold water and collected into a 10 mL graduated cylinder. The gas was collected since the start

of heating. After the reaction was completed, the reactor was cooled down to room temperature and the product fractions were weighed. The values of %conversion and %yield were calculated based on the equations as follows:

$$\%\text{Conversion} = \frac{\text{mass of liquid fraction + mass of gas fraction}}{\text{mass of HFO}} \times 100$$

$$\%\text{Yield of liquid} = \frac{\text{mass of liquid fraction}}{\text{mass of HFO}} \times 100$$

Mass of gas fraction = mass of the reactor with plastic and catalyst before reaction
mass of the reactor with residue and used catalyst after reaction
- mass of liquid fraction

The cracking products were classified into three fractions: gas fraction (products which were not condensed at temperature of cooling water), liquid fraction and residue. The gas products were analyzed by gas chromatograph (GC). The liquid fraction was frozen under liquid nitrogen in order to reduce pressure before distillation at 300°C as shown in Figure 2.2. The distillate oil was analyzed by a GC. The retention time of each component of the distillate oil from the GC column were compared with reference in form of n-paraffins by the temperature of boiling point. The regeneration of used catalyst was obtained by calcination at 550°C after washed with n-hexane.

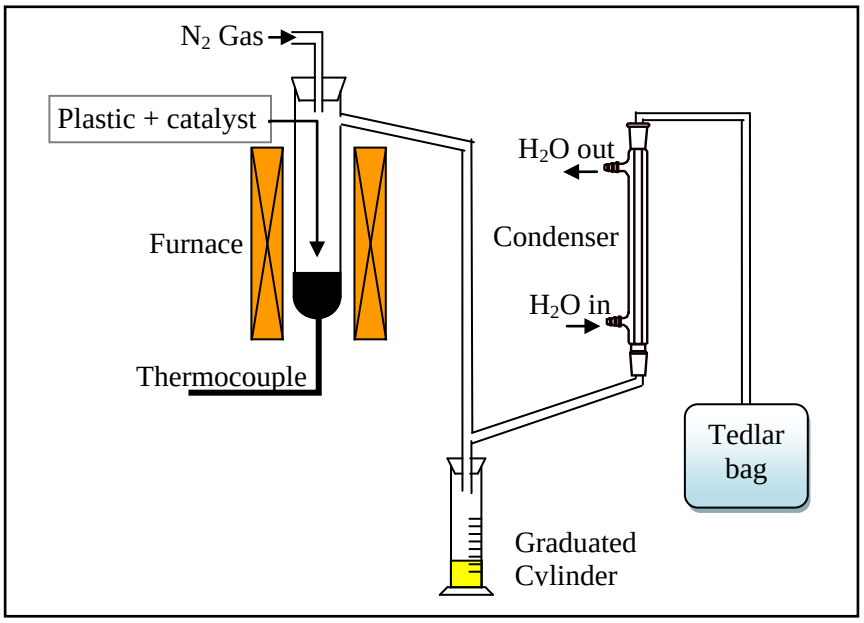

Figure 2.1 Catalytic cracking apparatus.

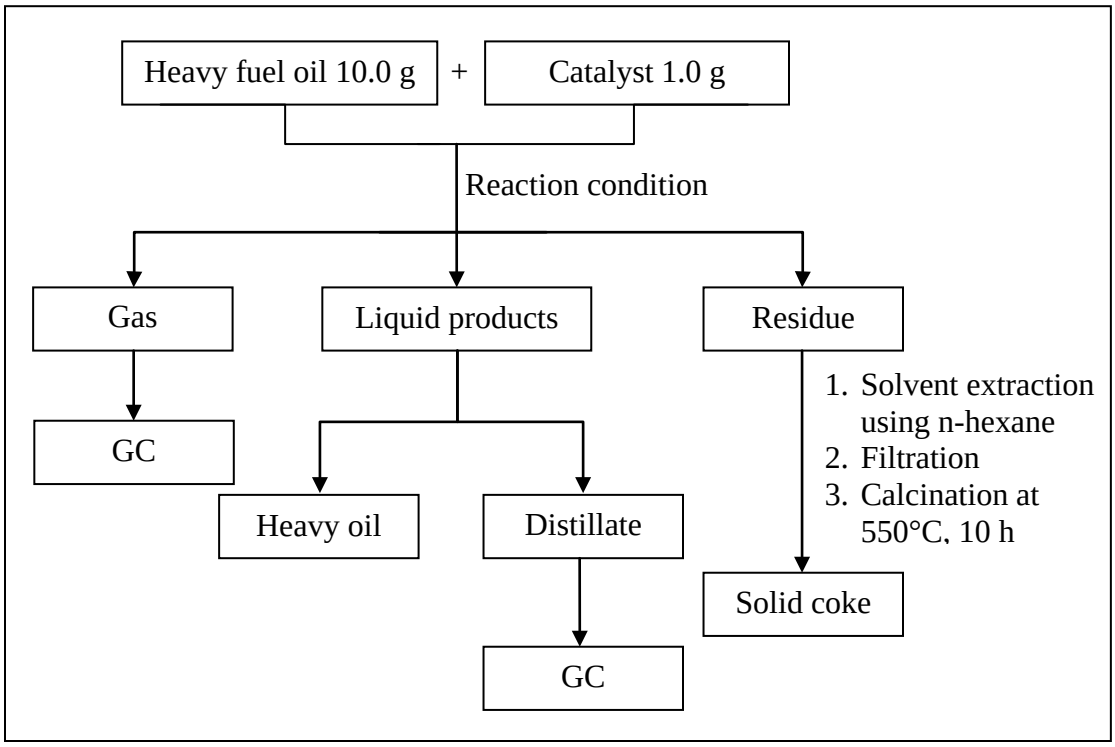

Scheme 2.7 Diagram of catalytic cracking process of heavy fuel oil using zeolite beta and enlarged-pore zeolite beta as catalyst.

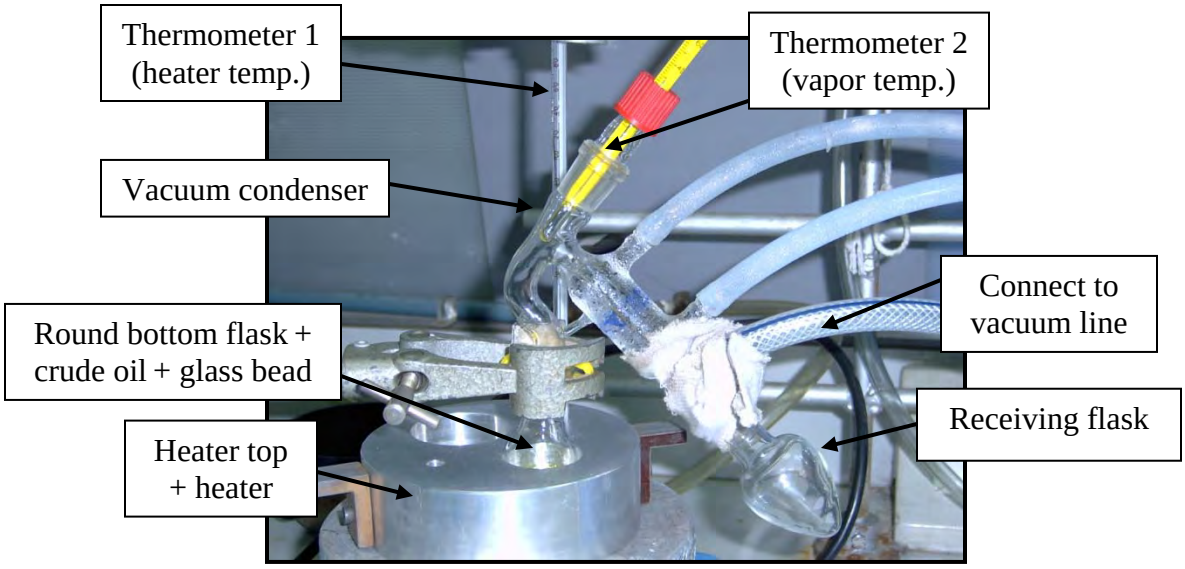

Figure 2.2 Vacuum distillation apparatus.

2.5.1 Effect of Catalyst

The effect of catalysts was investigated by catalytic cracking of HFO over zeolite beta and enlarged-pore zeolite beta catalysts at 380°C for 40 min, heating rate of 20°C/min, 10 wt% of catalyst to HFO, compared with thermal cracking.

2.5.2 Effect of Reaction Temperature

To investigate the effect of reaction temperature, the optimum catalyst (h-BEA) from Section 2.5.1 was used in catalytic cracking of HFO at 330, 350, 380 and 410°C for 40 min, heating rate of 20°C/min and 10 wt% of catalyst to HFO.

2.5.3 Effect of Reaction Time

The optimum temperature (380°C) from Section 2.5.2 was used in catalytic cracking of HFO over h-BEA for 30, 40 and 50 min, heating rate of 20°C/min and 10 wt% of catalyst to HFO.

2.5.4 Effect of Heavy Fuel Oil to Catalyst Ratio

The effect of catalyst ratio was studied by catalytic cracking of HFO over h-BEA at 380°C for 40 min, heating rate of 20°C/min and 5 wt% and 10 wt% of catalyst to HFO.

2.6 Catalyst Regeneration

The used catalyst (h-BEA) from HFO cracking at the reaction temperature of 380°C from each cycle was regenerated by calcination in air at 550°C for 10 h after washed with n-hexane. The regenerated catalyst was characterized by XRD, SEM, N_2 adsorption and tested for its activity by catalytic cracking of HFO at the reaction temperature of 380°C for 40 min, heating rate of 20°C/min and 10 wt% of catalyst to HFO. The reaction was performed in the same way as described in section 2.5.

CHAPTER III

RESULTS AND DISCUSSION

3.1 Characterization of Material

3.1.1 Hexagonal Mesoporous Silica (Si-HMS)

3.1.1.1 Powder X-ray Diffraction (XRD)

Hexagonal mesoporous silica (Si-HMS) was synthesized with the gel mole composition of $1SiO_2$: 0.25HDA: 8.3EtOH: $100H_2O$ reported by Tuel *et al.* [57]. The powder X-ray diffractograms (XRD patterns) of as-synthsized and calcined Si-HMS were shown in Figure 3.1. The well-defined XRD patterns were indexed on the basis of the Bragg peak. A prominent diffraction peak of (100) at the 2θ range of 1.5-2.0° indicating the hexagonal mesoporous structure of HMS was observed in both as-synthsized and calcined samples. After calcination in air at 550°C for 10 h, the hexagonal structure remained and the peak intensity increased, suggesting the removal of template from the pores of materials. Since the materials are not crystalline at the atomic level, no reflections at higher angles are observed. However mesoporous materials usually have long range order, the pore walls are amorphous. In the absence of such short range order, they can be interpreted as semi-crystalline solid [59].

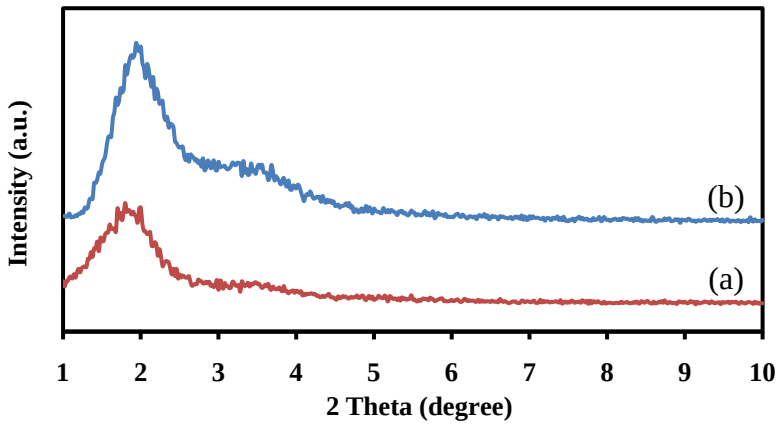

Figure 3.1 XRD patterns of (a) as-synthesizd and (b) calcined Si-HMS.

3.1.1.2 Nitrogen Adsorption-Desorption

The N_2 adsorption-desorption isotherm of the Si-HMS was shown in Figure 3.2. Si-HMS showed the type IV isotherm with the hysteresis loop between relative intensity (p/p_0) 0.45 to 0.6, which is the characteristic of ordered mesoporous materials.

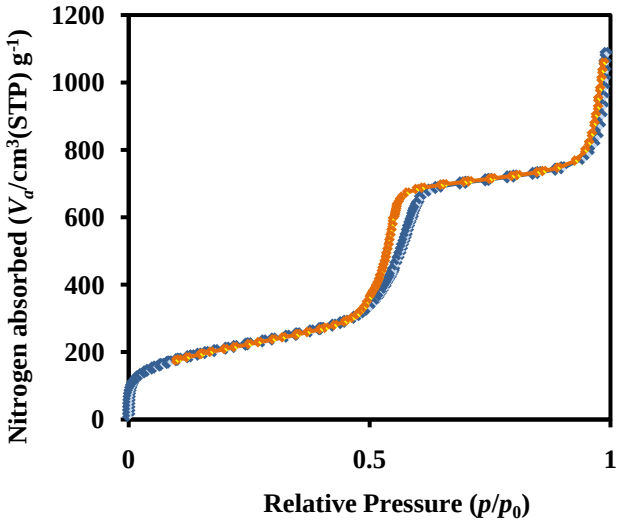

Figure 3.2 Nitrogen adsorption-desorption isotherm of Si-HMS.

The specific surface area, total pore volume and the pore diameter calculated from the N_2 adsorption of Si-HMS using the BET and BJH model, respectively, were presented in Table 3.1. The uniform pore size distribution of Si-HMS was shown in Figure 3.3.

Table 3.1 Physical properties of the Si-HMS sample

Sample	Specific Surface Area (m^2g^{-1})[a]	Total pore volume ($cm^3\ g^{-1}$)[a]	Pore Diameter (nm)[b]
Si-HMS	753	1.67	4.76

[a] Determined by BET method

[b] Determined by BJH-plot method

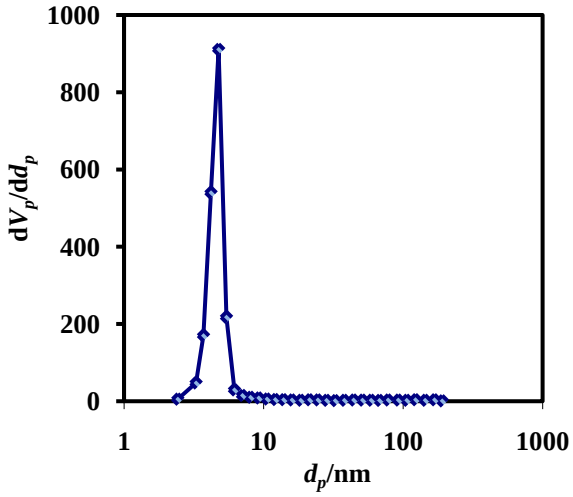

Figure 3.3 The pore size distribution diagram of Si-HMS from the BJH calculation.

3.1.1.3 Scanning Electron Microscope (SEM)

Figure 3.4 showed the SEM images of Si-HMS. Si-HMS exhibited an agglomeration of small particles.

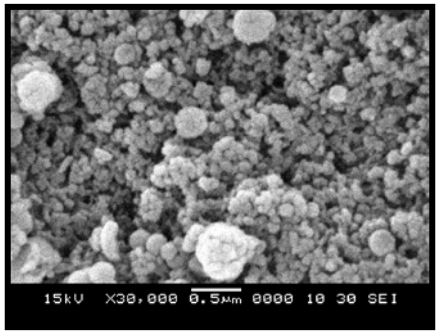

Figure 3.4 SEM images of Si-HMS with different magnification x30,000.

Both prepared sample: as-synthesized Si-HMS and calcined Si-HMS were used as silica source for further synthesis of enlarged-pore zeolite beta.

3.1.2 Enlarged-Pore Zeolite Beta

3.1.2.1 Effect of Silica Source

The enlarged-pore zeolite betas were synthesized using different silica sources: as-synthesized Si-HMS and calcined Si-HMS (denoted h'-BEA and h-BEA, respectively). The comparative zeolite beta was synthesized by Aguado method [50] using TEOS as silica source (denoted BEA), as described in 2.3.2.1.

3.1.2.1.1 Powder X-ray Diffraction (XRD)

The powder XRD patterns of as-synthesized and calcined BEA, h'-BEA and h-BEA were shown in Figures 3.5 and 3.6, respectively.

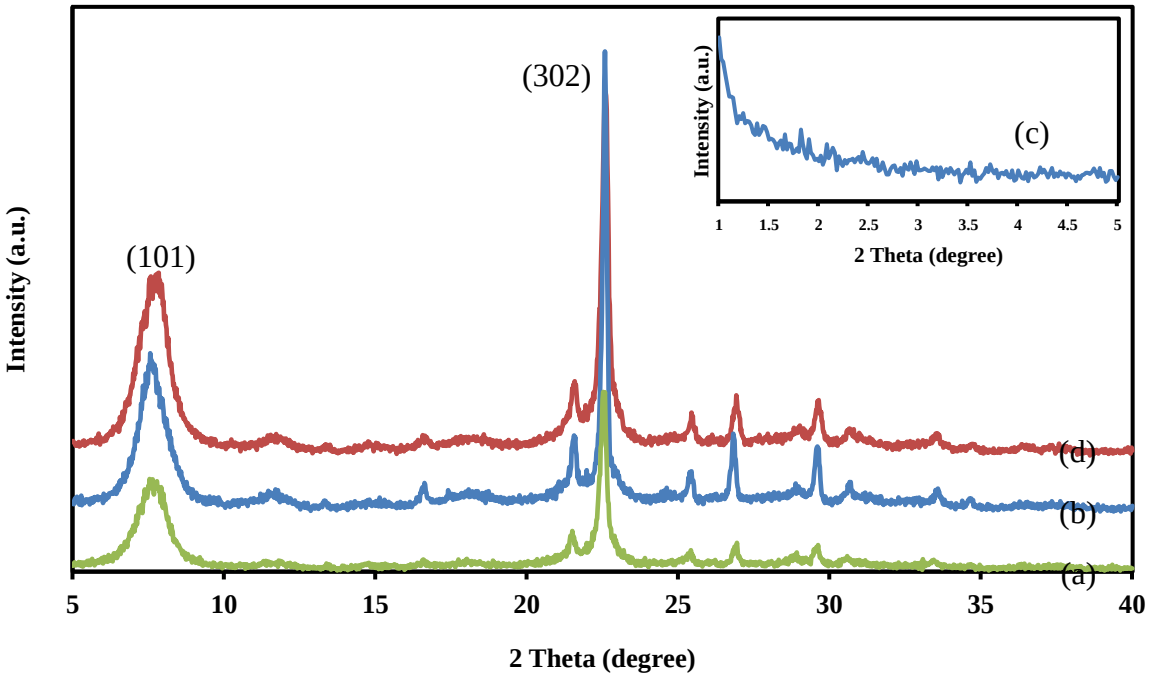

Figure 3.5 XRD patterns of as-synthesized (a) h'-BEA, (b)-(c) h-BEA and (d) BEA.

From Figure 3.5, it was found that as-synthesized h'-BEA, h-BEA and BEA had the characteristic peaks as the zeolite beta reported by Aguado *et al*. [50]. The well-defined XRD patterns were indexed on the basis of Bragg peaks. The broad diffraction peak of (101) plane was observed at the 2θ of 7.5° indicating the presence of

two isomorphs, A and B, which is hardly separated in zeolite beta. The most intense sharp peak at 22.4° was assigned to the diffraction of (302) plane, suggesting the high crystallinity of the zeolite beta [50].

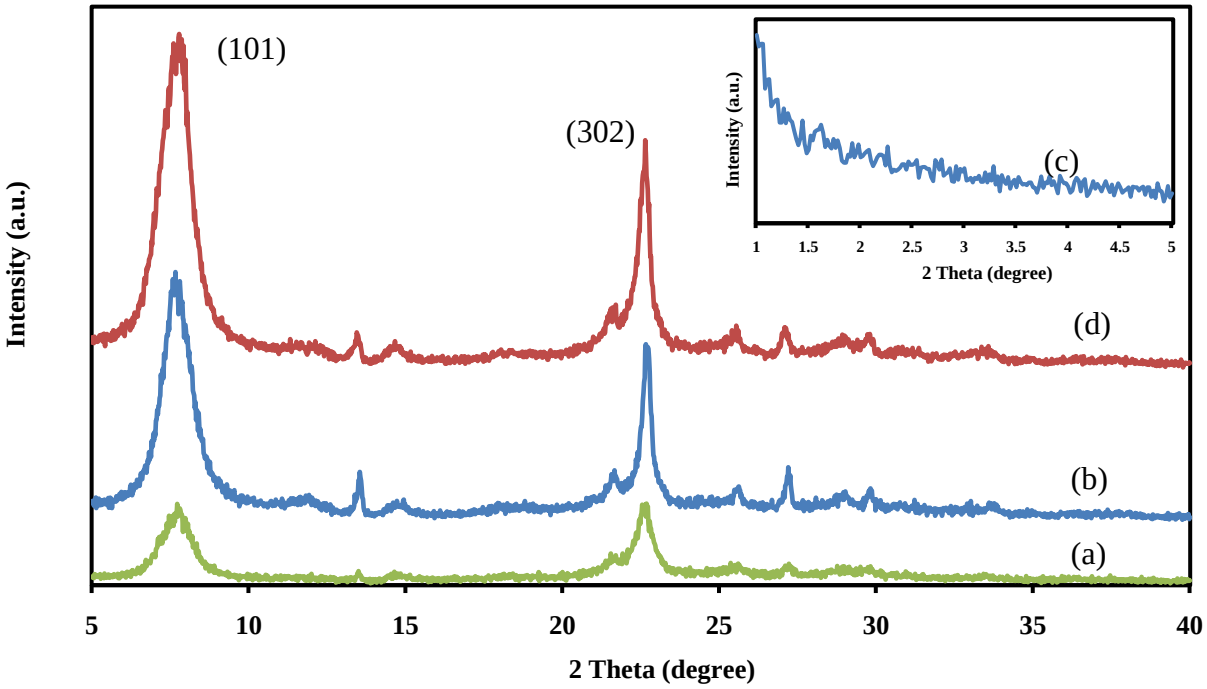

Figure 3.6 XRD patterns of calcined (a) h'-BEA, (b)-(c) h-BEA and (d) BEA.

From Figure 3.6, it was found that after the oxidative decomposition of template at 550°C for 5 h for BEA and 10 h for h'-BEA and h-BEA, the intensity of (101) broad peak (2θ at 7.5°) was increased because template was removed from channels of zeolite beta, whereas the intensity of (302) peak at 22.4° was decreased due to dealumination of aluminium from the tetrahedral framework. The dealumination can be evidenced by the appearance of ^{27}Al-NMR signal of octahedral aluminum at 0 ppm, as shown in Figure 3.19.

The XRD patterns of both h'-BEA and h-BEA did not show the (100) plane, which is the characteristic peak of HMS at low 2θ angle, as shown in Figure 3.6 (c). It was suggested that Si-HMS structure was completely changed to zeolite beta structure.

The intensity of characteristic peaks of h-BEA were higher than h'-BEA. This is due to different silica source. The calcined Si-HMS has higher crystallinity than the as-synthesized Si-HMS [60]. Thus, the h-BEA prepared from the calcined Si-HMS might get the heredity from higher crystallinity than the h'-BEA which was prepared from the as-synthesizd Si-HMS [49].

3.1.2.1.2 Nitrogen Adsorption-Desorption

The N_2 adsorption-desorption isotherms of the BEA, h'-BEA and h-BEA were shown in Figure 3.7. All samples showed N_2 sorption isotherms of type I with high adsorption at low relative pressure (p/p_0) and a plateau at relative pressure higher than 0.02, which is the characteristic of micropore.

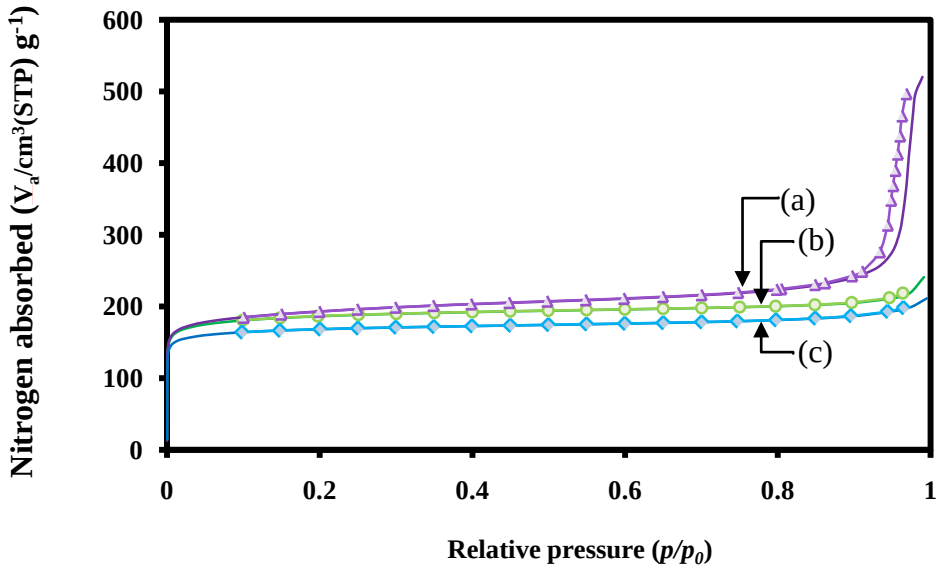

Figure 3.7 Nitrogen adsorption-desorption isotherm of (a) BEA, (b) h'-BEA and (c) h-BEA

The specific surface area, external surface area, pore diameter and micropore volume of BEA, h'-BEA and h-BEA were presented in Table 3.2 and the pore size distribution of these samples were shown in Figure 3.8. The sample of h-BEA provided specific surface area and external surface area higher than h'-BEA. Both h'-BEA

and h-BEA provided specific surface area and micropore volume lower than BEA. When comparing, external surface area observed as h-BEA > BEA > h'-BEA while the trend of pore diameter can be observed as h-BEA > h'-BEA≈ BEA. These results were influenced by the structure of silica source, as described in the previous section. It can be concluded that as-synthesized and calcined Si-HMS can be used for preparation of enlarged-pore zeolite beta by maintaining its high crystalinity of zeolite beta. Because h-BEA showed more advantage, such as, higher crystallinity, larger micropore volume, specific surface area and especially pore diameter than h'-BEA. Thus h-BEA was chosen for further study on synthesis parameters.

Table 3.2 Physical properties of the calcined BEA, h'-BEA and h-BEA samples

Sample	**Specific Surface Area (m^2g^{-1})[a]**	**External Surface Area (m^2g^{-1})[b]**	**Micropore Volume (cm^3g^{-1})[a]**	**Pore Diameter (nm)[b]**
BEA	743	47	170.84	0.59
h'-BEA	637	28	146.55	0.59
h-BEA	721	70	165.72	0.62

[a] Determined by BET method

[b] Determined by *t*-plot method

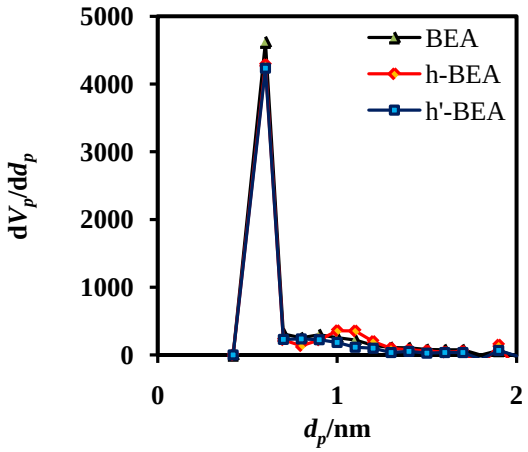

Figure 3.8 Pore size distribution of (a) BEA, (b) h'-BEA and (c) h-BEA from MP-plot.

3.1.2.1.3 Scanning Electron Microscope (SEM)

The morphology of calcined BEA, h'-BEA and h-BEA were displayed in Figure 3.9. BEA presented a uniform round granular with the average size of particles around 250 ± 5 nm. Although the h'-BEA and h-BEA presented granulars, the particles sizes of h-BEA and h'-BEA were 560 ± 5 nm and 187 ± 5 nm, respectively.

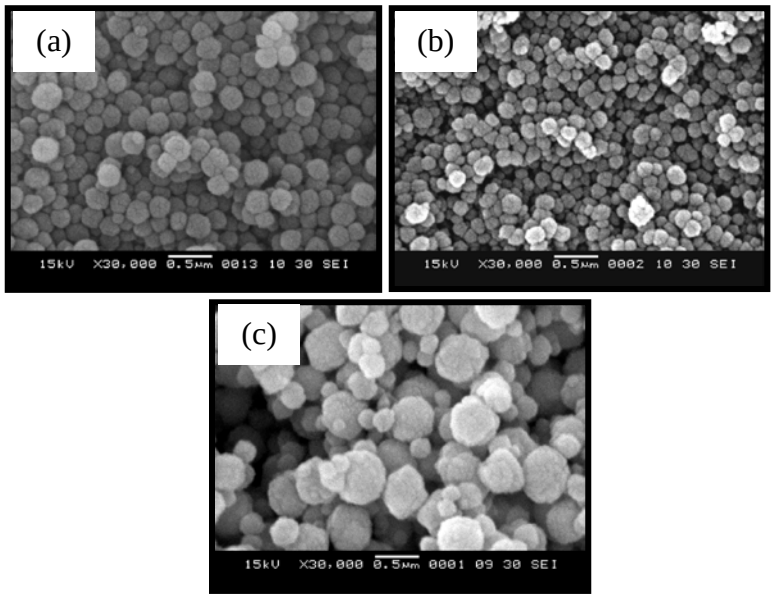

Figure 3.9 SEM images of (a) BEA, (b) h'-BEA and (c) h-BEA.

3.1.2.2 Effect of Templates

The enlarged-pore zeolite beta prepared from calcined Si-HMS was investigated for the effect of templates, *e.g.* TEAOH, HDA and mixed template between TEAOH and HDA, as summarized in Table 2.2 (page 38) at crystallization temperature of 135°C for 3 days.

3.1.2.2.1 Powder X-ray Diffraction (XRD)

The powdered XRD patterns of as-synthesized and calcined enlarged-pore zeolite beta were shown in Figures 3.10 and 3.11, respectively.

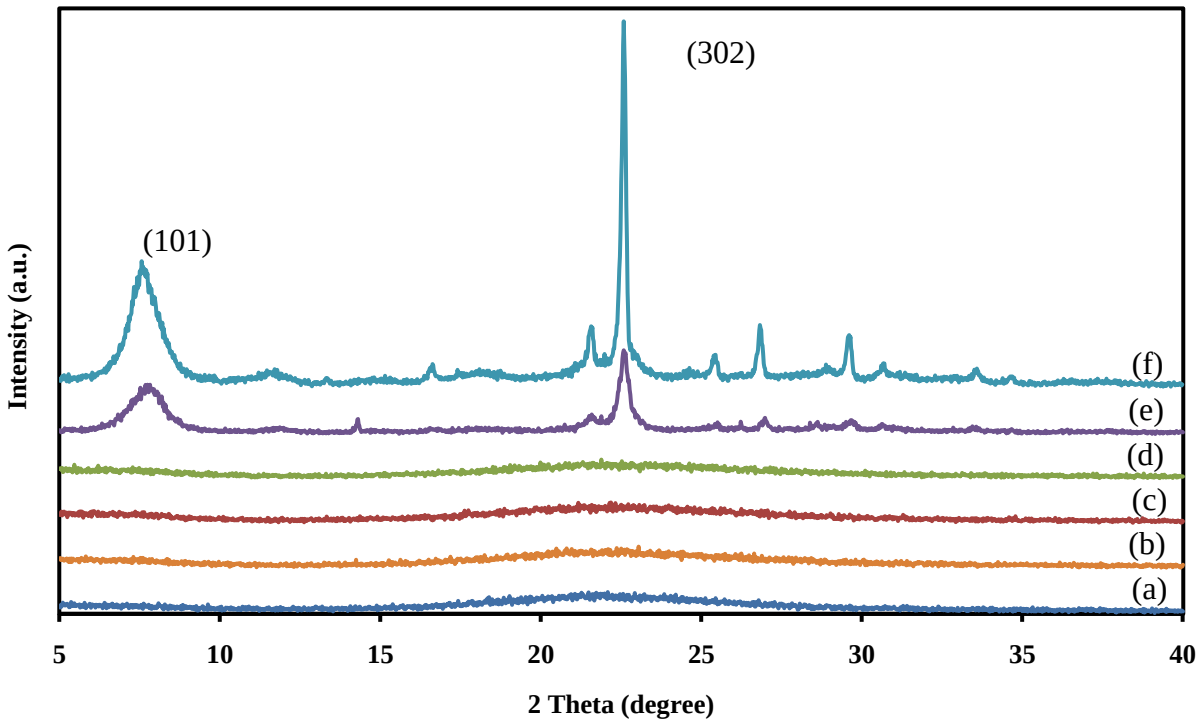

Figure 3.10 XRD patterns of as-synthesized enlarged-pore zeolite beta: (a) h-BEA-M1-135-3, (b) h-BEA-M2-135-3, (c) h-BEA-M3-135-3, (d) h-BEA-M4-135-3, (e) h-BEA -M5-135-3 and (f) h-BEA.

It was found that h-BEA prepared from only TEAOH template showed high crystallinity of characteristic peak of zeolite beta [50]. The peak intensity of

enlarged-pore zeolite beta decreased when mixed template was used. Only h-BEA-M4-135-3 sample prepared from mixed template in ratio of 0.326TEAOH: 0.050HDA, showed the characteristic peak of zeolite beta structure but its intensity was low. The other ratios, h-BEA-Mn-135-3 where n as 0, 1, 2 and 3, showed very low crystallinity which can be seen from humps between 2θ of 6-8° and 21-24°, associated with the presence of amorphous structure [50]. It can be seen that when HDA template was increased, the crystallinity was decreased.

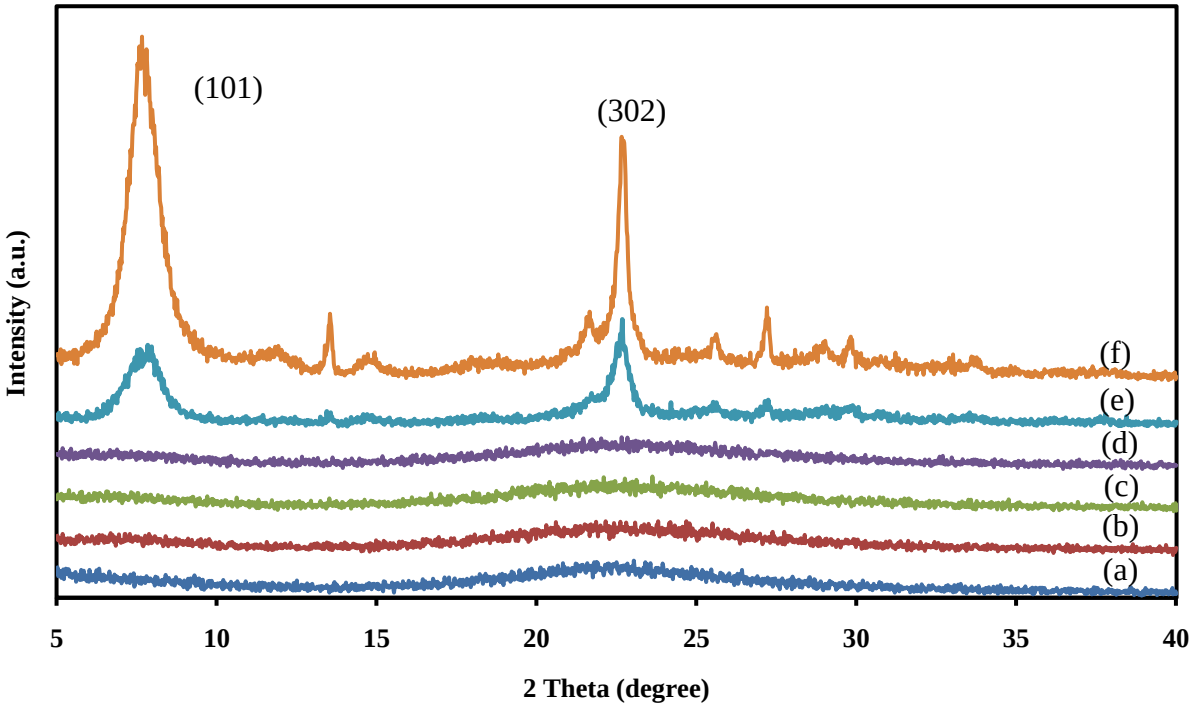

Figure 3.11 XRD patterns of calcined enlarged-pore zeolite beta: (a) h-BEA-M0-135-3, (b) h-BEA-M1-135-3, (c) h-BEA-M2-135-3, (d) h-BEA-M3-135-3, (e) h-BEA-M4-135-3 and (f) h-BEA.

Generally, the mechanism for zeolite synthesis is commonly understood as a solution-mediated process with two main steps: nucleation through the formation of very small crystalline entities and crystal growth through the progressive incorporation of soluble species around these nuclei previously formed [61]. The nucleation of zeolite beta can be achieved through H-bond interaction between the

TEAOH template and the inorganic species. When HDA template was partially added into TEAOH template, HDA was enriched at the liquid-solid interface through the H-bond interaction between the neutral inorganic precursor and the surfactant head group leading to crystallization of zeolite beta structure. However, high amount of added HDA and slightly acidic EtOH cosolvent reduced pH of solution and retarded the crystal growth process.

The increasing of HDA template ratio decreased the concentration of TEAOH template. It was corresponded with Matsukata's work [62]. They investigated the effect of concentration of TEA^+ on the synthesis of zeolite beta and found that when TEA^+ concentration was reduced, the amorphous or ZSM-12 or ZSM-5 phases were increased. On the contrary, TEA^+ concentration was increased, zeolite beta phase was increased. Therefore, the enlarged-pore zeolite beta with the gel mole composition of $1SiO_2$: $0.0083Al_2O_3$: 0.315TEAOH: 0.061HDA: 1.69EtOH: $17.95H_2O$ (h-BEA-M3-T_{crys}-t_{crys}) was chosen for investigation in order to increase its crystallinity.

3.1.2.2.2 Nitrogen Adsorption-Desorption

The h-BEA-M4-135-3 sample showed type I N_2 sorption isotherm with high adsorption at low relative pressure (p/p_0) and a plateau at relative pressure higher than 0.02, which is the characteristic of micropore, as shown in Figure 3.12.

Table 3.3 Physical properties of the calcined h-BEA-M4-135-3 sample

Sample	Specific Surface Area (m^2g^{-1})[a]	External Surface Area (m^2g^{-1})[b]	Micropore volume (cm^3g^{-1})[a]	Pore Diameter (nm)[b]
h-BEA-M4-135-3	639	30	146.84	0.59

[a] Determined by BET method

[b] Determined by *t*-plot method

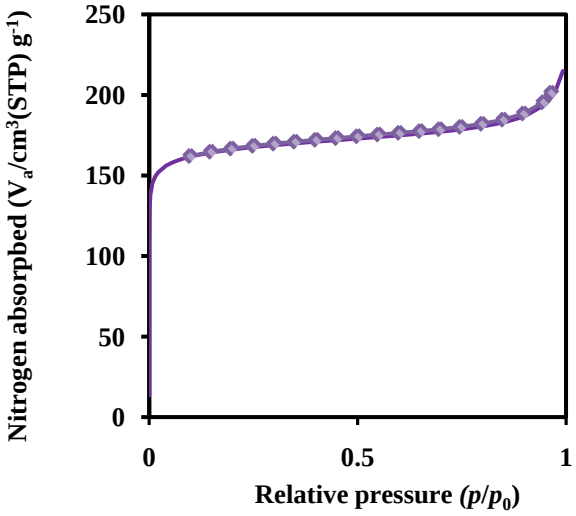

Figure 3.12 Nitrogen adsorption-desorption isotherm of h-BEA-M4-135-3 sample.

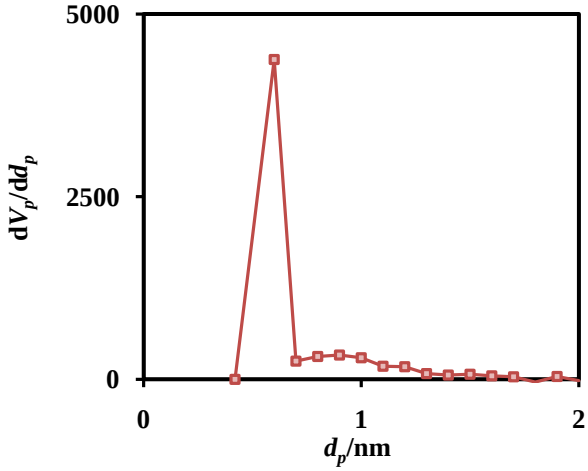

Figure 3.13 Pore sized distribution of h-BEA-M4-135-3 from MP-plot.

The specific surface area, external surface area, micropore volume and pore diameter of h-BEA-M4-135-3 were calculated and presented in Table 3.3 and the pore size distribution of this sample was shown in Figure 3.13. The specific surface area, external surface area, pore diameter and micropore volume of h-BEA-M4-135-3 were lower than h-BEA, in Table 3.2.

3.1.2.3 Effect of Crystallization Temperature and Time

The enlarged-pore zeolite beta with the gel mole composition $1SiO_2$: $0.0083Al_2O_3$: 0.315TEAOH: 0.061HDA: 1.69EtOH: $17.95H_2O$ (h-BEA-M3-T_{crys}-t_{crys}) was investigated for the effect of crystallization time for 6, 9, 12 and 15 days at temperature of 135, 140 and 145°C.

3.1.2.3.1 Powder X-ray Diffraction (XRD)

The powder XRD patterns of as-synthesized and calcined of h-BEA-M3-T_{crys}-t_{crys} at the various crystallization time and temperatures were shown in Figure 3.14 and 3.15, respectively. At crystallization temperature of 135°C, Figure 3.15 (a), enlarged-pore zeolite beta crystallized for 6 and 9 days (denoted h-BEA-M3-135-6 and h-BEA-M3-135-9, respectively) showed broad peaks between 2θ of 6-8° and 21-25°, indicating the presence of amorphous structure. After crystallization for 12 days (denoted h-BEA-M3-135-12), little diffraction peaks at 2θ of 7.5° and 22.4° were observed, indicating the presence of zeolite beta phase.

From Figures 3.15 (b) and 3.15 (c), the enlarged-pore zeolite beta crystallized at 140 and 145°C for 6 days (denoted h-BEA-M3-140-6 and h-BEA-M3-145-6) showed broad peaks between 2θ of 6–8° and 21-25° which are amorphous. Whereas after crystallization for 9 days, a crystalline enlarged-pore zeolite beta was obtained with ZSM-12 coexist phase at both temperatures. The phase change was indicated by a splitting of the beta peak at 7.5° to peaks at 7.5°, 7.6° and 8.9°, a fading of the peak at 22.4° and an emerging of a new peak at 21° [56]. It can be seen that the crystallization of zeolite beta was rapidly taken place by ZSM-12 phase when increasing crystallization time.

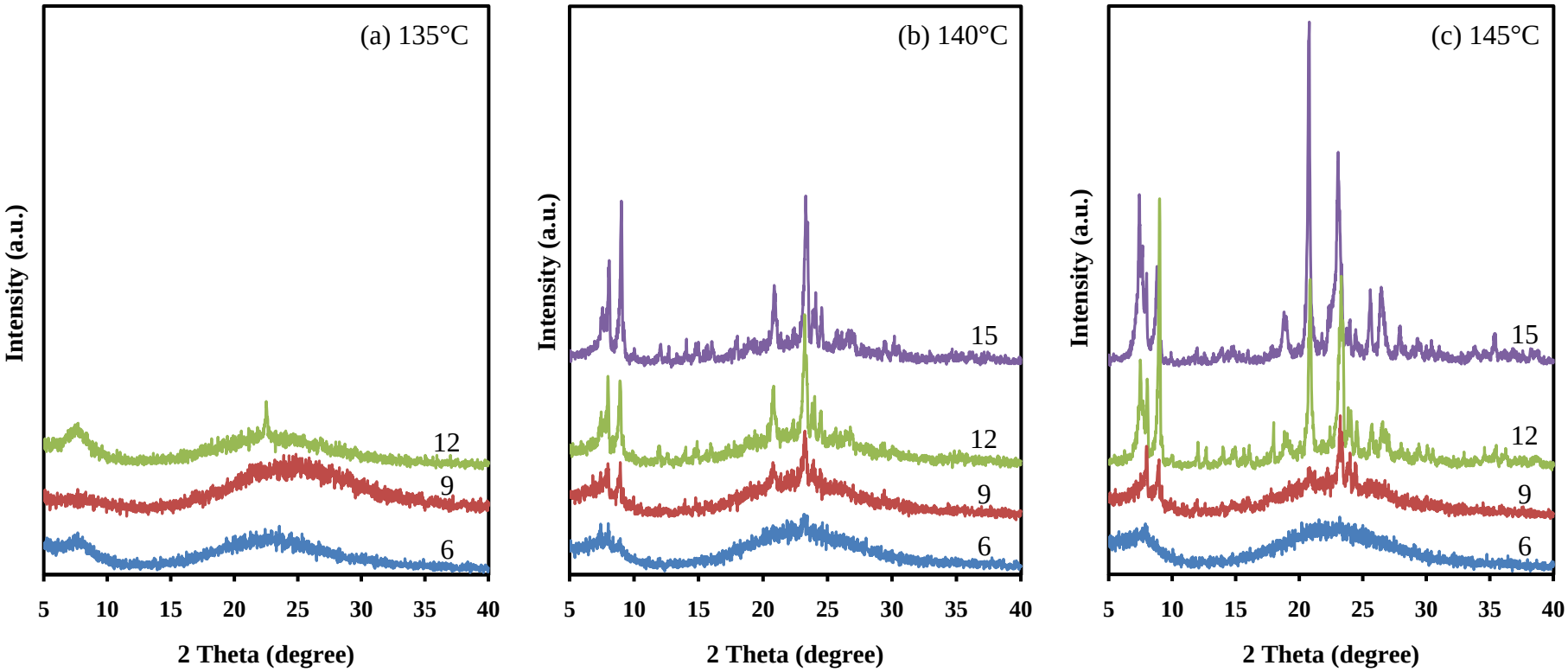

Figure 3.14 XRD patterns of as-synthesized enlarged-pore zeolite beta with mixed templates (h-BEA-M3-T_{crys}-t_{crys}), crystallization for 6, 9, 12 and 15 days at temperature of (a) 135, (b) 140 and (c) 145°C.

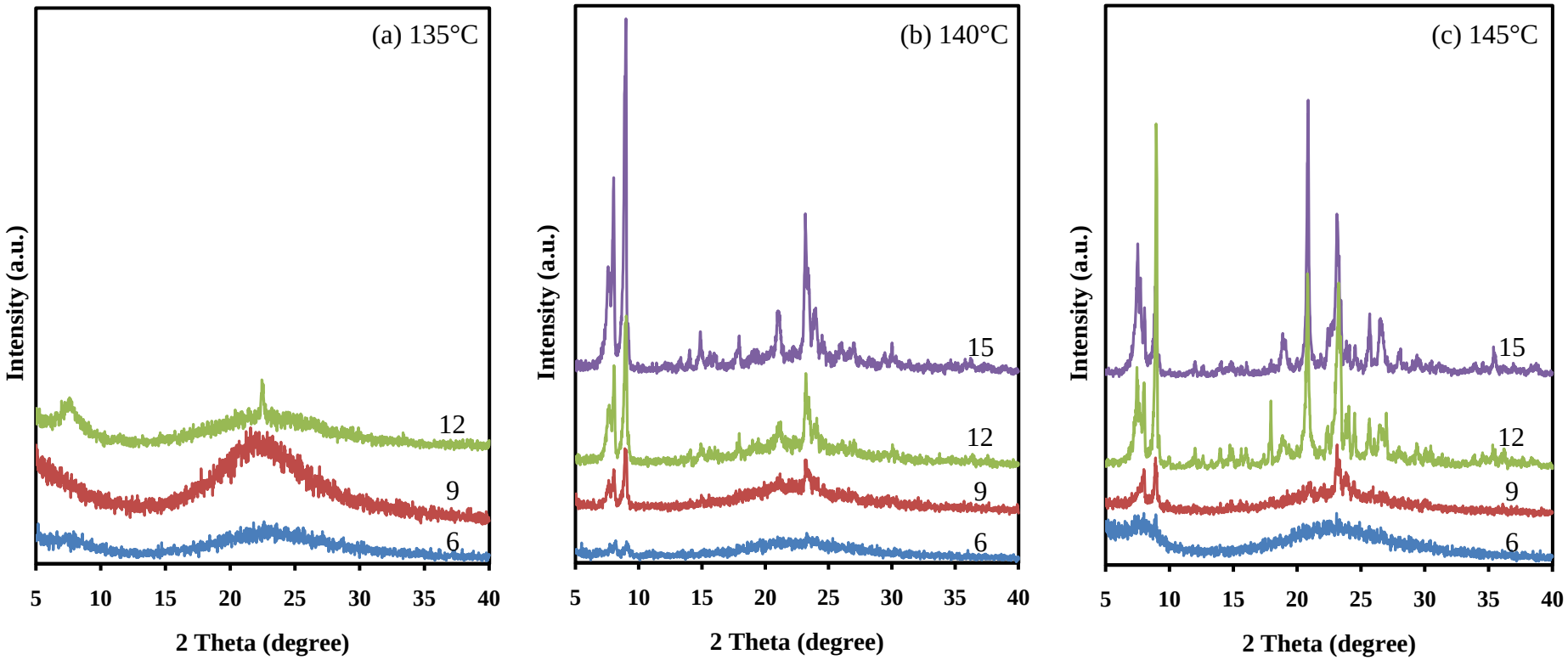

Figure 3.15 XRD patterns of calcined enlarged-pore zeolite beta with mixed templates (h-BEA-M3-T_{crys}-t_{crys}), crystallization for 6, 9, 12 and 15 days at temperature of (a) 135, (b) 140 and (c) 145°C.

To determine the degree of phase change from zeolite beta to ZSM-12 in the samples, the ratio of peak area of the most intense XRD peak of Beta (2θ = 22.4°) to that of ZSM-12 (2θ = 21.0°) was determined and summarized in Table 3.4. Note that the ZSM-12 peaks at 7.5 and 7.6 were not used because they overlapped with beta peaks [63].

Table 3.4 Calculated ratio of peak area of zeolite ZSM-12 and zeolite beta

Crystallization temperature (°C)	**Crystallization time (day)**	**Peak area at 2θ= 22.4 (Beta)**	**Peak area at 2θ= 21.0 (ZSM-12)**	**Peak area Ratio ZSM-12/Beta**
	9	826	430	0.52
140	12	4961	1076	0.22
	15	10658	1807	0.17
	9	1788	780	0.44
145	12	7017	5830	0.83
	15	7022	6559	0.94

The ZSM-12/Beta ratios were plotted versus crystallization time in Figure 3.16 and a linear correlation was observed. It was found that at crystallization temperature of 145°C, the higher crystallization time the increase in the ratio was observed, and the phase change was increased. While at 140°C, the ratios were decreased as crystallization time increased, according to Eapen's work [64]. They studied crystallization of zeolite beta and found that high crystallization temperature resulted in formation of impurity phase while low crystallization temperature was more favorable for crystallization of zeolite beta.

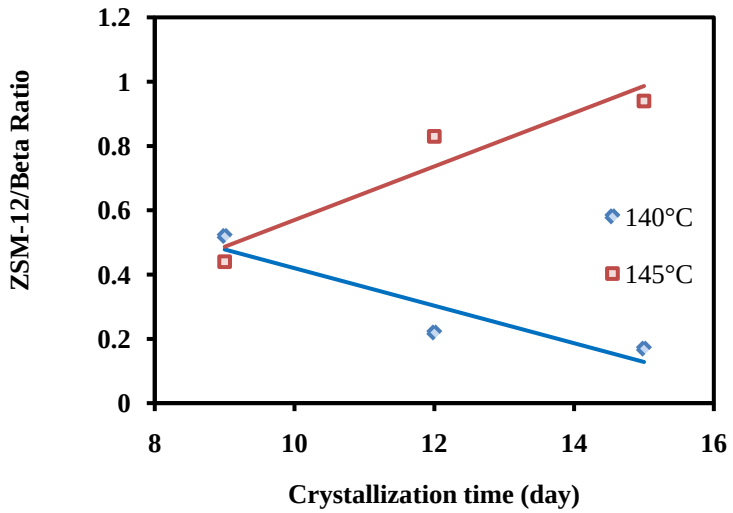

Figure 3.16 The relationship between the peak area of zeolite ZSM-12 and Beta versus the crystallization time.

3.1.2.3.2 Nitrogen Adsorption-Desorption

The N_2 adsorption-desorption isotherms of the enlarged-pore zeolite beta prepared from mixed template crystallized for 9, 12 and 15 days at 140 and 145°C (h-BEA-M3-140-t_{crys} and h-BEA-M3-140-t_{crys}, respectively) were shown in Figure 3.17. It can be seen that h-BEA-M3-140-9, h-BEA-M3-140-12, h-BEA-M3-140-15 and h-BEA-M3-145-12 samples showed a low absorption at low pressure and increase in adsorbed nitrogen and hysteresis loop when the relative pressure (p/p_0) was higher than 0.5, which meant that there are monolayer and multilayer sorption characteristics, process micropore and mesopore characteristics [65]. While h-BEA-M3-145-15 gave N_2 sorption isotherms type I with high adsorption at low relative pressure (p/p_0) and a plateau at relative pressure higher than 0.02, which is the characteristic of micropore.

The specific surface area, external surface area, micropore volume and pore diameter of h-BEA-M3-140-t_{crys} and h-BEA-M3-145-t_{crys} samples were presented in Table 3.5. It was found that when crystallization temperature and time increased, pore diameter and external surface area were decreased while the specific surface area and micropore volume were increased.

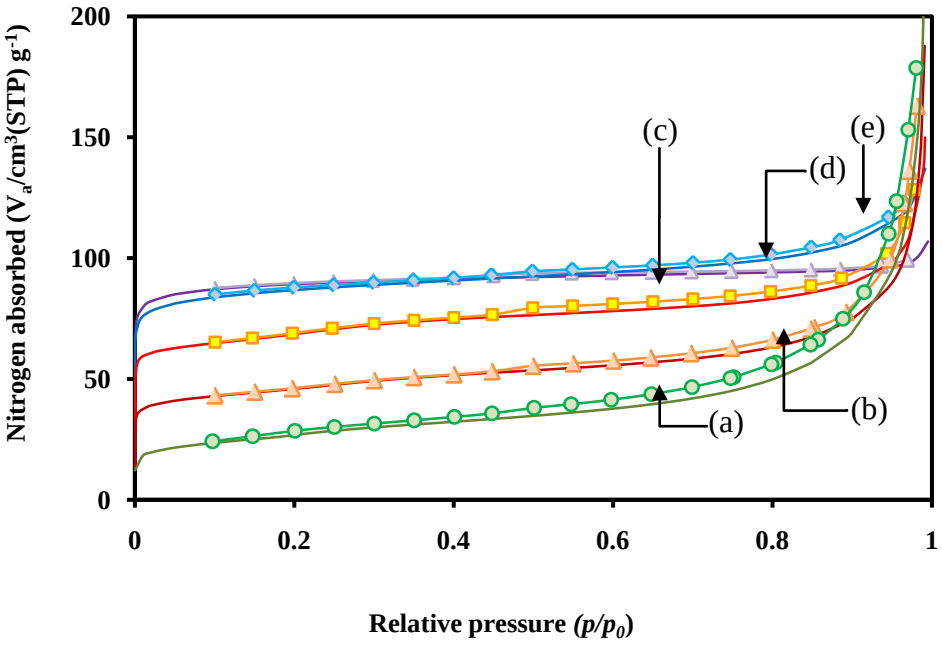

Figure 3.17 Nitrogen adsorption-desorption isotherms of (a) h-BEA-M3-140-9, (b) h-BEA-M3-140-12, (c) h-BEA-M3-140-15, (d) h-BEA-M3-140-12 and (e) h-BEA-M3-145-15.

Table 3.5 Physical properties of the calcined h-BEA-M3-T_{crys}-t_{crys} samples

Sample	Specific Surface Area (m^2g^{-1})[a]	External Surface Area (m^2g^{-1})[b]	Micropore volume (cm^3g^{-1})[a]	Pore Diameter (nm)[b]
h-BEA-M3-140-9	94	60	21.62	0.66
h-BEA-M3-140-12	164	41	37.76	0.63
h-BEA-M3-140-15	245	30	56.31	0.63
h-BEA-M3-145-12	315	33	72.55	0.59
h-BEA-M3-145-15	342	11	78.68	0.59

[a] Determined by BET method

[b] Determined by *t*-plot method

Normally, the high porosity of zeolite beta is obtained by crystallization at lower temperature and short period of time while low porosity zeolite beta does at higher temperature and long period [66]. Thus, when compared at the same crystallization time, the higher crystallization temperature produced smaller pore diameter as well as the increasing crystallization temperature.

3.1.2.3.3 Scanning Electron Microscope (SEM)

Morphology of the h-BEA-M3-140-9, h-BEA-M3-140-12 and h-BEA-M3-140-15 was shown in Figure 3.18. It was found that morphology of the h-BEA-M3-140-9 exhibited small particles, similar to the Si-HMS in Figure 3.4. The h-BEA-M3-140-12 and h-BEA-M3-140-15 samples exhibited inhomogeneous agglomeration of small particles which increased when crystallization time was increased, as showed in Figure 3.9.

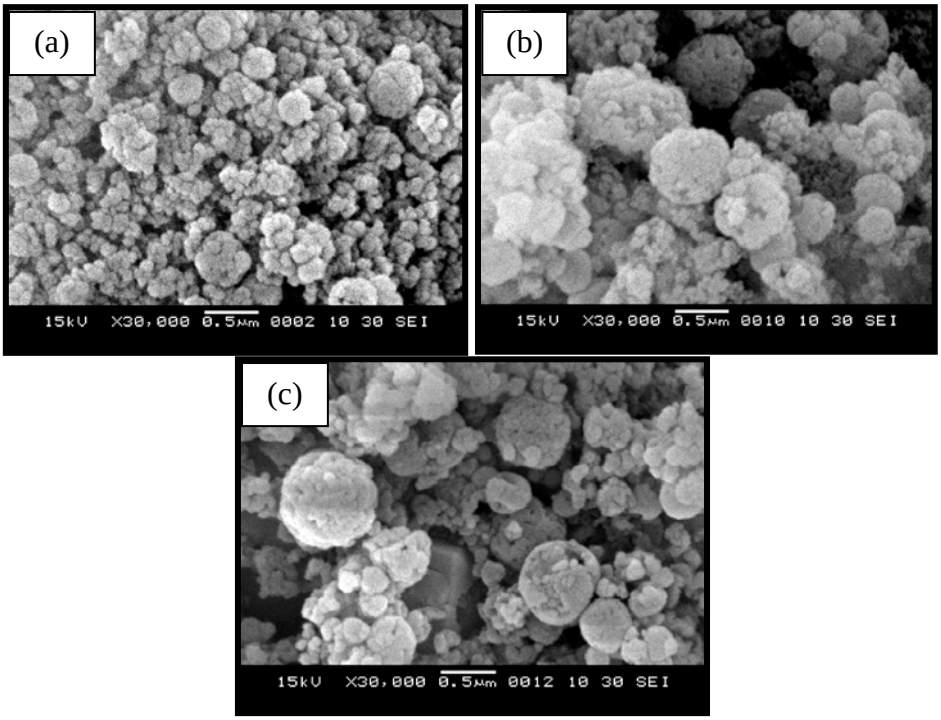

Figure 3.18 SEM images of (a) h-BEA-M3-140-9, (b) h-BEA-M3-140-12 and (c) h-BEA-M3-140-15.

3.1.3 Elemental Analysis

In this work, ICP-AES technique was used for determination of aluminum contents. The Si/Al mole ratios in gel and in catalyst of BEA, h-BEA and h-BEA-M3-140-t_{crys} samples were shown in Table 3.6. It was clearly observed that the Si/Al mole ratios in catalyst of all prepared samples in this work were less than Si/Al mole ratios in gel which were calculated from reagent quantities. For BEA and h-BEA samples, there were no significant difference between Si/Al ratio in catalyst and Si/Al ratio in gel, suggesting all aluminum ions were incorporated in the samples. While Si/Al ratio in catalyst of the h-BEA-M3-140-t_{crys} samples showed clearly higher than Si/Al ratio in the gel, suggesting that some aluminum ions were not incorporated in the samples. Thus, it can be concluded that the enlarged-pore zeolite beta with mixed template samples have lower acidity than the h-BEA and BEA.

Table 3.6 Comparison of Si/Al mole ratios of BEA, h-BEA and h-BEA-M3-140-t_{crys} samples

Sample	Si/Al molar ratio in gel [a]	Si/Al molar ratio in catalyst [b]
BEA	60	59
h-BEA	60	72
h-BEA-M3-140-9	60	144
h-BEA-M3-140-12	60	159
h-BEA-M3-140-15	60	185

[a] calculated from reagent quantities.

[b] Alumimum (Al) was determined by ICP-AES and Si was calculated from the deduction of Al_2O_3 from sample weight

3.1.4 ^{27}Al-MAS-NMR Spectra

The ^{27}Al-MAS-NMR spectra of calcined BEA, h-BEA and h-BEA-M3-140-t_{crys} samples were presented in Figure 3.19. The spectra of h-BEA-M3-140-t_{crys} samples showed signal only at 55 ppm. It indicates that aluminum is in tetrahedral

(T_d) framework. While the spectra of BEA and h-BEA showed signals at 0 ppm and 55 ppm that is assigned for aluminum species in octahedral (O_h) non-framework, and tetrahedral (T_d) framework, respectively [67]. The non-framework aluminum species were generated during calcination process [68].

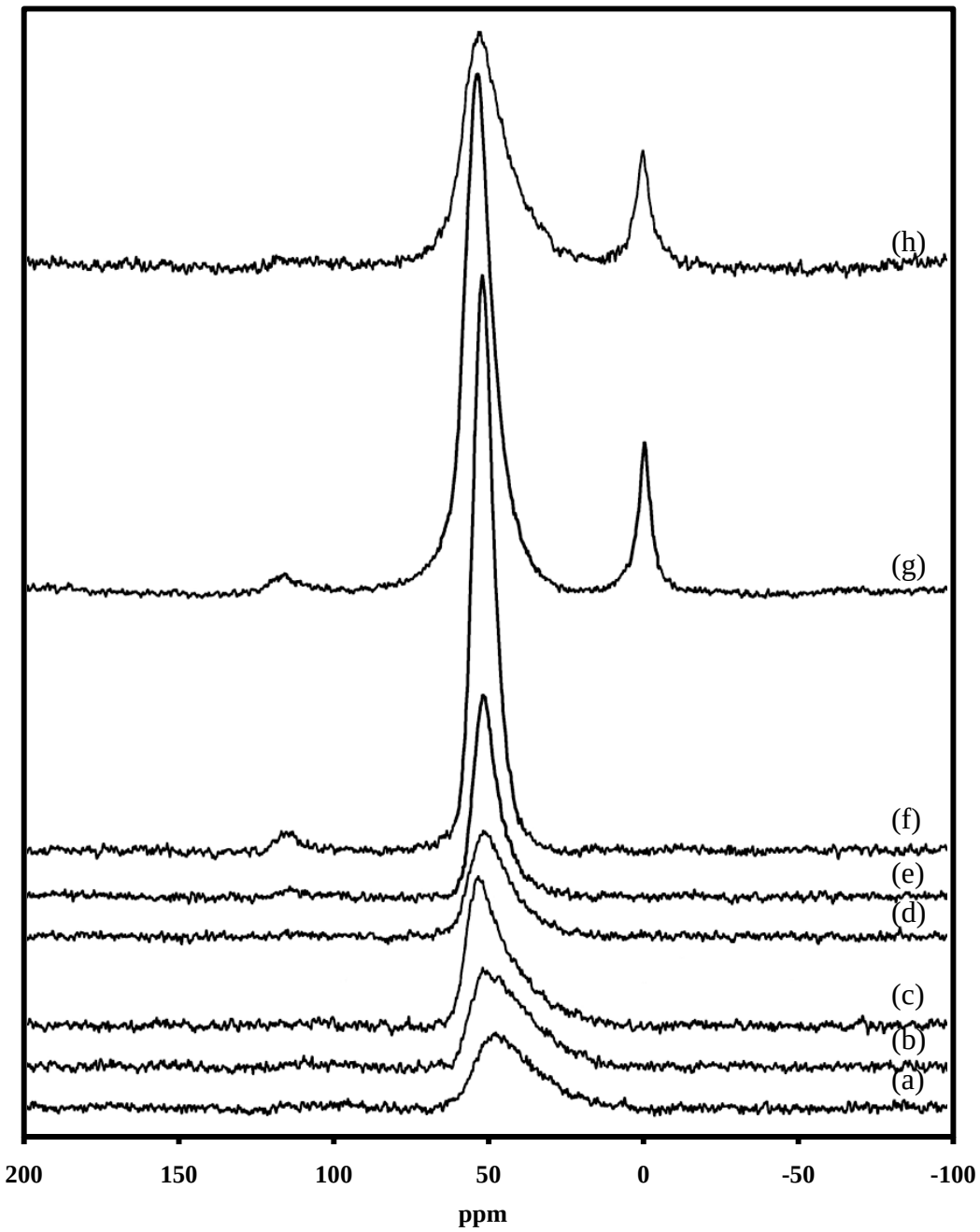

Figure 3.19 ^{27}Al-MAS-NMR spectra of calcined (a) h-BEA-M3-140-9, (b) h-BEA-M3-140-12, (c) h-BEA-M3-140-15, (d) h-BEA-M3-145-9, (e) h-BEA-M3-145-12, (f) h-BEA-M3-145-15, (g) h-BEA and (h) BEA.

3.2 Catalytic Cracking of Heavy Fuel Oil

To test the catalytic activity of prepared catalyst in this work, heavy fuel oil (HFO) was selected as feedstock.

3.2.1 Effect of Catalyst

The heavy fuel oil (HFO) was degraded over various catalysts: BEA, h-BEA, h-BEA-M3-140-9, h-BEA-M3-140-12 and h-BEA-M3-140-15 at 380°C for 40 min, heating rate 20°C/min, 10 wt% of catalyst to HFO. The thermal cracking was also tested in comparison. The values of %conversion and product yield for thermal and catalytic cracking of HFO over the various catalysts were shown in Table 3.7.

Table 3.7 Thermal and catalytic cracking of HFO at 380°C

	Thermal	BEA	h-BEA	h-BEA-M3-140-9	h-BEA-M3-140-12	h-BEA-M3-140-15
%Conversion (%wt)*	44.55	55.79	60.97	66.52	63.49	61.17
%Yield (%wt) *						
1.Gas	10.74	12.79	14.54	17.29	16.33	15.34
2. Liquid	33.82	43.01	46.43	49.22	47.15	45.53
- Distillate oil	0.42	1.83	3.62	0.17	0.32	0.60
- Heavy oil	33.40	41.18	42.80	49.05	46.83	49.93
3.Residue	55.44	44.21	39.03	33.49	36.52	39.13
Liquid fraction density (g/cm^3)	0.83	0.83	0.85	0.85	0.84	0.85

Condition: reaction temperature of 380ºC, reaction time of 40 min, 10 wt% of catalyst to HFO and N_2 flow of 20 cm^3/min. *Deviation within ±0.60 for conversion, ±0.80 for yield of gas fraction, ±0.60 for yield of liquid fraction, and ±0.50 for yield of residue.

The BEA, h-BEA and h-BEA-M3-140-t_{crys}, exhibited a high performance with the conversion of HFO over 55% in all reaction with small amount of residue. The conversion and obtained product yield were higher than those of thermal cracking which gave conversion of 44.55%. This result was caused by the acidity and surface area of the catalysts enhancing the cracking activity. Considering the product yields, thermal cracking and catalytic cracking of HFO over zeolite beta and enlarged-pore zeolite beta catalysts produced higher yield of liquid fraction than gas fraction. The yields of liquid fraction were in range of 33-49% while yields of gas fraction were in range of 10-17%.

Comparing the degradation of HFO over enlarged-pore zeolite beta (h-BEA and h-BEA-M3-140-t_{crys} samples) and comparative zeolite beta, the conversion and products yields were increased whereas the amounts of residue fractions were decreased. This result may be affected by pore diameter. Due to the increasing of pore diameter, the large molecules in HFO can effectively enter and diffuse inside the pore of enlarged-pore zeolite beta and degrade inside the pore to increase conversion and product yields [69].

When comparing the degradation of HFO over the enlarged-pore zeolite beta between the h-BEA and the h-BEA-M3-140-t_{crys}, the conversion and products yields were more increased, whereas the amounts of residue fractions were decreased. The result may be affected by pore diameter, coexistence of ZSM-12 phase and also acidity of catalysts. The effect of pore diameter was as described earlier. For the coexistence of ZSM-12 phase, the ZSM-12 exhibits characteristic properties of the one-dimensional 12-membered ring (diameter of 5.6×6.2 Å) [70] leading to the diffusion of large molecule to access and degrade at the active site inside the pore.

For the acidity of catalysts, although the h-BEA samples have higher acidity than h-BEA-M3-140-t_{crys}, some aluminum species of the h-BEA were not only in the tetrahedral framework but also in octrahedral non-framework, inert species, as followed in Section 3.1.4. It resulted in the reduction of catalytic activity of the h-BEA. Thus, the h-BEA-M3-140-t_{crys} samples provided more conversion and products yields than the h-BEA.

The liquid product was then distilled to separate light oil from heavy oil. It was found that h-BEA-M3-140-9, h-BEA-M3-140-12 and h-BEA-M3-140-15

catalysts produce more heavy oil and less distillate oil, comparing with the BEA and h-BEA, which produces more distillate oil. It can be concluded that with increasing pore diameter, the selectivity to distillate oil is decreased. Since enlarged-pore zeolite betas had larger pore diameter, the large molecules of products formed within the pores can be more escaped from the pore leading to high composition of heavy oil in liquid product [71].

Figure 3.20 illustrated the relationship between the cumulative volume of liquid fraction with time. It was found that the cumulative volume of liquid fractions per minute of all catalysts were higher than thermal cracking. The volume of collected liquid fraction was ordered by h-BEA-M3-140-9 > h-BEA-M3-140-12 > h-BEA > h-BEA-M3-140-15 > BEA.

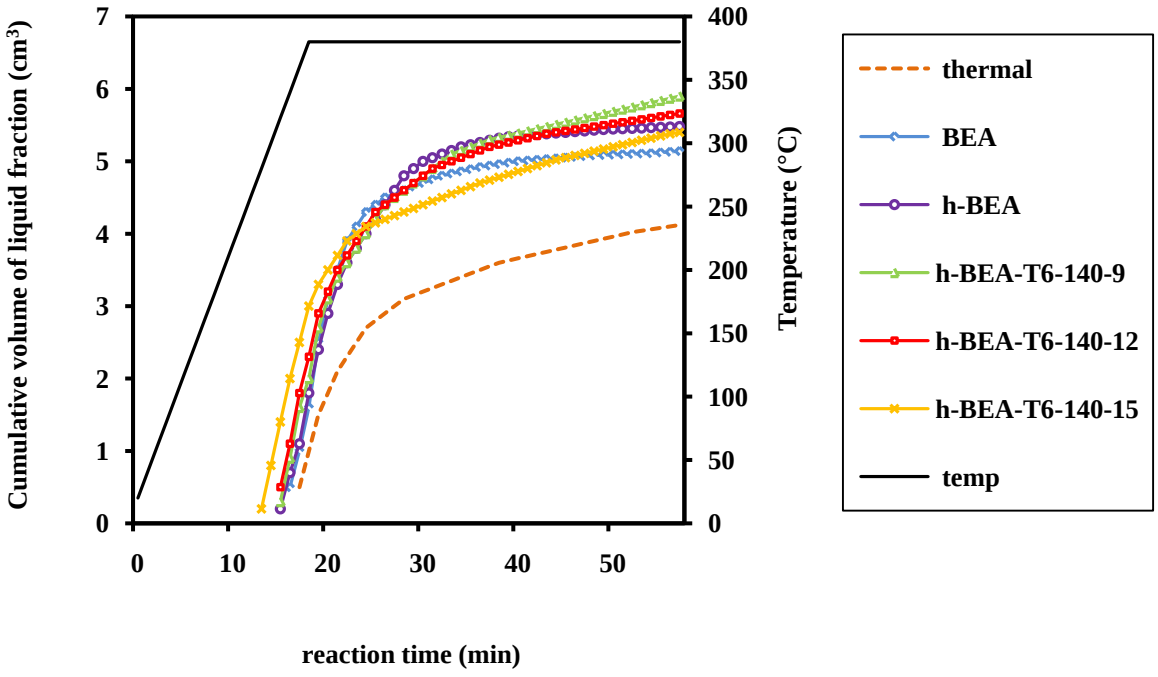

Figure 3.20 Cumulative volume of liquid fraction obtained by thermal and catalytic cracking of HFO over various catalysts.

Distribution of gas products in thermal and catalytic cracking reaction at 380°C was shown in Figure 3.21. Considering only gases were normally C_1 through C_5, the major components for thermal cracking were methane, ethane, propane, cyclopropane, propylene, i-butane, 1-butene, 1,3-butadiene, methyl acetate. However,

the vapor of C_5^+ (liquids at ambient condition) which has higher boiling point than that of C_5 (n-pentane) was obviously detected in the high amount. The gas fraction from catalytic cracking over BEA contained 1,3-butadiene and C_5^+ while the gas fraction from catalytic cracking over enlarged-pore zeolite beta catalysts (h-BEA and h-BEA-M3-140-t_{crys}) contained methane, ethane, propane, cyclopropane, 1,3-butadiene, methyl acetate and C_5^+. From distribution plots of HFO cracking over enlarged-pore zeolite beta, it seems to be that when increased pore diameter the selectivity of 1,3-butadiene decreased while light gas (C_1-C_3) increased. The results were affected by pore size and acidity of catalyst. When increasing pore diameter, the heavy gas molecule can move through the pore and degrade at the active site of catalyst, providing the lighter gas fraction, compared to small pore diameter [72].

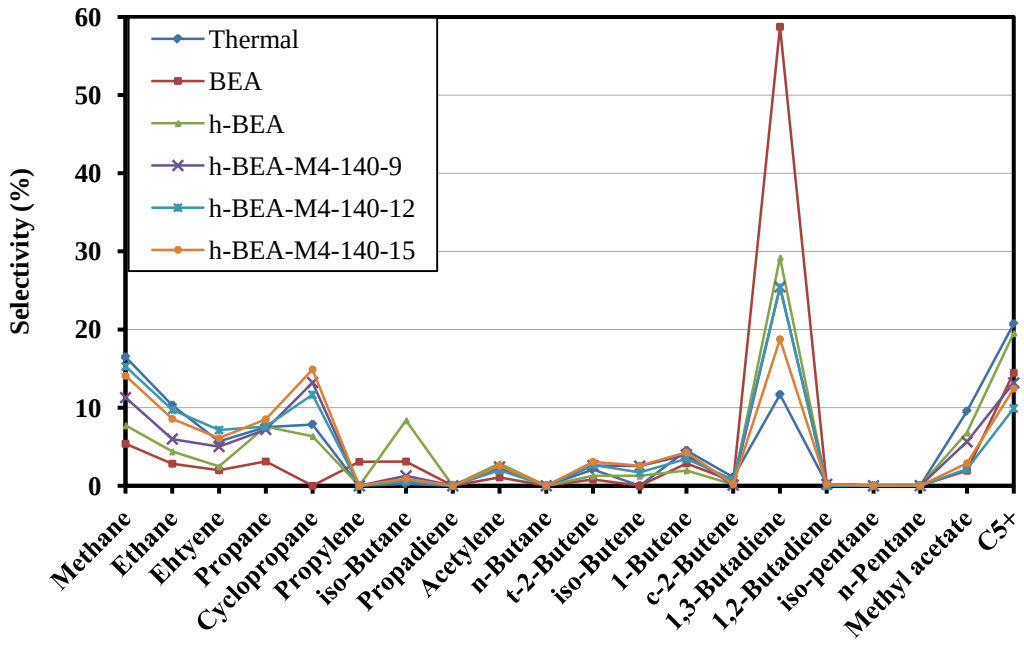

Figure 3.21 Distribution of gas fraction obtained by thermal cracking and catalytic cracking of HFO over BEA, h-BEA and h-BEA-M3-140-t_{crys} catalysts.

The compositions of distillate oil and heavy oil were analyzed by GC. Since the h-BEA-M3-140-9, h-BEA-M3-140-12 and h-BEA-M3-140-15 provided low quantity of distillate oil, the product distributions of distillate oil obtained by thermal cracking and catalytic cracking over BEA and h-BEA at 380°C were only

investigated and presented in Figure 3.22. Liquid products were investigated with the C_{np} value which relates to the boiling point of normal paraffin. For thermal cracking the liquid fraction was in range of C_5 to C_{14} but mainly in C_7 to C_{10}. For catalytic cracking, it was found that the distillate oil over BEA and h-BEA catalyst was also composed of C_5-C_{14} hydrocarbons which were similar to hydrocarbons in the gasoline range, as shown in Figure 3.23. Considering catalytic cracking over BEA, the distillate oil components were mainly in the range of C_6 to C_9 while over h-BEA, the distillate oil components were mainly in the range of C_6 to C_{10}. These result showed that BEA and h-BEA exhibited good catalytic activity for producing light hydrocarbon liquids, compared to thermal cracking. The h-BEA showed a range of larger hydrocarbon than that of BEA. It was caused by effect of pore size as above-mentioned. The composition of heavy oil was mainly distributed in C_{10}-C_{20}, or kerosene range, as shown in Figure 3.24.

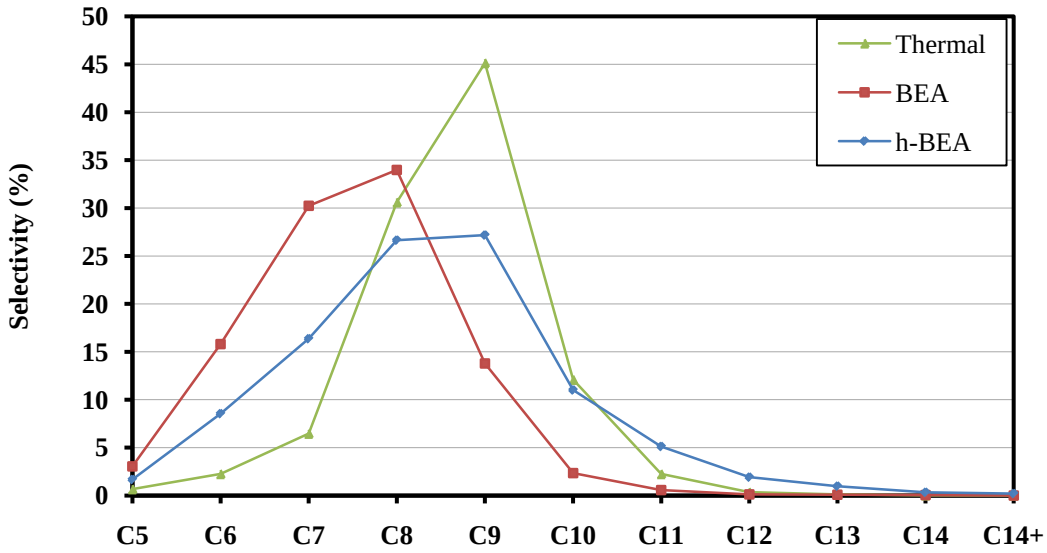

Figure 3.22 Carbon number distribution of distillate oil obtained by thermal cracking and catalytic cracking of HFO over BEA and h-BEA catalysts.

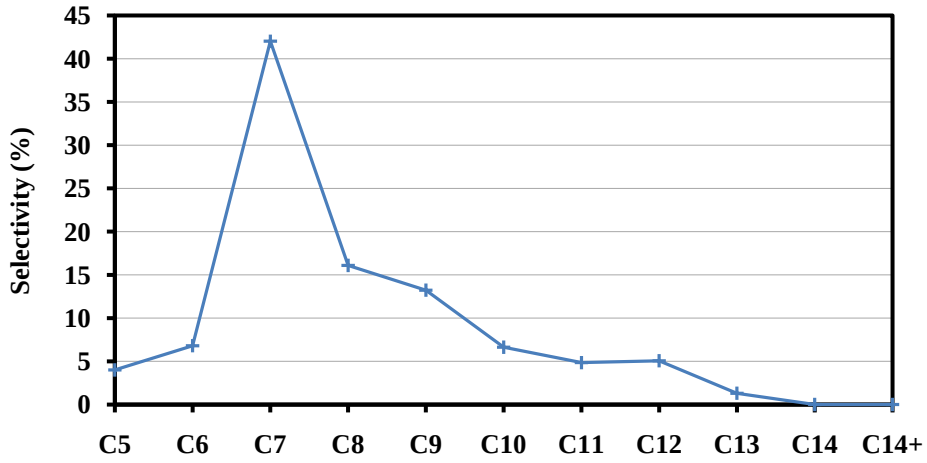

Figure 3.23 Carbon number distribution of standard gasoline.

It can be concluded that the synthesized enlarged-pore zeolite betas had more efficiency in catalytic cracking of HFO than comparative zeolite beta and thermal cracking. The enlarged-pore zeolite beta (h-BEA) provided high yield of distillate oil in the range of gasoline while the h-BEA-M3-140-t_{crys} provided high yield of heavy oil in the range of kerosene. Thus, the enlarged-pore zeolite betas can be adapted for catalytic cracking of HFO depending on customaries requirement. In this work, the researcher is focusing on the light hydrocarbon in gasoline range. Therefore, the h-BEA was chosen for further studies.

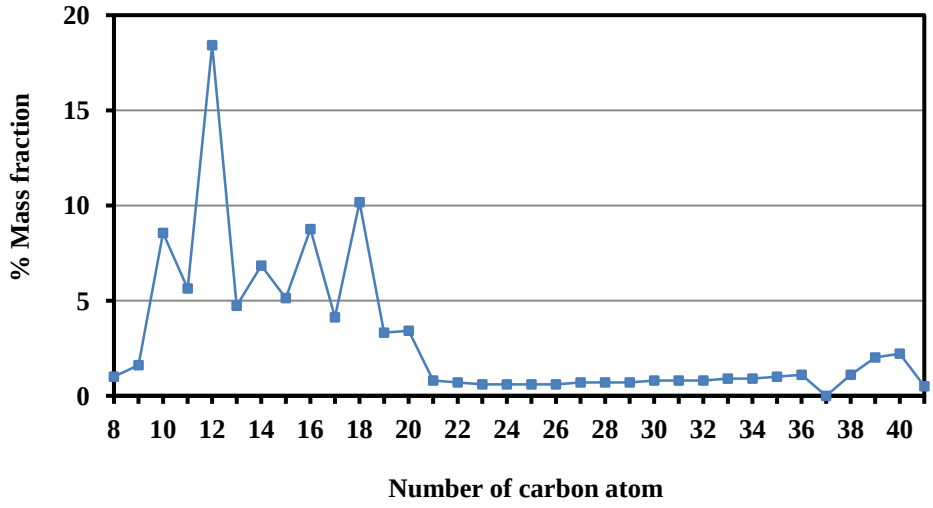

Figure 3.24 Carbon number distribution of heavy oil fraction obtained by catalytic cracking of HFO over h-BEA-M3-140-12 sample.

3.2.2 Effect of Reaction Temperature

The h-BEA catalysts were used to investigate the effect of temperature on its activity. The values of %conversion and the product yields from catalytic cracking of HFO over h-BEA catalysts at 330, 350, 380 and 410°C were shown in Table 3.8. The value of %conversion of h-BEA was continually increased from 35.68% to 76.26% when reaction temperature was increased from 330°C to 410°C. The yields of both gas and liquid products are also increased. The products were mainly in liquid fraction and the minor products were gas fraction. The liquid fractions obtained from the reaction at 330°C and 350°C, whereas brown for 380°C and dark brown for 410°C. Considering the yield of distillate oil, it was found that at the temperature of 380°C, the highest selectivity and yield of distillate oil were obtained. Therefore, reaction temperature of 380°C was chosen to study effect of reaction time in catalytic cracking of HFO.

Table 3.8 Catalytic cracking of HFO over h-BEA at various reaction temperatures

	Reaction temperature (°C)			
	330	350	380	410
%conversion*	35.68	41.21	60.97	76.26
%yield of product*				
1. Gas	4.95	5.84	14.54	22.54
2. Liquid	30.73	35.36	46.43	53.72
- Distillate oil	1.28	1.65	3.62	3.38
- Heavy oil	29.62	33.71	42.80	50.35
3. Residue	64.32	58.79	39.03	23.74
Liquid fraction density (g/cm^3)	0.84	0.83	0.85	0.86

Condition: reaction time for 40 min, 10 wt% of catalyst to HFO and N_2 flow of 20 cm^3/min. *Deviation within ±0.60 for conversion, ±0.70 for yield of gas fraction, ±0.90 for yield of liquid fraction, and ±0.60 for yield of residue.

Figure 3.25 showed the relationship between the cumulative volume of liquid fractions with time obtained by catalytic cracking of HFO over h-BEA samples at reaction temperature of 330, 350, 380 and 410°C. When the temperature was increased, the total volume of liquid fractions was in order: 410°C >380°C >350°C > 330°C.

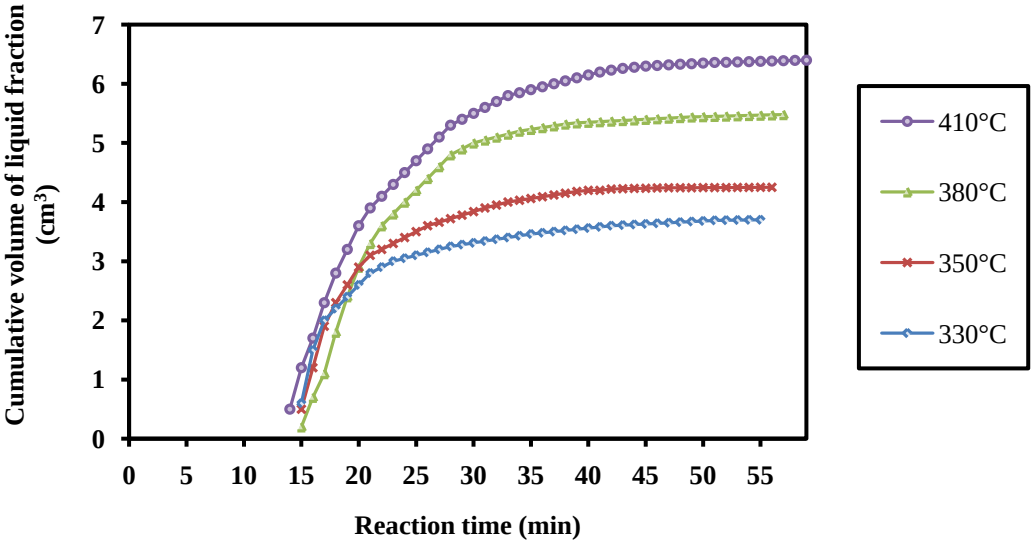

Figure 3.25 Cumulative volume of liquid fraction obtained by catalytic cracking of HFO over h-BEA sample at different reaction temperatures.

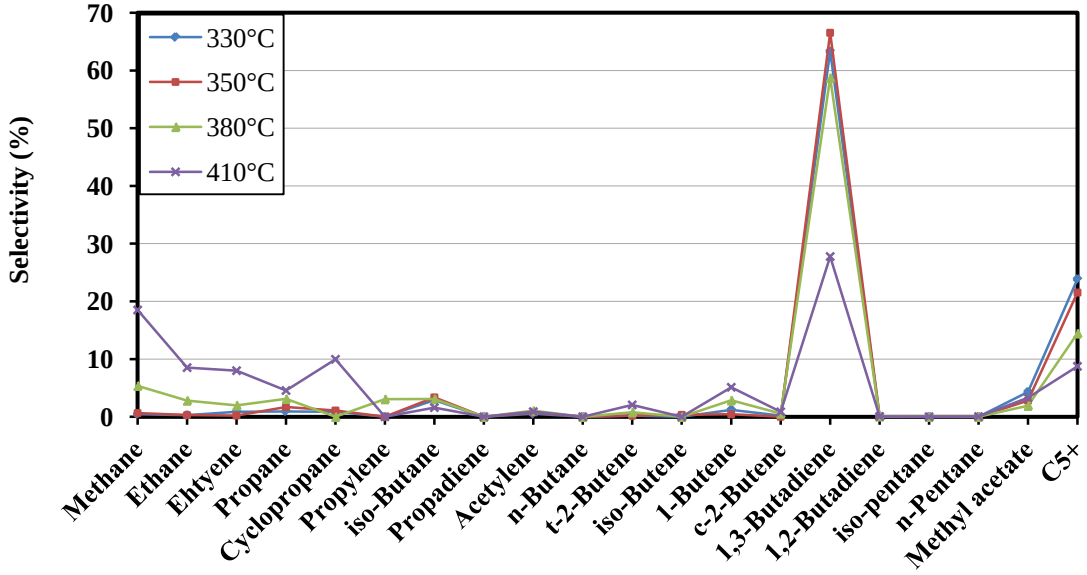

Figure 3.26 Distribution of gas fraction obtained by catalytic cracking of HFO over h-BEA catalyst at different reaction temperatures.

Figure 3.26 showed distribution of gas fraction obtained by catalytic cracking of HFO over h-BEA sample at 330, 350, 380 and 410°C. The major components for catalytic cracking over h-BEA was C_4 (1,3-butadiene) and C_5^+. The results were found that reaction temperature effected distribution of gas fraction products. When the reaction temperature increased, the gas fraction of lighter hydrocarbon (C_1-C_3) increased, while that of heavier hydrocarbon (1-butene and 1,3-butadiene) decreased. The increasing of volatile components by effect of temperature could be caused by the thermal stability of large molecule. Hydrocarbons are reduced their thermal stability with increasing temperature [73-74]. The C-C bonds were cracked more easily at 410°C than at lower temperature, and it resulted in higher yield of volatile products.

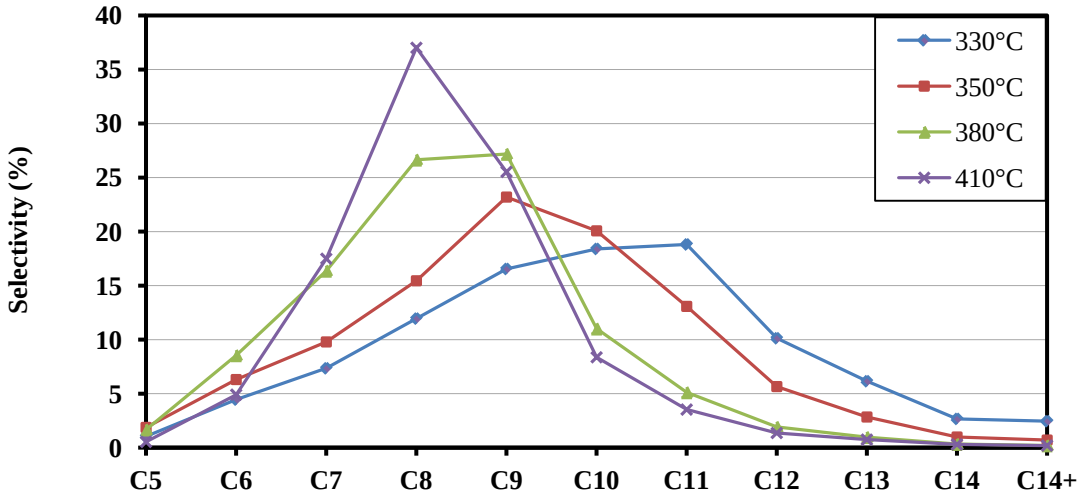

Figure 3.27 Carbon number distribution of distillate oil obtained by catalytic cracking of HFO over h-BEA catalyst at different reaction temperatures.

Figure 3.27 showed product distribution of distillate oil obtained by catalytic cracking of HFO over h-BEA catalysts at 330, 350, 380 and 410°C. It was found that the distillate oil components at 330°C were mainly in the range of C_9 to C_{12} while at 350°C were mainly in the range of C_9 to C_{10}. When the reaction temperature was increased to 380°C and 410°C, the liquid fractions of lighter hydrocarbon (C_8 to C_9) were increased while that of heavier hydrocarbon (C_{10}-C_{12}) decreased. This result indicated that liquid product distribution depended on temperature. Moreover, the higher quantity of distillate oil was obtained at the temperature of 380°C.

3.2.3 Effect of Reaction Time

The h-BEA catalysts were used to investigate the effect of time on its activity. Table 3.9 summarized the value of %conversion and the %yields obtained in the catalytic cracking of HFO over h-BEA catalysts at 380°C with reaction time for 30, 40 and 50 min. The value of %conversion of h-BEA continually increased from 55.07% to 61.05% when reaction temperature increased from 30 to 50 min. That indicated both conversion and the yields (gases and liquids) were affected by reaction time. The increasing of product yields was caused by the thermal stability of large hydrocarbon molecules, since C-C bond strength of hydrocarbons was weaken with increasing reaction time [75]. Thus, the large hydrocarbon molecules were consequently degraded to light product.

Table 3.9 Catalytic cracking of HFO over h-BEA sample at 380°C various reaction time

	Reaction time (min)		
	30	40	50
%conversion*	55.07	60.97	61.05
%yield of product*			
1. Gas	9.49	14.54	13.5
2. Liquid	45.58	46.43	47.55
- Distillate oil	3.67	3.62	3.02
- Heavy oil	41.91	42.8	43.53
3. Residue	45.63	39.03	35.45
Liquid fraction density (g/cm^3)	0.85	0.85	0.86

Condition: reaction temperature at 380°C, 10 wt% of catalyst to HFO and N_2 flow of 20 cm^3/min. *Deviation within ±0.40 for conversion, ±0.60 for yield of gas fraction, ±0.20 for yield of liquid fraction, and ±0.40 for yield of residue.

Figure 3.28 showed the relationship between the cumulative volume of liquid fraction with time obtained by catalytic cracking of HFO over h-BEA samples at reaction time for 30, 40 and 50 min. When the time was increased, the total volume of liquid fractions was slightly difference in order of 50≈40 >30. It was indicated that after 40 min, cracking reaction was nearly in equilibrium. Since the reaction time at 40 min gave high distillate oil comparing to reaction at 50 min, it was chosen to be a suitable reaction time for further studies in this work.

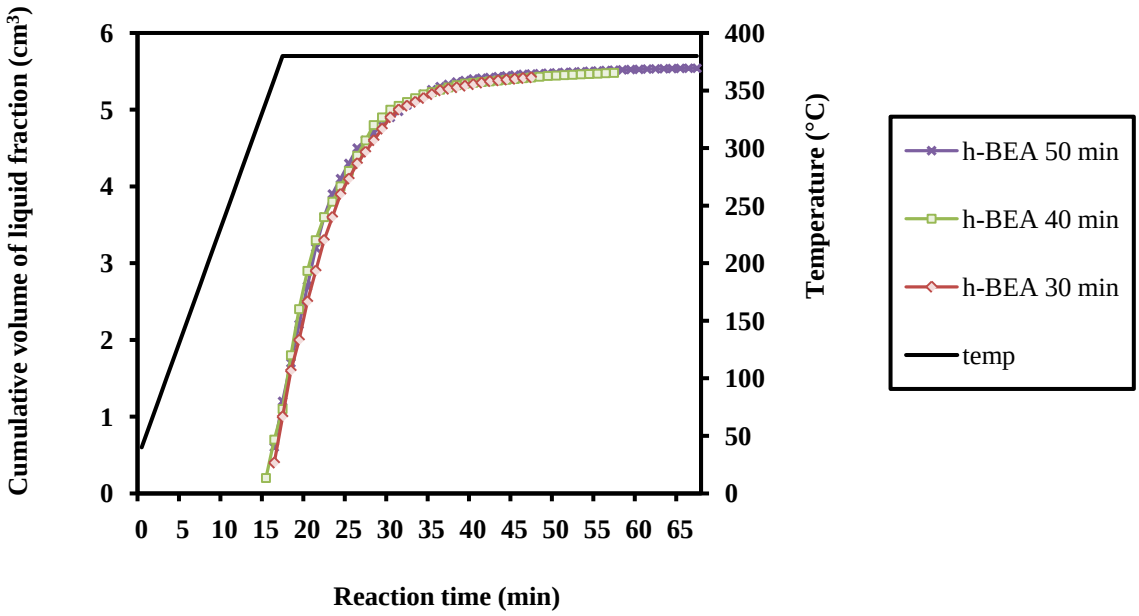

Figure 3.28 Cumulative volume of liquid fraction obtained by catalytic cracking of HFO over h-BEA sample at different reaction time.

Distribution of gas products in catalytic cracking reaction at 380°C with three reaction times were shown in Figure 3.29. The major components for catalytic cracking over h-BEA with reaction time for 40 and 50 min were 1,3-butadiene and C_5^+ while the gas fraction with reaction time for 30 min mainly contained propadiene, 1,3-butadiene, methyl acetate and C_5^+. It was noticed that reaction time for 30 min provided lighter gas fractions and less amount of 1,3-butadiene. This may be because at short period of reaction time, the hydrocarbon molecules had less time to react with active site of catalyst. The lighter hydrocarbon molecules, which were easily degraded, moved out quickly from catalyst. When increased reaction time to 40 min

and 50 min, the heavy hydrocarbon molecules had more time to react with catalyst and produced more products leading to high yield. Therefore, in the case of reaction time for 40 min, 1,3-butadiene was increased more than 30 min. But after 40 min, the heavy gases were degraded to light gases leading to increasing of light gas and less 1,3-butadiene compared to 40 min. It was indicated that when increasing reaction time, large hydrocarbon molecules were broken to small hydrocarbon molecules.

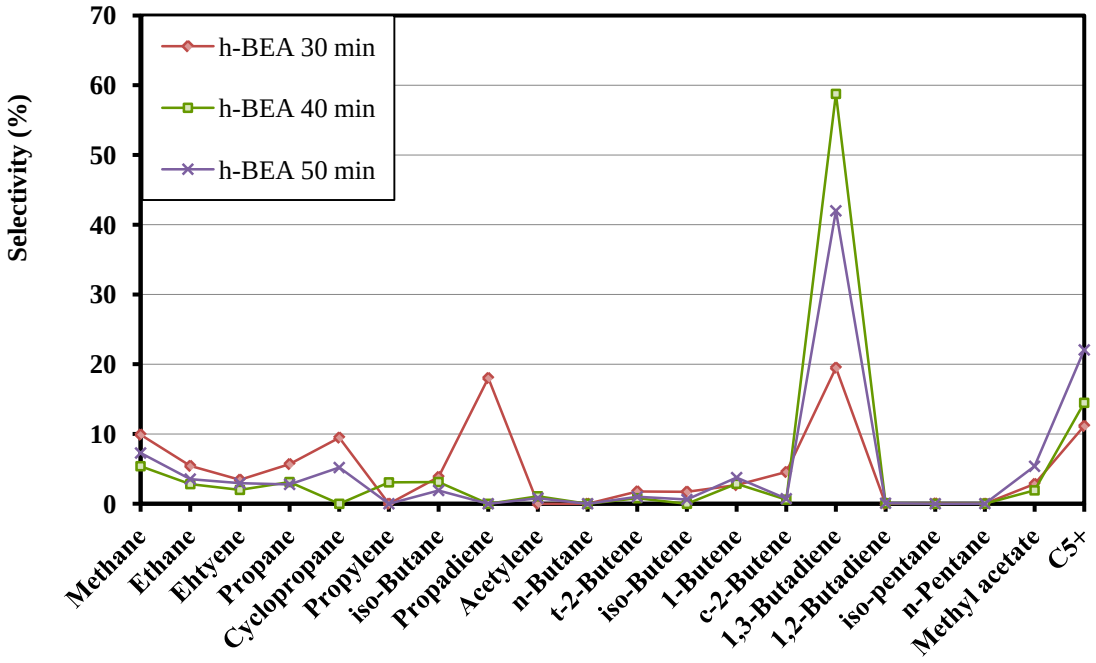

Figure 3.29 Distribution of gas fraction obtained by catalytic cracking of HFO over h-BEA catalyst with different reaction time.

Figure 3.30 showed product distribution of distillate oil obtained by catalytic cracking of HFO over h-BEA catalysts at 380 °C with reaction time for 30, 40 and 50 min. It was found that the distillate oil components with reaction temperature for 30 min were mainly in the range of C_8 to C_{11} while at 40 min were mainly in the range of C_8 to C_9. When the reaction time was increased to 50 min, the liquid fractions of lighter hydrocarbon (C_7 to C_9) increased while that of heavier hydrocarbon (C_9-C_{12}) decreased. This result indicated that liquid product distribution depended on reaction time, as described earlier.

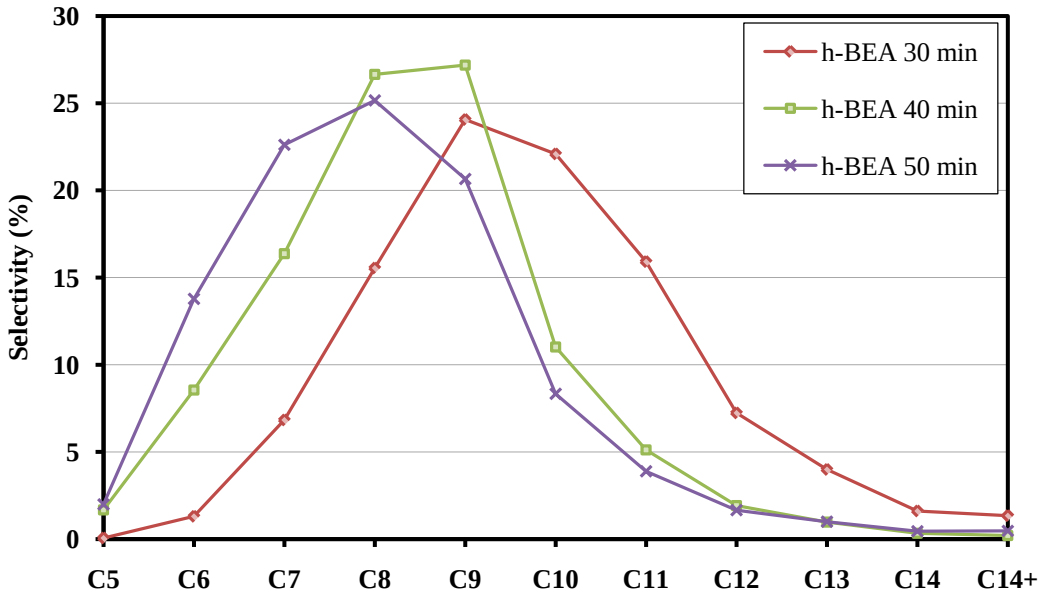

Figure 3.30 Carbon number distribution of distillate oil obtained by catalytic cracking of HFO over h-BEA catalyst with different reaction time.

3.2.4 Effect of Heavy Fuel Oil to Catalyst Ratio

Values of conversion and product yield obtained by catalytic cracking of HFO at 380°C over h-BEA catalyst with different amounts of 5 wt%, 10 wt% and 20 wt% to HFO were shown in Table 3.10. The high conversion value obtained from 20 wt% catalyst amount was reduced from 68.33% to 49.08% when catalyst amount was reduced to 5 wt%. It was indicated that the conversion strongly depended on the catalyst content. In addition, yields of gas and liquid fractions decreased when amount of catalyst was reduced. The yield of distillate oil and heavy oil in liquid fraction were also affected by catalyst content and was ordered by amount of catalyst as 20 wt% > 10 wt% > 5 wt%. Generally, the decreasing of catalyst amount leads to the reducing of acidity and product yields [76]. On the other hand, the amount of residue was increased.

Table 3.10 Catalytic cracking of HFO over h-BEA sample at 380°C various amounts of catalyst

	Catalyst amount to HFO		
	5 wt%	10 wt%	20 wt%
%conversion*	49.08	60.97	68.33
%yield of product*			
1. Gas	9.4	14.54	16.38
2. Liquid	39.68	46.43	51.95
- Distillate oil	1.83	3.62	6.88
- Heavy oil	41.18	42.80	45.07
3. Residue	50.92	39.03	31.67
Liquid fraction density (g/cm^3)	0.85	0.85	0.81
Distillate oil to catalyst amounts ratio	2.76	3.62	3.44

Condition: reaction temperature at 380°C, reaction time for 40 min and N_2 flow of 20 cm^3/min. *Deviation within ±0.60 for conversion, ±0.50 for yield of gas fraction, ±0.20 for yield of liquid fraction, and ±0.60 for yield of residue.

Figure 3.31 showed the relationship between the cumulative volume of liquid fraction with time obtained by catalytic cracking of HFO over h-BEA with various catalyst amounts. When catalyst amount was increased, the cumulative volume of liquid fractions per minute of liquid formation and total volume of liquid fraction were in order: 20 wt% > 10 wt% > 5 wt%, due to acidity of catalyst as mentioned above.

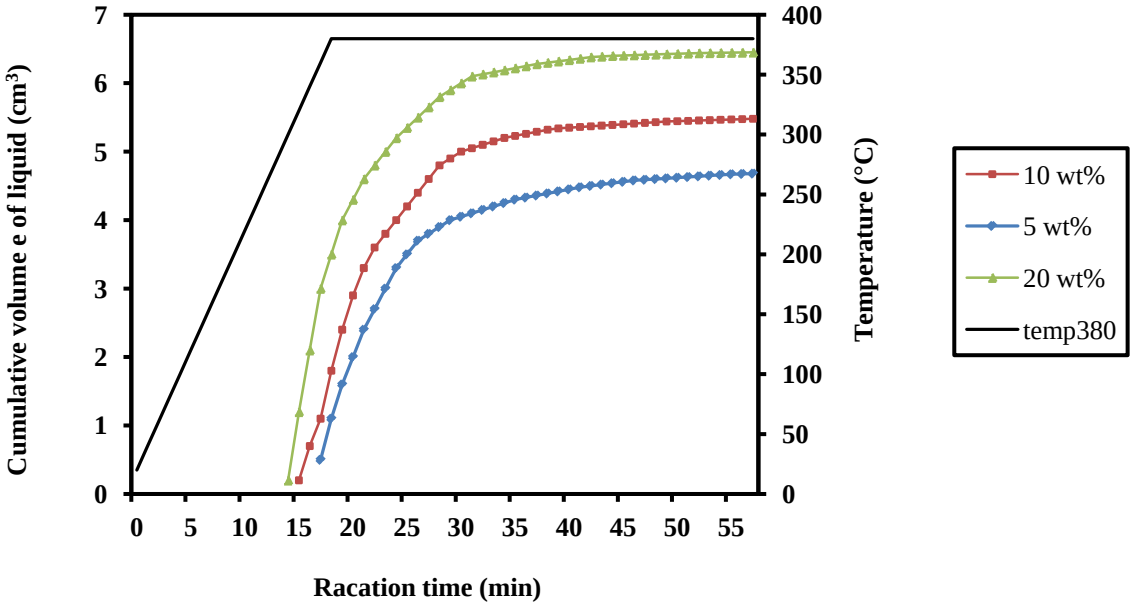

Figure 3.31 Cumulative volume of liquid fraction obtained by catalytic cracking of HFO over h-BEA sample various catalyst amounts.

Distribution of gas products in catalytic cracking reaction at 380°C with various catalyst amounts were shown in Figure 3.32. The mainly gas fraction from HFO cracking over h-BEA with 5 wt% catalyst amount were 1,3-butadiene and C_5^+ which are similar to 10 wt% and 20 wt% catalyst amount. It can be concluded that HFO to catalyst ratios did not affect to gas product distribution.

Figure 3.33 showed product distribution of distillate oil obtained by catalytic cracking of HFO over h-BEA catalysts at 380 °C with various catalyst amounts. It was found that the product distribution of liquid phase for 5 wt%, 10 wt% and 20 wt% catalyst amounts were different. The obtained liquid products from 10 wt% catalysts were mainly in the range of C_7 to C_{10}. When catalyst amount was decreased to 5 wt%, the liquid products in the range of C_8 to C_9 were increased and the selectivity of C_5 to C_6 was decreased. On the other hand, when catalyst amount was increased to 20 wt%, the liquid products in the range of C_8 to C_9 were decreased while the selectivity of C_5 to C_7 was clearly increased. It indicated that the volume of light liquid hydrocarbon was affected by increasing of catalyst amounts due to the acidity. It seems to be that 20 wt% catalyst amounts was the best condition in this work, however when considering the yield of distillate oil to catalyst amounts ratio, it was found that 10

wt% catalyst amount yielded the highest ratio. Thus, in this work, 10 wt% catalyst amount was used for the best condition according to the higher %conversion and selectivity to light liquid hydrocarbon.

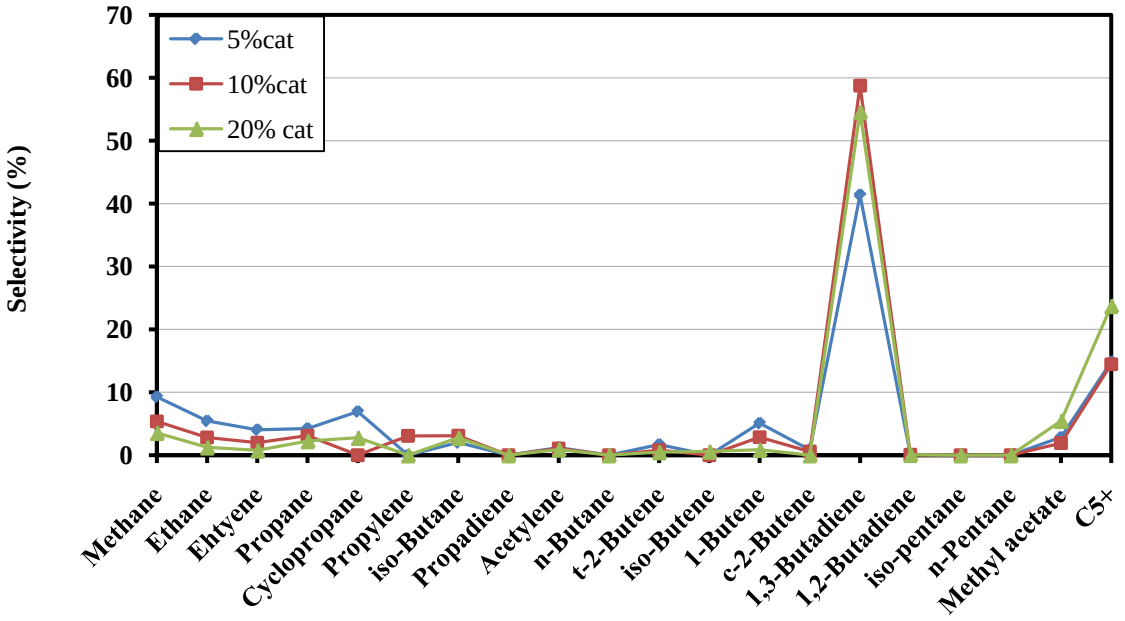

Figure 3.32 Distribution of gas fraction obtained by catalytic cracking of HFO over h-BEA sample with various catalyst amounts.

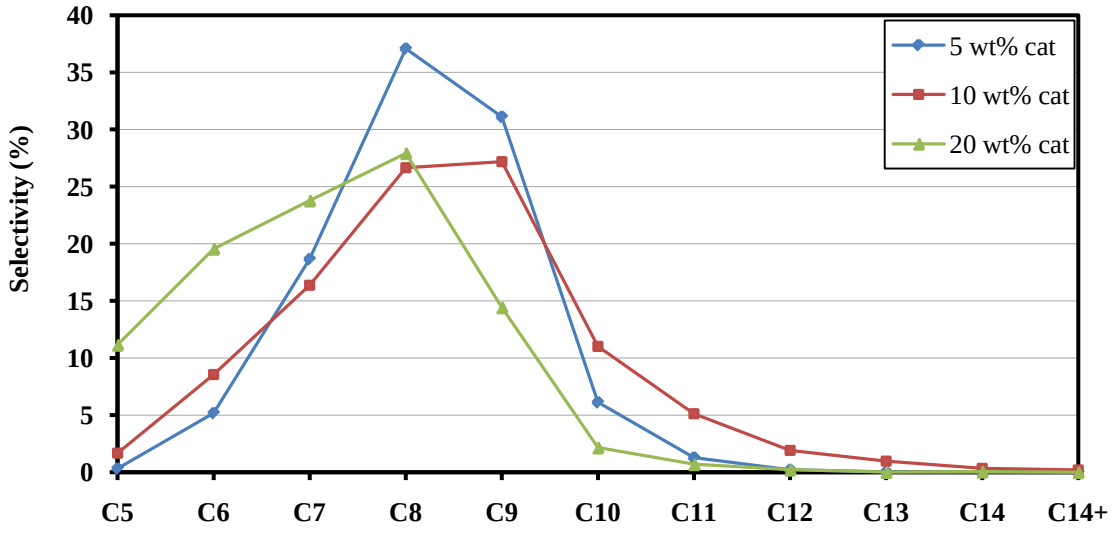

Figure 3.33 Carbon number distribution of distillate oil obtained by catalytic cracking of HFO over h-BEA sample with various catalyst amounts.

From the experimental investigation, it had been concluded that the catalytic cracking at 380°C for 40 min, using 10 wt% of catalyst and N_2 flow of 20 cm^3/min, is the optimal condition for heavy fuel oil cracking over h-BEA in this study.

3.3 Catalyst Regeneration

The spent h-BEA catalysts from HFO cracking at the reaction temperature of 380˚C were regenerated by calcination in air at 550°C for 10 h. The regenerated catalyst was characterized by XRD, SEM, N_2 sorption and tested for its activity by catalytic cracking of HFO at the reaction temperature of 380°C for 40 min. The reaction was performed in the same way as what described in section 2.5.

3.3.1 Powder X-ray Diffraction (XRD)

The used h-BEA was turned to white powder after calcination at 550°C for 10 h. The XRD pattern of the regenerated catalyst was presented in Figure 3.34, compared with the calcined fresh catalyst. The crystallinity of zeolite beta peaks was not different between the regenerated and the fresh h-BEA.

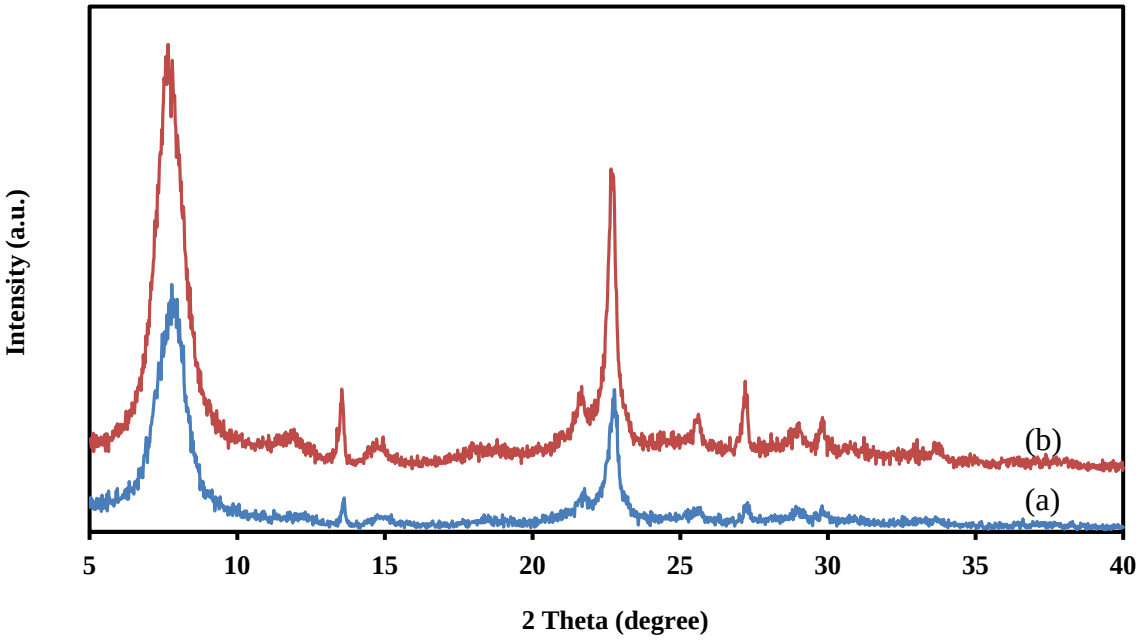

Figure 3.34 XRD patterns of calcined samples: (a) regenerated h-BEA and (b) calcined fresh h-BEA.

3.3.2 Nitrogen Adsorption-Desorption

The N_2 adsorption-desorption isotherms of the regenerated h-BEA was shown in Figure 3.35. The regenerated catalyst exhibited the characteristic isotherm of microporous material and gave specific surface area of 720 m^2g^{-1} and pore diameter of 0.61 nm. The physical properties of regenerated catalyst were not different from the fresh catalyst which gave specific surface area and pore diameter of 721 m^2g^{-1} and 0.62 nm, respectively.

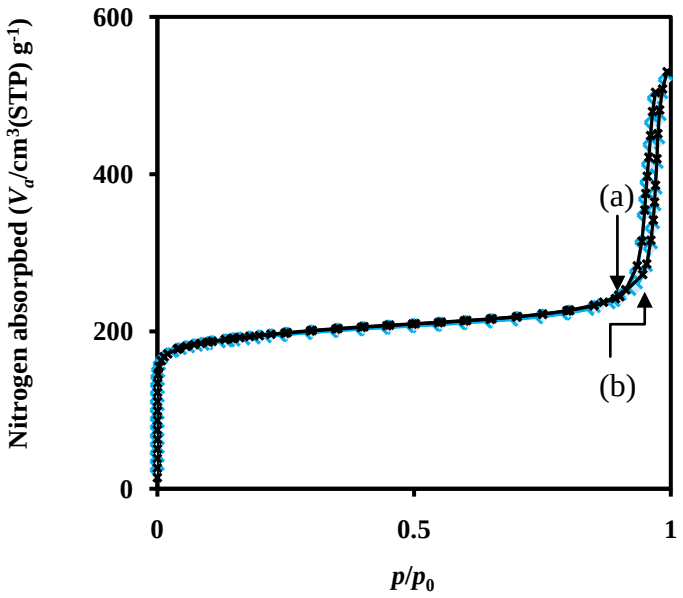

Figure 3.35 The N_2 adsorption-desorption isotherms (a) fresh h-BEA and (b) regenerated h-BEA.

3.3.3 Scanning Electron Microscope (SEM)

SEM Image of the regenerated h-BEA sample was shown in Figure 3.36. After the cracking, the regenerated h-BEA sample showed sphere particles as same as the fresh catalyst which had been shown in Figure 3.9 (c).

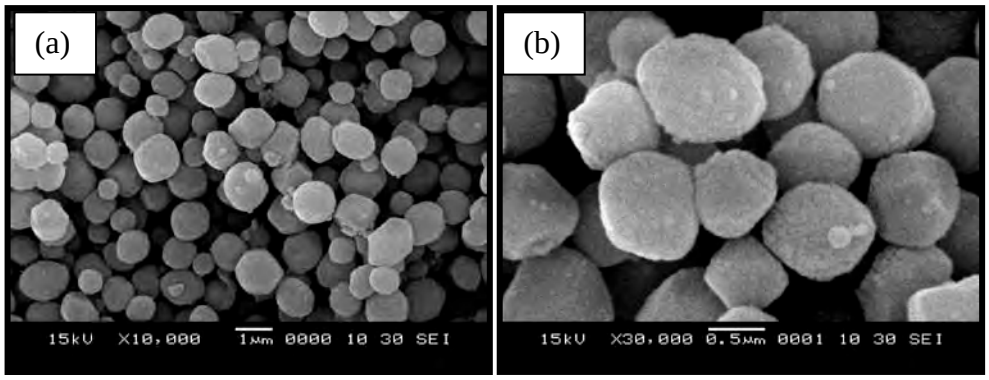

Figure 3.36 SEM images of the regenerated h-BEA with different magnification (a) x10,000 and (b) x30,000.

3.3.4 Activity of Regenerated Enlarged-Pore Zeolite Beta in Heavy Fuel Oil Cracking

Table 3.10 summarized the values of %conversion and %yield obtained in the catalytic cracking of HFO over regenerated h-BEA at 380°C for 40 min. The both conversion and product yield of regenerated h-BEA were slightly decreased from fresh catalyst. The slightly lower yield of distillate oil was obtained by regenerated catalyst comparing to the fresh catalyst. The specific surface area and pore diameter of catalyst is important roles. The large hydrocarbon molecules diffused through the pore and degraded on surface area of fresh catalyst. The regenerated catalyst showed almost equal surface area but slightly smaller pore diameter leading to little lower selectivity to distillate oil.

Figure 3.37 showed the relationship between the cumulative volume of liquid fraction with time obtained by catalytic cracking of HFO over fresh h-BEA and regenerated h-BEA samples. The cumulative volume of liquid fraction per minute of liquid formation had no significant different between fresh and regenerated catalysts. The regenerated catalyst provided slightly lower volume of liquid fraction than fresh catalyst due to pore diameter as described mentioned above.

Table 3.11 Catalytic cracking of HFO over fresh h-BEA and regenerated h-BEA samples at 380°C

	Regenerated h-BEA	Fresh h-BEA
%conversion*	58.27	60.97
%yield of product*		
1. Gas	12.49	14.54
2. Liquid	45.78	46.43
- Distillate oil	3.39	3.62
- Heavy oil	42.39	42.80
3. Residue	41.73	39.03
Liquid fraction density (g/cm^3)	0.85	0.85

Condition: 10 wt% of catalyst to HFO, N_2 flow of 20 cm^3/min, reaction temperature at 380°C and reaction time of 40 min. *Deviation within ±0.60 for conversion, ±0.50 for yield of gas fraction, ±0.20 for yield of liquid fraction, and ±0.60 for yield of residue.

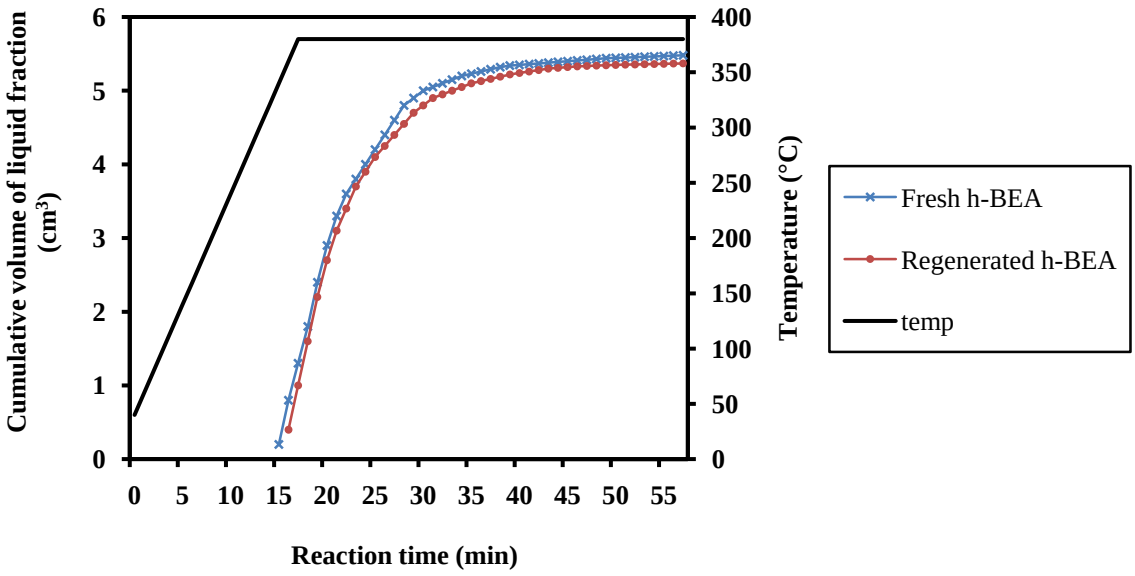

Figure 3.37 Cumulative volume of liquid fraction obtained by catalytic cracking of HFO over h-BEA and regenerated h-BEA samples.

Distribution of gas components catalytic cracking reaction over fresh h-BEA and regenerated h-BEA at 380°C for 40 min were shown in Figure 3.38. The major components for catalytic cracking over fresh h-BEA contained 1,3-butadiene and C_5^+ while the gas fraction of regenerated h-BEA were cyclopropane, 1,3-butadiene and C_5^+. This result may be due to pore diameter. The smaller pore diameter of regenerated h-BEA enhanced the selectivity of smaller products.

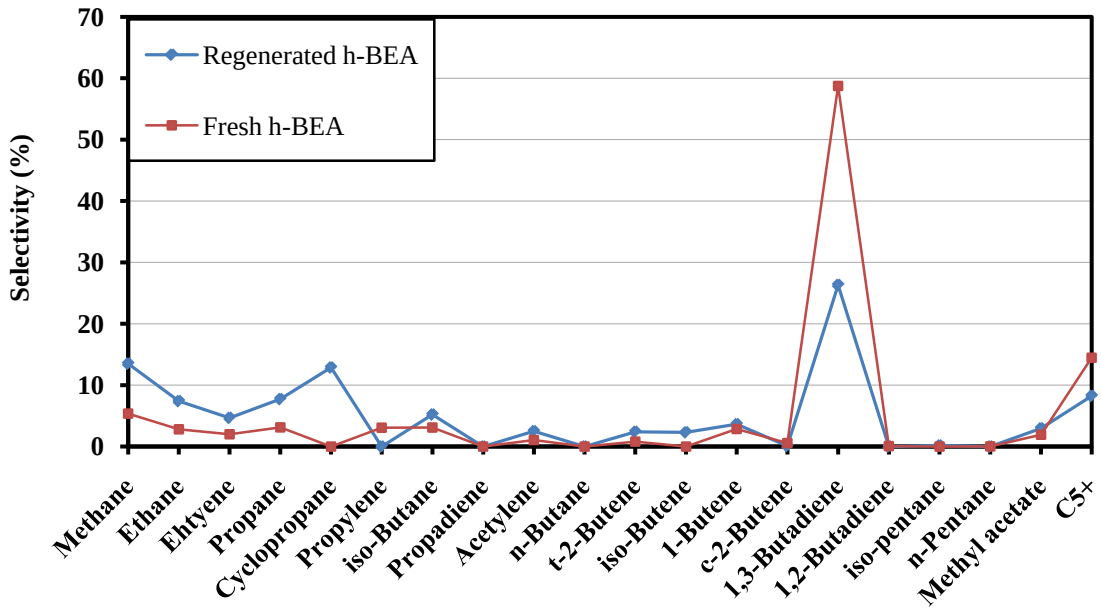

Figure 3.38 Distribution of gas fraction obtained by catalytic cracking of HFO over fresh h-BEA and regenerated h-BEA catalysts.

Figure 3.29 showed product distribution of distillate oil obtained by catalytic cracking reaction over fresh h-BEA and regenerated h-BEA at 380°C for 40 min. It was found that the distillate oil components obtained from regenerated h-BEA were mainly in the range of C_8 to C_9 as same as fresh catalyst.

It was indicated that enlarged-pore zeolite beta was stable and can be easily regenerated in a furnace. Its catalytic activity was no significantly difference between the fresh and regenerated catalysts.

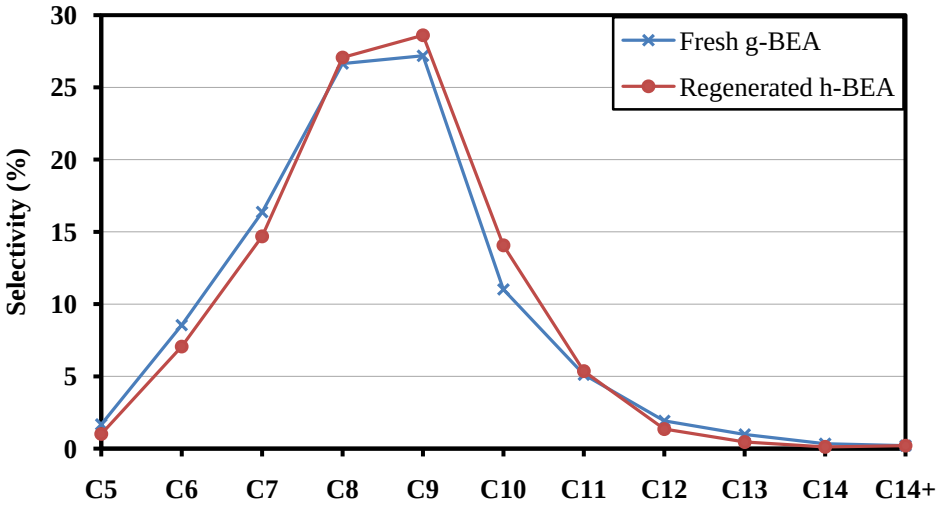

Figure 3.39 Carbon number distribution of distillate oil obtained by catalytic cracking of HFO over fresh h-BEA and regenerated h-BEA catalysts.

CHAPTER IV

CONCLUSION

The enlarged-pore zeolite beta materials had been synthesized under hydrothermal condition. The effects of silica source, templates and crystallization temperature and time were investigated. The enlarged-pore zeolite beta (h-BEA) prepared from calcined Si-HMS did not affect the crystallinity. The formation of zeolite beta structure can be achieved after crystallization at 135°C for 3 days. The h-BEA material exhibits a type I isotherm which is typical of microporous materials, and shows larger pore diameter than zeolite beta prepared form TEOS. When HDA template was also used with TEAOH to synthesize enlarged-pore zeolite beta (h-BEA-Mn-T_{crys}-t_{crys}), increasing of HDA template ratio in mixed template system reduced crystallinity of zeolite structure. The samples also show a type I isotherm. When h-BEA-M3-T_{crys}-t_{crys} samples were studied for crystallization temperature and time at 135, 140 and 145°C for 6, 9, 12 and 15 days, increasing crystallization temperature and time had significantly affected on crystallinity and phase of materials. The XRD pattern shows that the formation of zeolite beta phase can be achieved after crystallization at 140 and 145°C for 9 days with ZSM-12 coexisting phase. At crystallization temperature of 145°C, the zeolite beta phase was rapidly taken place by ZSM-12 while at 140°C, the coexistence of ZSM-12 was decreased. The h-BEA-M3-T_{crys}-t_{crys} samples at low crystallization temperature and time show low absorption at low pressure and increase in adsorption with a hysteresis loop at higher pressure, indicating monolayer and multilayer sorption characteristics, that is micro- and mesoporous characteristics. The pore diameter of h-BEA-M3-T_{crys}-t_{crys} samples can be controlled by varying crystallization time. The Si/Al ratios in catalyst of comparative zeolite beta and the enlarged-pore zeolite beta (h-BEA) were higher than Si/Al ratio in gel and become greater in enlarged-pore zeolite beta when prepared from TEAOH-HDA mixed template. ^{27}Al MAS NMR spectra of h-BEA-M3-T_{crys}-t_{crys} materials indicate all of the aluminum atoms remained in the tetrahedral oxygen coordination at framework positions for zeolite beta while comparative zeolite beta

and h-BEA materials indicate partial aluminum atoms remained in the tetrahedral oxygen coordination at framework positions and another remained in the octahedral non-framework.

The catalytic property of synthesized enlarged-pore zeolite beta materials was investigated in catalytic cracking of heavy fuel oil at 380°C for 40 min. The enlarged-pore zeolite beta catalysts had efficiency in the cracking of large molecules in heavy fuel oil to lighter hydrocarbon liquid more than the comparative zeolite beta and thermal cracking. The heavy fuel oil conversions and yields of products depend on properties of catalyst, the cracking temperature and time and heavy fuel oil to catalyst ratio. The conversions and yields of products increase when pore diameter of catalyst, reaction temperature and time and heavy fuel oil to catalyst ratio increase. The product selectivity is also affected by pore diameter of catalyst, reaction temperature and time and heavy fuel oil to catalyst. The selectivity to light hydrocarbon products decreased when pore diameter increased, while cracking temperature and time and heavy fuel oil to catalyst ratio increase. The gas products obtained by heavy fuel oil catalytic cracking are mainly 1,3-butadiene and C_5^+. The distillate liquid products obtained by heavy fuel oil catalytic cracking are mainly C_6 to C_{10} which are in gasoline range (based on boiling point range using n-paraffins as reference) while heavy liquid products are mainly in C_{10}-C_{20} which are in kerosene range. Thus, the enlarged-pore zeolite betas can be adapted for catalytic cracking of heavy fuel oil depending on customers' requirement. The optimum condition of catalytic cracking of heavy fuel oil is over h-BEA at 380°C for 40 min, 10 wt% of catalyst to heavy fuel oil and N_2 flow of 20 cm^3/min. The used catalyst can be regenerated by calcination in air and its property and activity were not significantly different from the fresh catalyst.

The suggestions for future work

To investigate the effect of Si/Al ratio in the range of 5-30 in the synthesis of enlarged-pore zeolite beta due to the increasing of Si/Al ratio lead to increasing of the ZSM-12 coexisting phase. Whereas zeolite betas with the decreasing gel Si/Al ratios lead to the pure phase of beta.

REFERENCES

[1] World oil recoveries over 10 year periods [Online]. 2006. Available from: http:// www.caseyresearch.com/displayCdd.php?id=273 [2009, October 05]

[2] Mrak, M., Tušar, N. T., Logar, N. Z., Mali, G., Kljajić, A., Arčon, I., Launay, F., Gedeon, A. Kaučič, V. Titanium containing microporous/mesoporous composite (Ti,Al)-Beta/MCM-41: Synthesis and characterization. *Microporous and Mesoporous Materials* 95(2006): 76-85.

[3] Zhoa, S. X., Lu, G. Q., Millar G. J. Advances in Mesoporous Molecular Sieve MCM-41. *Industrial & Engineering Chemistry Research* 35(1996): 2075-2090.

[4] Products Made from a Barrel of Crude Oil [Online]. 2006. Available from: http:// www.heatingoil.com. [2009, February 17]

[5] Kolpack, R. L. Sinking of oil in Los Angeles harbor, California following the destruction of the *Sansinena.* In: Proceedings of the conference on assessment of ecological impacts of oil spills. *American Institute of Biological Sciences* 39(1978): 378-392.

[6] Orr, A. S., Van Sant, Jr. R. W. *Residual fuel oils. In: Guthrie, V.B. (Petroleum Products Handbook Ed.).* pp. 8.1-8.31. New York: McGraw-Hill, 1960.

[7] Guard, H. E., Cobet, A. *Fate of petroleum hydrocarbons in beach sand. Final Report No. CG-D-8-75.* Washington DC: US Coast Guard, 1972.

[8] CONCAWE: *Health aspects of petroleum fuels - potential hazards and precautions for individual classes of fuels. Report No. 85/51.* Brussels: CONCAWE, 1985.

[9] Cruzan, G., Low, L. K., Cox, C. E., Meeks, J. R., Mackerer, C. R., Craig, P. H., Singer, E. J., Mehlman, M. A. Systemic toxicity from subchronic dermal exposure, chemical characterization, and dermal penetration of catalytically cracked clarified slurry oil. *Toxicology and Industrial Health* 2(1986): 429-444.

[10] Energy uses by fuel type in 1970 to 2000 [Online]. 2006. Available from: http:// www.nrcan.gc.ca. [2009, July 24]

[11] Comparison of ex-refinery oil price. 2009. Available from: Ministry of energy, Thailand [2010, January 17]

[12] Scheirs, J. *Polymer Recycling. 1st Ed.* New York: John Wiley and Sons, 1998.

[13] Olah, G. A., Molnar, A.P. *Hydrocarbon Chemistry. 1st Ed.* New York: John Wiley and Sons, 1995.

[14] Matar, S., Hatch, L. F. *Chemistry of Petrochemical Process. 1st Ed.* Texas: Gulf Publishing Company, 1994.

[15] Speight, J. G. *The Chemistry and Technology of Petroleum. 2nd Ed.* New York: Marcel Dekker, 1991.

[16] Ding, W., Liang, J., Anderson, L. L. Hydrocracking and hydroisomeriaztion of high-density polyethylene and waste plastic over zeolite and silica-aluminasupported Ni and Ni-Mo sulfides. *Energy & Fuel* 11(1997): 1219-1224.

[17] Sing, K. S. W., Everett, D. H., Haul, R. A. W., Moscou, L., Pierotti, R. A., Rouquerol, J., Siemieniewska, T. Reporting physisorption data for gas/solid systems with special reference to the determination of surface area and porosity. *International Union of Pure and Applied Chemistry* 57(1985): 603-619.

[18] Barrer, R. M. Synthesis of a zeolite mineral with chabasitelike sorptive properties. *Journal of Chemical Society* (1948): 127-132.

[19] Milton R. M. Molecular sieve science and technology. A historical perspective. *ACS Symposium (zeolite synth.)* 398(1989): 1-10.

[20] Breck, D. W. *Zeolite Molecular sieve: Structure, Chemistry and use.* pp. 3-20. New York: John Wiley and Sons, 1997.

[21] Baerlocher, Ch., Meier, W. M., Olsen, D. H. *Atlas of Zeolite Framework Types*. Elseviers, 2001.

[22] Loewenstein W. The distribution of aluminum in the tetrahedral of silicates and aluminate. *American Mineralogist* 39(1954): 92-96.

[23] Chen, N. Y., Kaedin W. W., Dwyer, F. G. Para-directed aromatic reactions over shape-selective molecular sieve zeolite catalysts. *Journal of the American Chemical Society* 101(1979): 6783-6784.

[24] Jeanvoine, Y., Angyan, J. G., Kresse, G., Hafner, J. Brønsted acid sites in HSAPO-34 and chabazite: An abolition structural study. *Journal of Physical Chemistry B* 102(1998): 5573-5580.

[25] Ding, L., Zheng Y. Effect of template concentration and gel dilution on crystallization and particle size of zeolite beta in the absence of alkali cations. *Microporous and Mesoporous Materials* 103(2007): 94-101.

[26] Ding, L., Zheng Y. Nanocrystalline zeolite beta: The effect of template agent on crystal size. *Materials Research Bulletin* 42 (2007): 584-590

[27] Millini, R., Frigerio, F., Bellussi, G., Pazzuconi, G., Perego, C., Pollesel, P., Romano, U. A priori selection of shape-selective zeolite catalysts for the synthesis of 2,6-dimethylnaphthalene. *Journal of Catalysis* 217(2003): 298-309.

[28] Weitkamp, J. Zeolites and catalysis. *Solid State Ionics* 131(2000): 175-188.

[29] Zones, S. I., Davis, M. S. Zeolite material: Resent discovery and future prospects. *Current Opinion in Solid State & Materials Science* 1(1996): 107-117.

[30] Wadlinger, R. L., Kerr, G. T., Rosinski, E. J. A crystalline zeolite with improved adsorption and catalytic properties. *United States Patent* 3308069 (1967)

[31] Treacy, M. M. J., Newsam, J. M. Two new three-dimensional twelve-ring zeolite frameworks of which zeolite beta is a disordered intergrowth. *Nature* 332(1988): 249-251.

[32] Baerlocher, C., Meier, W. M., Olson, D. H. *Atlas of zeolite framework types 5th Ed.* Amsterdam: Elsevier, 2001.

[33] De Vries, A. H., Sherwood, P., Collins, S. J., Rigby, A. M., Rigutto, M., Kramer, G. J. Zeolite structure and reactivity by combined quantum chemical-classical calculations. *Journal of Physical Chemistry B* 103(1999): 6133-6141.

[34] Rungsirisakun, R., Jansang, B., Pantu, P., Limtrakul, J. The adsorption of benzene on industrially important nanostructured catalysts (H-BEA, H-ZSM-5, and H-FAU): confinement effects. *Journal of Molecular Structure* 733(2005): 239-246.

[35] Newsam, J. M., Treacy, M. M. J., Koetsier, W. T., de Gruyter, C. B. Structural characterization of zeolite beta. *Proceeding of Royal Society A* 420(1988): 375-405.

[36] Guisnet, M., Ayrault, P., Coutanceau, C., Alvarez, M. F., Datka, J. Acid properties of dealuminated beta zeolites studied by IR spectroscopy. *Journal of Chemical Society, Faraday Transactions* 93(1997): 1661-1665.

[37] Zhang, H., Li, Y. Preparation and characterization of Beta/MCM-41 composite zeolite with a stepwise-distributed pore structure. *Powder Technology* 183(2008): 73-78.

[38] Beck, J. S., Vartuli, J. C., Roth, W. J., Leonowicz, M. E., Kresge, C. T., Schmitt, K. K., Chu, C. TW., Olson, D. H., Sheppard, E. W., McCullen, S. B., Higgins, J. B., Schlenker J. L. A new family of mesoporous molecular mieves prepared with liquid crystal templates. *Journal of the American Chemical Society* 114(1992): 10834-10843.

[39] Kresge, C. T., Leonowicz, M. E., Roth, W. J., Vartuli, J. C., Beck, J. S. Ordered mesoporous molecular sieves synthesized by a liquid-crystal template mechanism. *Nature* 359(1992): 710-712.

[40] Schubert, U., Hüsing, N. *Synthesis of Inorganic Materials.* Weinheim: WILEY-VCH, 2000.

[41] Huo, Q., Margolese, D. K., Ciesla, U., Feng, P., Gier, T. E., Sieger, P., Leon, R., Petroff, P. M., Schuth, F., Stucky, G. D. Generalized synthesis of periodic surfactant/inorganic composite materials. *Nature* 368(1994): 317-323.

[42] Liu, H., Lu, G. Z., Guo, Y. L., Wang, J. S. Synthesis of framework-substituted Fe-HMS and its catalytic performance for phenol hydroxylation, *Nanotechnology* 17(2006): 997-1003.

[43] Bagshaw, S. A., Prouzet, E., Pinnavaia, T. J. Templating of mesoporous molecular-sieves by nonionic polyethylene oxide surfactants, *Science* 269(1995) p. 1242.

[44] Mokaya, R., Jones, W. Synthesis of acidic aluminosilicate mesoporous molecular sieves using primary amines. *Journal of Chemical Society. Chemical Communication* (1996): 981-193.

[45] Tanev, P. T., Pinnavaia, T. J. A neutral templating route to mesoporous molecular sieves. *Science* 267(1995): 865-867.

[46] Tanev, P. T., Pinnavaia, T. J. mesoporous silicas molecular sieves prepared by ionic and neutral surfactant templating: A Comparison of Physical Properties, *Chemistry of Materials* 8(1996): 2068-2079.

[47] Prouzet, E., Pinnavaia, T. J. Assembly of mesoporous molecular mieves containing wormhole motifs by a nonionic surfactant pathway: control of pore size by synthesis temperature. *Angewandte Chemie International Edition* 36(1997) 516.

[48] Chiranjeevi, T., Muthu K. G., Gupta, J. K., Murali D. G. Synthesis and characterization of acidic properties of Al-HMS materials of varying Si/Al ratios. *Thermochimica Acta* 443(2006): 87-92.

[49] Chen, S., Yang, Y., Zhang, K., Wang, J. BETA zeolite made from mesoporous material and its hydrocracking performance. *Catalysis Today* 116(2006): 2-5.

[50] Aguado, J., Serrano, D. P., Escola, J. M., Garagorri, E., Fernández, J. A. Catalytic conversion of polyolefins into fuels over zeolite. *Polymer Degradation and Stability* 69(2000), 11-16.

[51] Groen, J. C., Abelló, S., Villaescusa, L. A., Pérez-Ramírez, J. A new family of mesoporous molecular mieves prepared with liquid crystal templates. *Microporous and Mesoporous Materials* 114(2008): 93-102.

[52] Guo, W., Huang, L., Deng, P., Xue Z., Li Q. Characterization of Beta/MCM-41 composite molecular sieve compared with the mechanical mixture. *Microporous and Mesoporous Materials* 44(2001), 427-434.

[53] Van O. C. J., Stevens, W. J. J., Bruijn, E., Mertens, M., Lebedev, O. I., Van T. G., Meynen, V., Cool, P. Formation of a combined micro- and mesoporous material using zeolite Beta nanoparticles. *Microporous and Mesoporous Materials* 120(2009): 29-34.

[54] Cassiers, K., Linssen, T., Mathieu, M., Benjelloun, M., Schrijnemakers, K., Van D. V. P., Cool, P., Vansant, E. F. A Detailed Study of thermal, hydrothermal and mechanical stabilities of a wide range of surfactant

assembled mesoporous silicas. *Chemistry of Materials* 14(2002): 2317-2324.

[55] Li, X., Shen, B., Guo, Q., Gao, J. Effects of large pore zeolite additions in the catalytic pyrolysis catalyst on the light olefins production. *Catalysis Today* 125(2007): 270-277.

[56] Loiha, S., Prayoonpokarach, S., Songsiriritthigun, P., Wittayakun J. Synthesis of zeolite beta with pretreated rice husk silica and its transformation to ZSM-12. *Materials Chemistry and Physics* 115(2009): 637-640.

[57] Tuel, A., Gontier, S. Synthesis and characterization of trivalent metal containing mesoporous silicas obtained by a neutral templating route. *Chemistry of Materials 8*(**1996)**: 114-122.

[58] Pauly, T. R., Lu, Y., Pinnavia, T. J., Billinger, S. J. L. Riker, T. P. Textural mesoporosity and the catalytic activity of mesoporous molecular sieves with wormhole framework structures. *Journal of the American Chemical Society* **121**(1999): 8835-8842.

[59] Selvam, P., Bhatia, S. K., Sonwane, C. G. Recent advances in processing and characterization of periodic mesoporous MCM-41 silicate molecular sieves. *Industrial & Engineering Chemistry Research* 40(2001): 3237-3261.

[60] Raman, N., Anderson, M. T., Brinker, C. J. Template-based approaches to the preparation of amorphous, nanoporous silicas. *Chemistry of Materials* 8(1996): 1682-1701.

[61] Kong, L., Chen, H., Tai J., Shen J., Zhang, S., Chen, J. Synthesis of small crystal zeolite beta in a biphasic H_2O–CTAB–alcohol system. *Materials Letters* 63(2009), 343-345.

[62] Matsukata, M., Ogura, M., Osaki, T., Kikuchi, E., Mitra, A. Quantitative analyses for TEA^+ and Na^+ contents in zeolite beta with a wide range of Si/2Al ratio. *Microporous and Messoporous Materials* 48(2001): 23-29.

[63] Gopal, S., Yoo, K., Smirniotis P. G. Synthesis of Al-rich ZSM-12 using TEAOH as template. *Microporous and Mesoporous material* 49(2001): 149-156.

[64] Eapen, M. J., Reddy, K. S. N., Shiralkar, V. P. Hydrothermal crystallization of zeolite beta using tetraethylammonium bromide. *Zeolites* **14**(1994): 295-302.

[65] Wei, X., Smirniotis P. G. Development and characterization of mesoporosity in ZSM-12 by desilication. *Microporous and Mesoporous material* 97(2006): 53-63.

[66] Gläser, R., Li, R., Hunger, M., Ernst, S., Weitkamp, J. Zeolite HNU-87: synthesis, characterization and catalytic properties in the shape-selective conversion of methylnaphthalenes. *Catalysis Letters* 50(1998): 141-148.

[67] Conesa, J. A., Fant, R., Marcilla, A., Garcia, A. N. Pyrolysis of polyethylene in a fluidized bed reactor. *Energy Fuels* 8(1994): 1238-1245.

[68] Kaminsky, W., Schesselmann, B., Simon, C. Olefins from polyolefins and mixed plastic by pyrolysis. *Journal of Analytical and Applied Pyrolysis* 32(1995): 19-25.

[69] Védrine, J. C., Auroux, A., Dejaifve, P., Ducarme, V., Hoser, H., Zhou, Sh. Catalytic and propertiesof phosphorus-modified ZSM-5 zeolite. *Journal of Catalysis* 73(1982): 147-160.

[70] Araujo, A. S., Silva, A. O. S., Souza, M. J. B., Coutinho, C. S. L. S., Aquino J. M. F. B., Moura, J., Pedrosa, A. M. G. Crystallization of ZSM-12 zeolite with different Si/Al ratio. *Adsorption* 11(2005): 159–165.

[71] Kaeding, W. W., Chu, C., Young, L. B., Welnsteln, B., Butter, S.A. Selective alkylation of toluene with methanol to produce para-Xylene. *Journal of Catalysis* 67(1981): 159-174.

[72] Kaeding, W. W., Chu, C., Young, L. B., Butter, S. A. Shape-selective reactions with zeolite catalysts: II. Selective disproportionation of toluene to produce benzene and *p*-Xylene. *Journal of Catalysis* 69(1981): 392-403.

[73] Masuda, T., Kuwahara, H., Mukai, S. R., Hashimoto, K. Production of high quality gasoline from waste polyethylene derived heavy oil over Ni-REY catalyst in steam atmosphere. *Chemical Engineering Science* 54(1999): 2773-2779.

[74] Joo, H. S., Guin, J. A. Continuous upgrading of a plastic pyrolysis liquid to an environmentally favorable gasoline range product. *Fuel Processing Technology* 57(1998): 25-40.

[75] Vitolo, S., Bresci, B., Seggiani, M., Gallo, M. G. Catalytic upgrading of pyrolytic oils over HZSM-5 zeolite: behavior of the catalyst when used in repeated upgrading-regenerating cycles. *Fuel* 80(2001): 17-26.

[76] Garforth, A. A., Lin, Y. H., Sharratt, P. N., Dwer, J. Production of hydrocarbons by catalytic degradation of high density polyethylene in a laboratory fluidized-bed reactor. *Applied Catalysis A: General* 169(1998): 331-342.

APPENDICES

A.1 Calculation of Selectivity to Other Hydrocarbon

% Selectivity of gas fraction and liquid fraction

$$\%\text{Selectivity of X} = \frac{\text{concentration of X}}{\text{total concentration of fraction}} \times 100$$

$$\text{Concentration of X} = \frac{b \times c}{a} \times 100$$

a = Peak area of X in standard gas or liquid fraction

b = %molar of X in standard gas or liquid fraction

a = Peak area of X in sample products

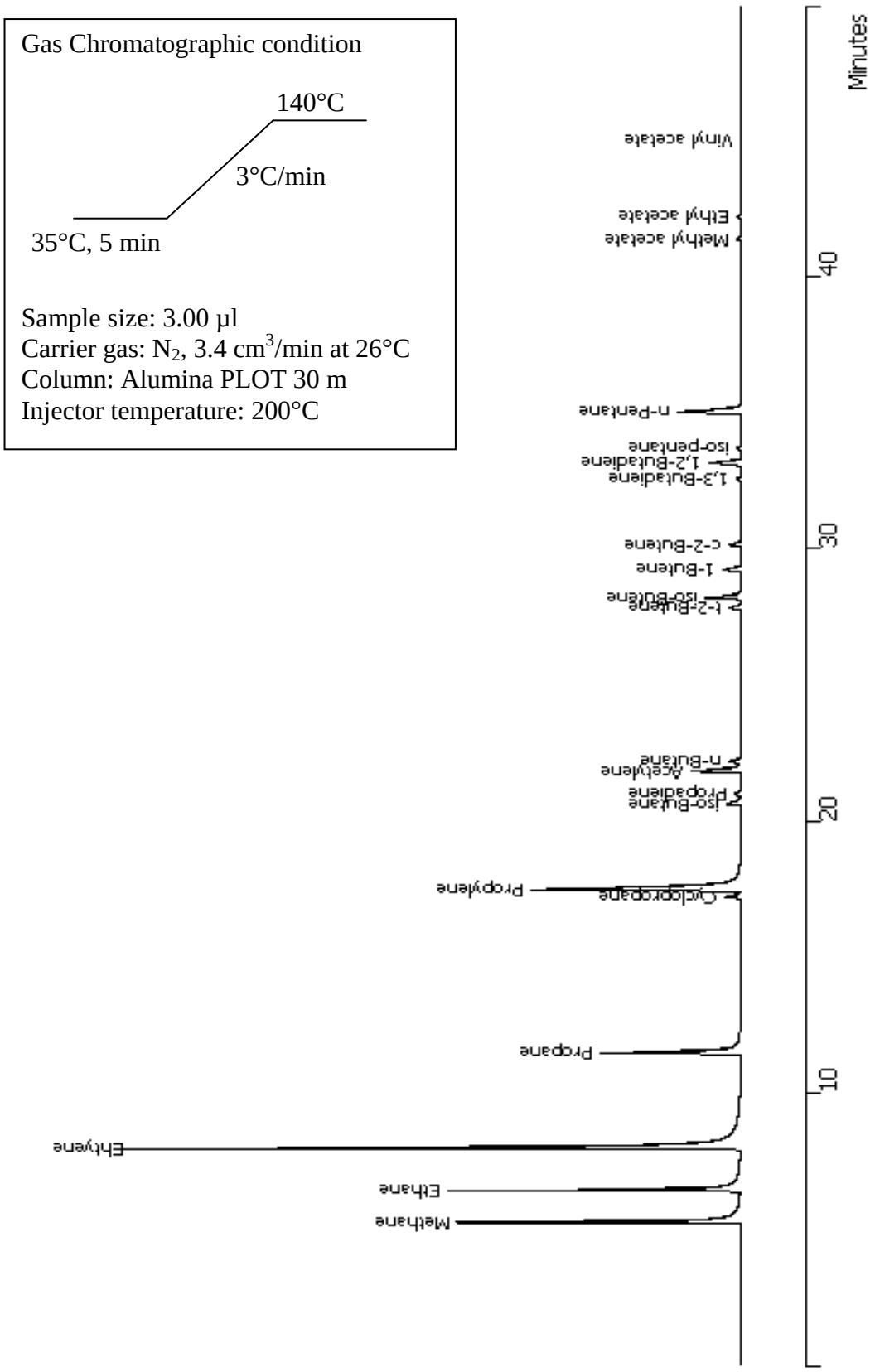

Figure A-1 Gas chromatogram of standard mixture gas

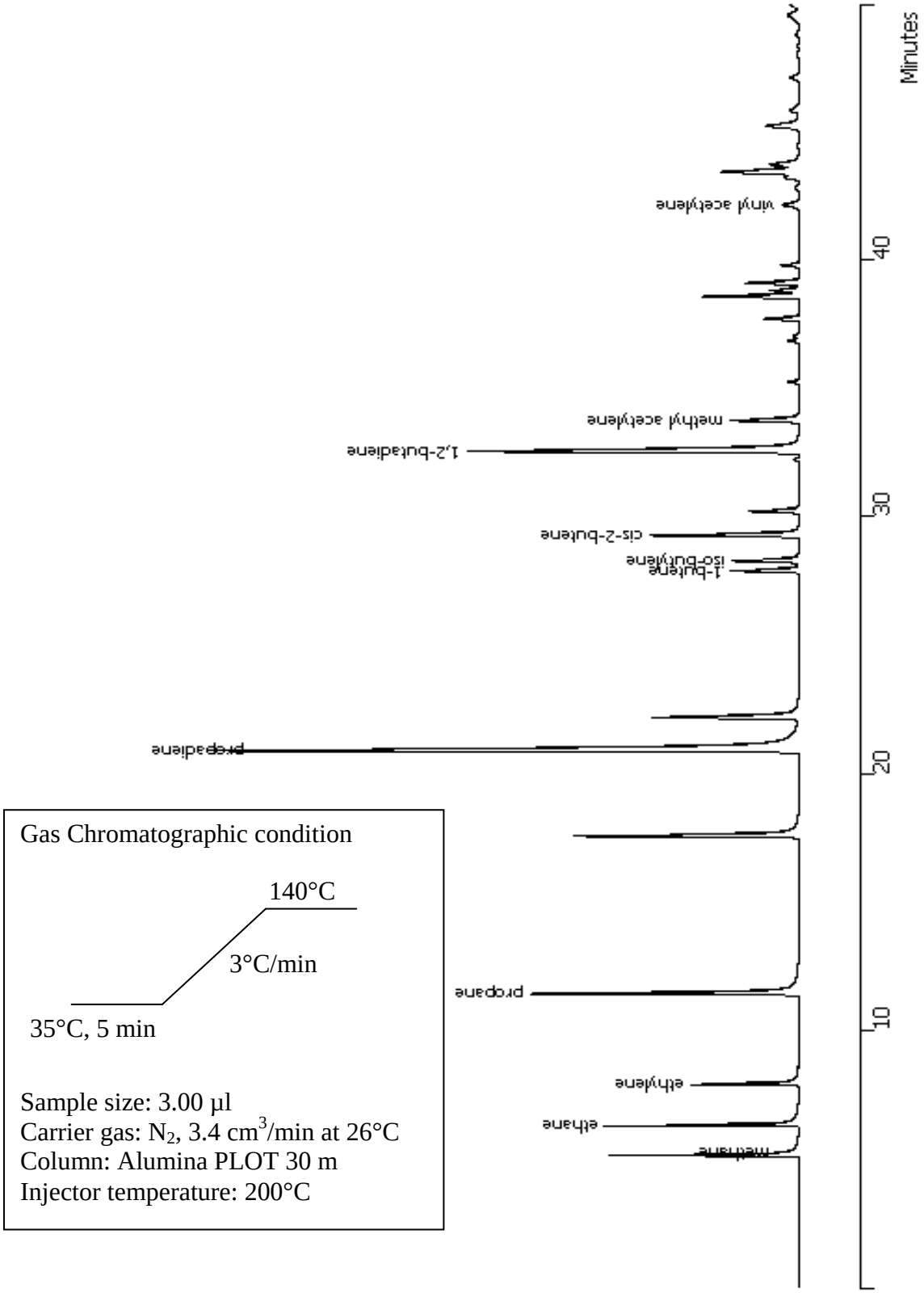

Figure A-2 Gas chromatogram of product obtained from catalytic cracking of HFO over h-BEA at 380°C for 40 min

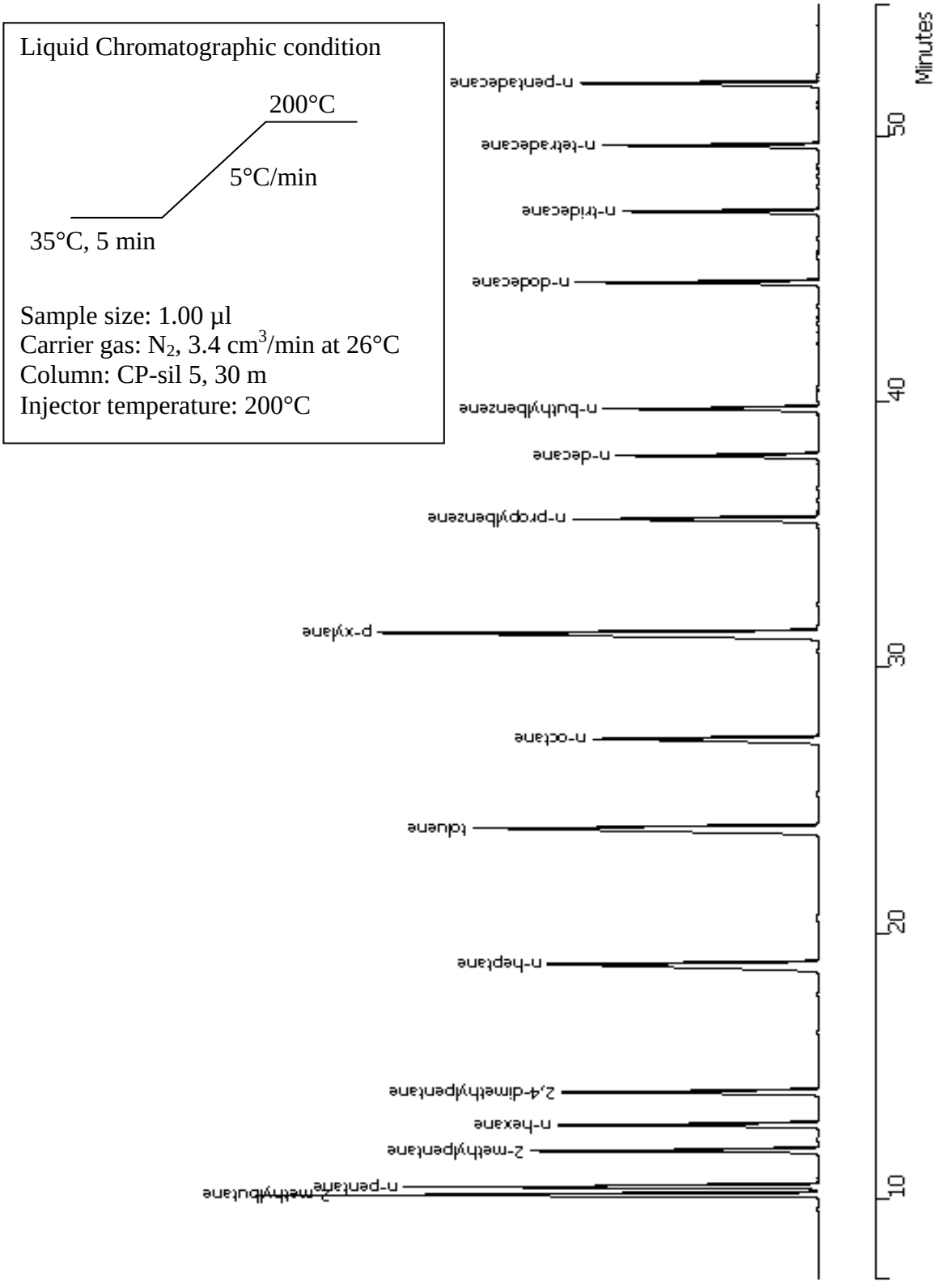

Figure A-3 Liquid chromatogram of standard quantitative calibration mix (SUPELCO)

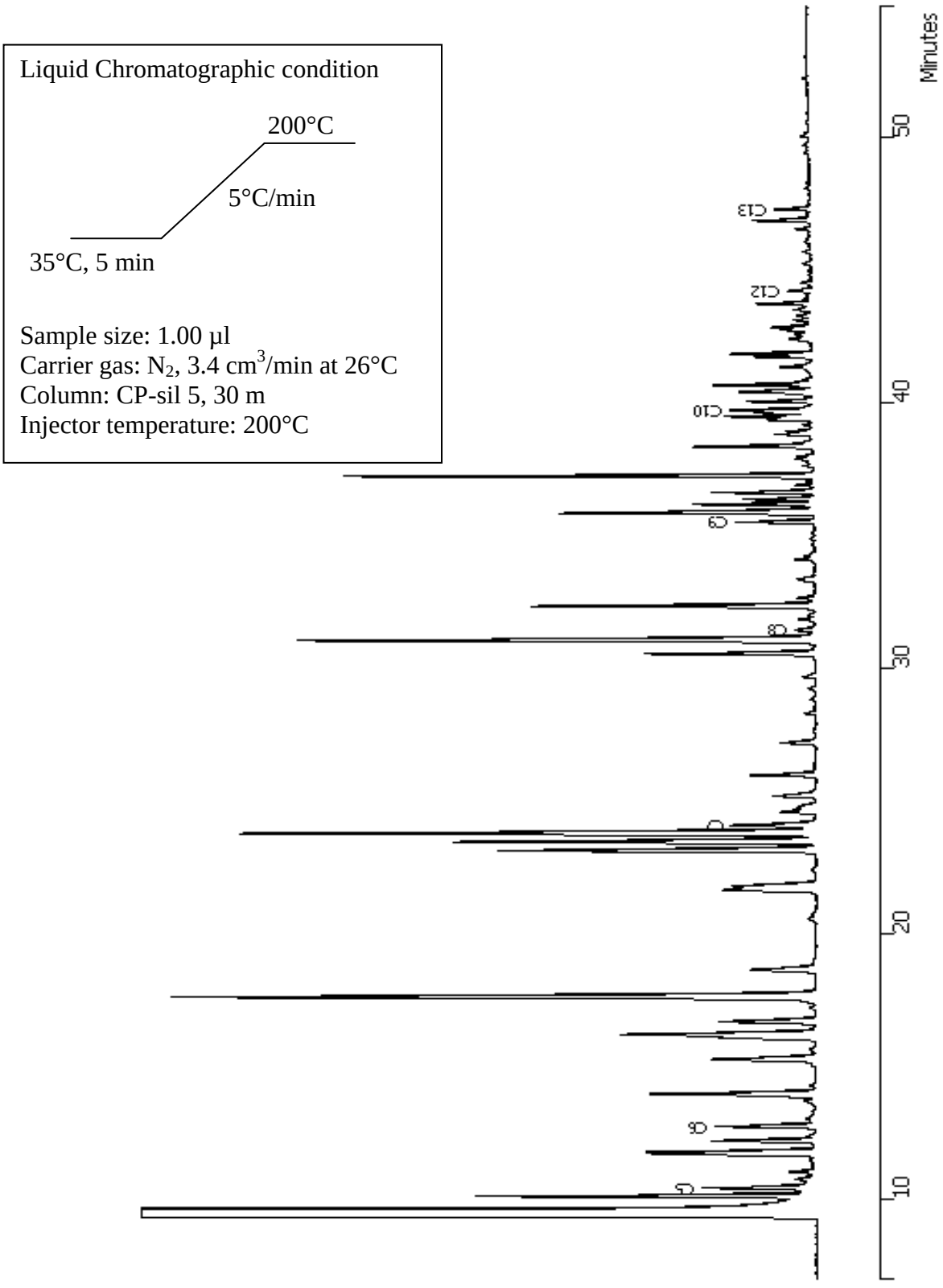

Figure A-4 Liquid chromatogram of standard gasoline (SUPELCO)

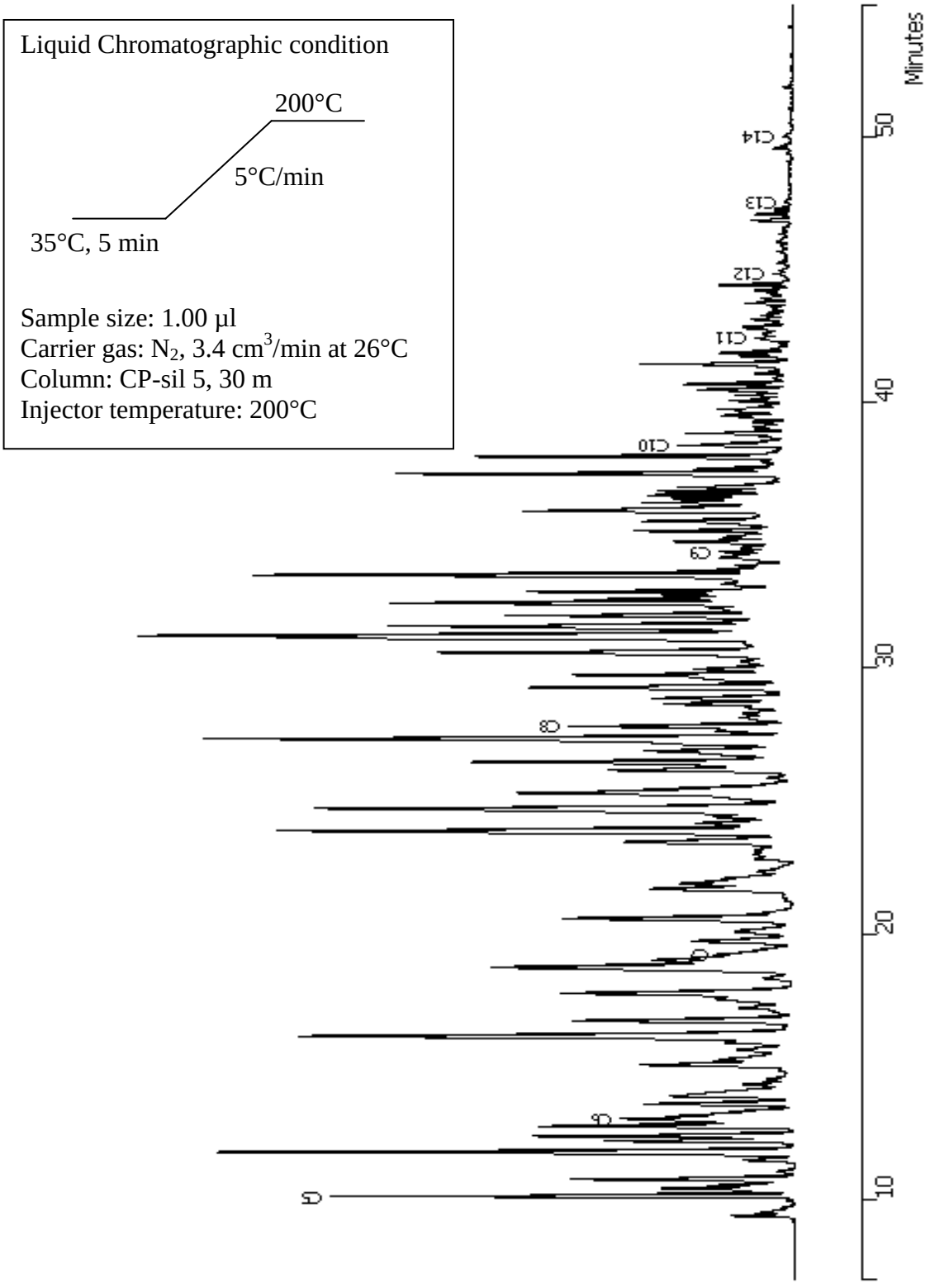

Figure A-5 Liquid chromatogram of product obtained from catalytic cracking of HFO over h-BEA at 380°C for 40 min

VITAE

Miss Nicharee Wongsawatgul was born on June 16, 1985 in Bangkok, Thailand. She graduated with Bachelor of Chemistry from Faculty of Science and Technology, Thammasat University in 2006. She continued her study in Petrochemical and Polymer Science, Chulalongkorn University in 2007 and completed in 2010. She participated in Pure and Applied Chemistry International Conference 2010 (PACCON 2010) on January 21-23, 2010 at Sunee Grand Hotel and Convention Center, Ubonratchathani, Thailand.